MICROBIAL ELECTROCHEMICAL SENSOR SYSTEMS FOR RAPID MEASUREMENT OF VOLATILE FATTY ACID INTERMEDIATES

A Thesis submitted by

Andrew Hill

BEng (Hons.)

For the award of

Doctor of Philosophy

2022

ABSTRACT

Biogas production from renewable sources is set to grow in Australia over the next decade. Anaerobic digestion is the key process employed to produce biogas and is being incorporated with other renewable energy production such as wind and solar. Biogas can contribute to stabilising energy supply-demand through steady baseload and on-demand variable biogas energy production. As adoption of more novel anaerobic digestion technologies increases, monitoring of key process parameters is becoming more crucial. Relatively poor process transparency accompanied with process sensitivity are key drivers to developing alternative monitoring options. One key parameter and indicator of process instability is the concentration of volatile fatty acids; metabolites formed during the anaerobic digestion process, and that build-up when the process is stressed. Current methods to measure volatile fatty acids include titration, gas chromatograph, and high-performance liquid chromatography. Unfortunately, these methods typically require an external laboratory, which can take several hours and/or require reliable manual sampling of the digestate to obtain a measurement. Consequently, there is a need for measurement alternatives to enable timely and reliable measurement of volatile fatty acids to monitor anaerobic digestion performance. Microbial electrochemical sensors show potential as a viable alternative to these problems but still face challenges in development. The themes within this thesis identify and investigate challenges to microbial electrochemical technologies. A cost-effective potentiostat design was presented as a way to overcome barriers associated with cost. As a sensor, a microbial electrochemical sensor needs to be capable of stable and predictable output, therefore a microbial electrochemical sensors biofilm growth long-term was explored in terms of cell performance to identify ageing effects on transduced signal. Lastly, to address the need for rapid measurements in high-rate anaerobic digesters, the conductivity impact on microbial electrochemical sensor biofilm response times and peak current was investigated. These interrelating studies contribute to further understanding of a promising alternate method for volatile fatty acid measurement, microbial electrochemical technologies.

CERTIFICATION OF THESIS

I Andrew Hill declare that this Ph.D. Thesis entitled “Microbial electrochemical sensor systems for rapid measurement of volatile fatty acid intermediates” is not more than 100,000 words in length including quotes and exclusive of tables, figures, appendices, bibliography, references, and footnotes.

This thesis is the work of the student, Andrew Hill, except where otherwise cited or acknowledged, with the majority of the contribution to the papers presented as a thesis by publication undertaken by the student. The work is original and has not previously been submitted for any other award, except where acknowledged.

Date:

Endorsed by:

Bernadette K. McCabe
Principal Supervisor

Stephan Tait
Associate Supervisor

Craig Ballie
Associate Supervisor

Peter Harris
Associate Supervisor

Student and supervisors’ signatures of endorsement are held at the University.

STATEMENT OF CONTRIBUTION

Paper I:

Hill, A., Tait, S., Ballie, C., Virdis, B., McCabe, B. (2021). Microbial electrochemical sensors for volatile fatty acid measurement in high strength wastewaters: A review. Biosensors and Bioelectronics, 165, 112409, https:// 10.1016/j.bios.2020.112409

Andrew Hill contributed 70% to this paper. Collectively Tait, S., Ballie, C., Virdis, B., McCabe, B. contributed the remainder.

Chapter 3:

Hill, A., Tait, S., Harris, P., Virdis, B., Ballie, C., McCabe, B. (2022). Design and analysis of a low-cost potentiostat combined with microbial electrochemical sensors for the accurate measurement of volatile fatty acids. **Submitted** to the journal *Applied Energy*.

Andrew Hill contributed 70% to this paper. Collectively Tait, S., Harris, P., Virdis, B., Ballie, C., McCabe, B. contributed the remainder.

Chapter 4:

Hill, A., Tait, S., Harris, P., Ballie, C., McCabe, B. (2022). Long-term biofilm growth in a microbial electrochemical sensor and the effect on transduced signal. **In preparation** for planned submission to *Journal of Environmental Chemical Engineering*.

Andrew Hill contributed 65% to this paper. Collectively Tait, S., Harris, P., Ballie, C., McCabe, B. contributed the remainder.

Chapter 5:

Hill, A., Tait, S., Harris, P., Ballie, C., McCabe, B. (2022). Conductivity effects on microbial electrochemical sensor biofilm peak current response times. **In preparation** for planned submission to the journal *Biotechnology and Bioengineering*.

Andrew Hill contributed 70% to this paper. Collectively Tait, S., Harris, P., Ballie, C., McCabe, B. contributed the remainder.

ACKNOWLEDGEMENTS

It is my privilege to have the opportunity to learn from principal supervisor Prof. Bernadette K. McCabe. Bernadette's invaluable input on my Ph.D. research contributed greatly. The feedback and constructive criticism greatly improve my Ph.D. research. Bernadette's guidance during this work enabled me to remain focused.

I would like to thank associate supervisor, Dr. Stephan Tait, for assisting me during the Ph.D. I greatly benefitted from Stephan's depth of knowledge, background, and experience. Stephan's contribution to my Ph.D. cannot be overstated.

I would like to thank associate supervisor Prof. Craig Ballie for providing a valuable perspective throughout the Ph.D. Craig enabled my work to continue despite challenges.

I would like to thank associate supervisor Dr. Peter Harris, for his guidance and critique which greatly shaped my Ph.D. research. Peter's friendship and availability were greatly appreciated.

Many thanks to the staff at the University of Southern Queensland, your support during my Ph.D. helped get me through, especially those who worked within the Centre for Agricultural Engineering.

To my wife and children, without whom this would not have been possible. The unwavering support and encouragement were invaluable. The love and kindness shown to me despite the long days and high workload helped shape the Ph.D. and me as a person. Thank you to all my family and friends for supporting me throughout my Ph.D.

This research has been supported by an Australian Government Research Training Program Scholarship. This research was supported by the Queensland Government's Advance Queensland Research Fellowships Program. This work was also partially supported by the Australia-Germany Joint Research Cooperation Scheme (a joint initiative of Universities Australia (UA) and the German Academic Exchange Service (DAAD)), with funds from the German Federal Ministry of Education and Research, and the University of Southern Queensland.

TABLE OF CONTENTS

LIST OF FIGURES

LIST OF TABLES

ABBREVIATIONS

µC	Microcontroller
ABS	Acrylonitrile-Butadiene Styrene
AD	Anaerobic Digestion
ADC	Analog to Digital Controller
ADC_m	Analog to Digital Controller Modified Value
ADC_v	Analog to Digital Controller Value
ALK	Alkalinity
BES	Bioelectrochemical System
BOD	Biological Oxygen Demand
CA	Chronoamperometry
CE_f	Coulombic Efficiency
CE	Counter Electrode
CE_t	Counter Electrode Terminal
CH_3COOH	Acetic Acid
COD	Chemical Oxygen Demand
CV	Cyclic Voltammetry
DAC	Digital to Analog Controller
EAB	Electroactive Biofilm
EET	Extracellular Electron Transfer
FID	Flame Ionisation Detector
FOG	Fats, Oils and Grease
GC	Gas Chromatography
HPLC	High-Performance Liquid Chromatography
KCL	Potassium Chloride

MESe	Microbial Electrochemical Sensor
MET	Microbial Electrochemical Technology
MFC	Microbial Fuel Cell
NaAc	Sodium Acetate
NaCl	Sodium Chloride
NH_4Cl	Ammonium Chloride
OA	Organic Acid
RE	Reference Electrode
RE_t	Reference Electrode Terminal
SD	Secure Digital
SEM	Standard Error of the Mean
TCA	Tricarboxylic Acid
TIA	Transimpedance Amplifier
USD	United States Dollar
VFA	Volatile Fatty Acid
WE	Working Electrode
WE_t	Working Electrode Terminal

CHAPTER 1: INTRODUCTION

Australian renewable energy consumption grew by 5 % (2018-2019), with renewables representing 20 % of total energy production (Australian Government, 2020). Biogas accounts for 4.1 % of renewable energy and annual biogas energy production is expected to grow by 3.0 % over the next 10 years (Australian Government, 2020).

Anaerobic digestion (AD) is the key process employed to degrade organic substrate for biogas production (Wu et al., 2019). Although substrates for anaerobic digestion can vary, organic agricultural wastes from facilities such as slaughterhouses, wineries, dairies, distilleries, and sugar production are all suitable. These substrates and others can be considered for AD due to costs associated with disposal and the benefit of reducing carbon emissions, energy production, and monetising waste material. Stability of the AD process can be affected due to changes in substrate, particularly high-strength wastewater, which can lead to a reduction in biogas and in extreme cases can cause failure of the anaerobic digestion process. Rapid monitoring of the process provides valuable information to operators, who can intervene if necessary. Volatile fatty acids are used to indicate stability in anaerobic digestion and currently require relatively long analysis times for accurate measurement. This presents a knowledge gap in timely monitoring of anaerobic digestion.

To facilitate an increase in renewable biogas production novel concepts will be required to meet changing energy demands. Biogas from traditional digesters can take several hours or even days to change the biogas production rate using a continuous feeding regime, which is unlikely to keep up with changing energy demands. Flexibility in substrate feeding is showing economic feasibility and may reduce storage requirements (Barchmann et al., 2016; Mauky et al., 2017). The adapted feedstock and loading rate could save between 10% and 45% of greenhouse gas emissions (Ertem, Martinez-Blanco, Finkbeiner, Neubauer, & Junne, 2016). To improve the uptake of flexible biogas production there is a need for additional stability monitoring of the anaerobic digestion process (Mauky et al., 2017).

This thesis is focused on MESe measurement of volatile fatty acids (VFA) in anaerobic digestion of high-strength wastewater, with application to wider industrial wastewaters. Integral to the anaerobic digestion process VFAs combined with alkalinity, provide a good indication of process stability (Thomas Schmidt, McCabe, & Harris, 2018). When

measuring acidity, high buffering capacity can mask the accumulation of VFA. Slaughterhouse wastewater often has high buffering capacity, which affects traditional (e.g. pH) sensor measurements. Therefore, VFAs need to be directly analysed, which currently requires manual sampling of the wastewater. Current methods to measure VFA in the anaerobic digestion process include gas chromatography and titration. More novel approaches to VFA measurement are being investigated, such as microbial electrochemical sensors (MESe). A strong relationship exists between VFA concentration and electrical current production in MESe (Jiang, Chu, & Zeng, 2019; Jin, Angelidaki, & Zhang, 2016; H. Sun, Zhang, Wu, Dong, & Angelidaki, 2019). By using MESe, VFA produced during AD could be directly measured.

Microbial electrochemical technologies (MET) are separated into primary and secondary categories. Primary METs use faraday or capacitive responses between microbes and electrodes, while secondary METs use more indirect methods to control or modify the reaction environment (Schröder, Harnisch, & Angenent, 2015). Primary METs include microbial fuel cells and microbial electrolysis cells (Schröder et al., 2015), which are capable of: producing hydrogen (A. Wang et al., 2011; W.-K. Wang et al., 2019; G. Q. Zhang, Zhou, & Yang, 2019), generating electricity from organics (H. Liu, Cheng, & Logan, 2005), measuring simple organic acids in wastewater (H. Sun, Zhang, et al., 2019), and producing liquid chemicals (Yu, Yuan, Tang, & Zhou, 2017). A primary MET, MESe are being investigated as a simple, cost-effective device for the measurement of VFAs.

A detailed description of MESe is provided in Chapter 2 and summarised here, MESe work by an electroactive biofilm community attached to an electrode respiring an organic metabolite (e.g. in this case acetate) and converting its chemical energy content into electrical current by donating electrons to an electrode which is then measured. This current and other associated electrode measurements can then be correlated with the concentration of the organic metabolite, thereby providing a concentration measurement.

Measurement of an MESe signals can be achieved using a potentiostat, although other methods exist (e.g. voltmeter). Combining a potentiostat with a MESe allows for accurate control of the cell's applied potential, which needs to change as the cell's series resistance changes. The use of a potentiostat eliminates the need for other measurement methods such as an external resistor, which negatively affects biofilm growth (Pasternak, Greenman, & Ieropoulos, 2018; Vilajeliu-Pons et al., 2016). Internal and external series resistance (e.g. electrical, microbial, mass transport) limit current flow, ideally all known

electrical resistance in the system should be eliminated or reduced to as low as practical. Unfortunately, there are several limitations, such as biofilm respiration that are known to limit electron transfer and therefore oppose current flow (i.e. electrical resistance) (J. Wang, 2000). Viewing a biofilm as and electrical circuit rather than just an organism is gaining popularity, with this paradigm shift potentiostat techniques (e.g. impedance spectroscopy) are revealing more information about biofilms than ever before (Call et al., 2017; Z. Li et al., 2020; Turick, Shimpalee, Satjaritanun, Weidner, & Greenway, 2019). Beneficially a potentiostat enables an MESe to operate at the most thermodynamically efficient potential (Korth & Harnisch, 2019). The potentiostat can also add additional flexibility such as data storage. Current laboratory potentiostats are relatively costly and can present a barrier to research. By designing a cost-effective and accurate potentiostat, researchers may not be restricted to methods that limit cell measurement.

Biofilms form a key element in an MESe (Ivars-Barceló et al., 2018), and as such, stable and predictable biofilm behaviour is required. It is well understood that most organic bacteria have growth cycles. For an MESe the model electroactive bacteria *Geobacter sulfurreducens* can typically have a replication time of 1-4 days, suggesting that a biofilm dominant in *Geobacter sulfurreducens* may vary in transduced signal every few days (Engel et al., 2019). This would require a biofilm be investigated over a sufficiently long period to ascertain the impact ageing may have on a sensor-transduced signal.

As more novel approaches to AD such as on-demand biogas production gain popularity, biofilm peak current response times will need to keep in step with increasing demands. Current novel sensor designs have response times >5 minutes (Jiang, Yang, Liang, Liu, & Huang, 2018) but it is unclear what impact electrolyte characteristics will have on these times. To gain a better understanding, biofilm response times will need to be investigated in response to compounds often found in wastewater, namely sodium chloride and ammonium chloride. These salts increase electrolyte conductivity, which can potentially affect biofilm response times.

1.1 Aims and objectives

The aim of the following literature review focused on a microbial electrochemical sensor for the rapid monitoring of VFA intermediates during anaerobic digestion. The thesis identifies three key knowledge gaps which have been addressed through the following objectives:

- Develop a low-cost potentiostat for use with microbial electrochemical cells;
- Investigate the poorly understood long-term effects of microbial electrochemical transduced signal;
- Investigate conductivity effects on biofilm output and relation to peak current response time.

The following chapters are organised as a series of papers to address these three knowledge gaps in the literature. The presentation of the chapters is structured as a series of papers for submission to respective journals as detailed below.

Chapter 1 – An introduction to biogas and the anaerobic digestion process, the current applications, and challenges, which includes an increased demand for better monitoring.

Chapter 2 – A literature review is presented to provide a thorough background of the anaerobic digestion process and microbial electrochemical technologies. The review investigates the role microbial electrochemical technologies have in monitoring anaerobic digestion and identifies knowledge gaps and key challenges from the literature.

Chapter 3 –The literature review presented in Chapter 2 highlighted a cost-effective potentiostat as a limiting factor, and necessary to operate microbial electrochemical sensors efficiently in further investigations. This necessitated a Methods paper describing a low-cost design of a potentiostat. The aim is to present a cost-effective, simple, and accurate potentiostat, which could be used by researchers investigating electrochemical cells and MESe as further investigated throughout this thesis.

Chapter 4: –Investigates the influence of long-term biofilm growth while measuring volatile fatty acids. Statistical analysis is used to identify significant temporal changes in the biofilms, in terms of coulombic efficiency and consumption of acetic acid as the measured metabolite.

Chapter 5 – Investigates the effects of increased electrolyte conductivity on biofilm peak current response time. Challenges of newer technologies such as on-demand high-rate anaerobic digesters require additional timely monitoring of the anaerobic process. Current response times of novel MESe are >5 minutes depending on cell configuration. Utilizing typical salts present in wastewater to affect conductivity, the investigations aimed to identify means to reliably shorten an MESe measurement response time without adverse effects on sensing performance.

Chapter 6 – Provides a discussion on themes presented in each Chapter and identifies areas for further investigation.

CHAPTER 2: PAPER I – LITERATURE REVIEW

This Chapter has been published as **Paper I** - Microbial electrochemical sensors for volatile fatty acid measurement in high strength wastewaters: A review. In Biosensors and Bioelectronics. Volume 165, 1 October 2020, 112409.

The following literature review sought to identify knowledge gaps in microbial electrochemical technologies and their use in anaerobic digestion. The literature review introduces the anaerobic digestion process, anaerobic digestion characteristics, and the monitoring of volatile fatty acids a key indicator of stability. Current methods to measure volatile fatty acids are identified and compared with microbial electrochemical technologies. Key elements of a microbial electrochemical cell are introduced. Identification of physical processes involved in reduction and oxidation reactions required for volatile fatty acid measurement.

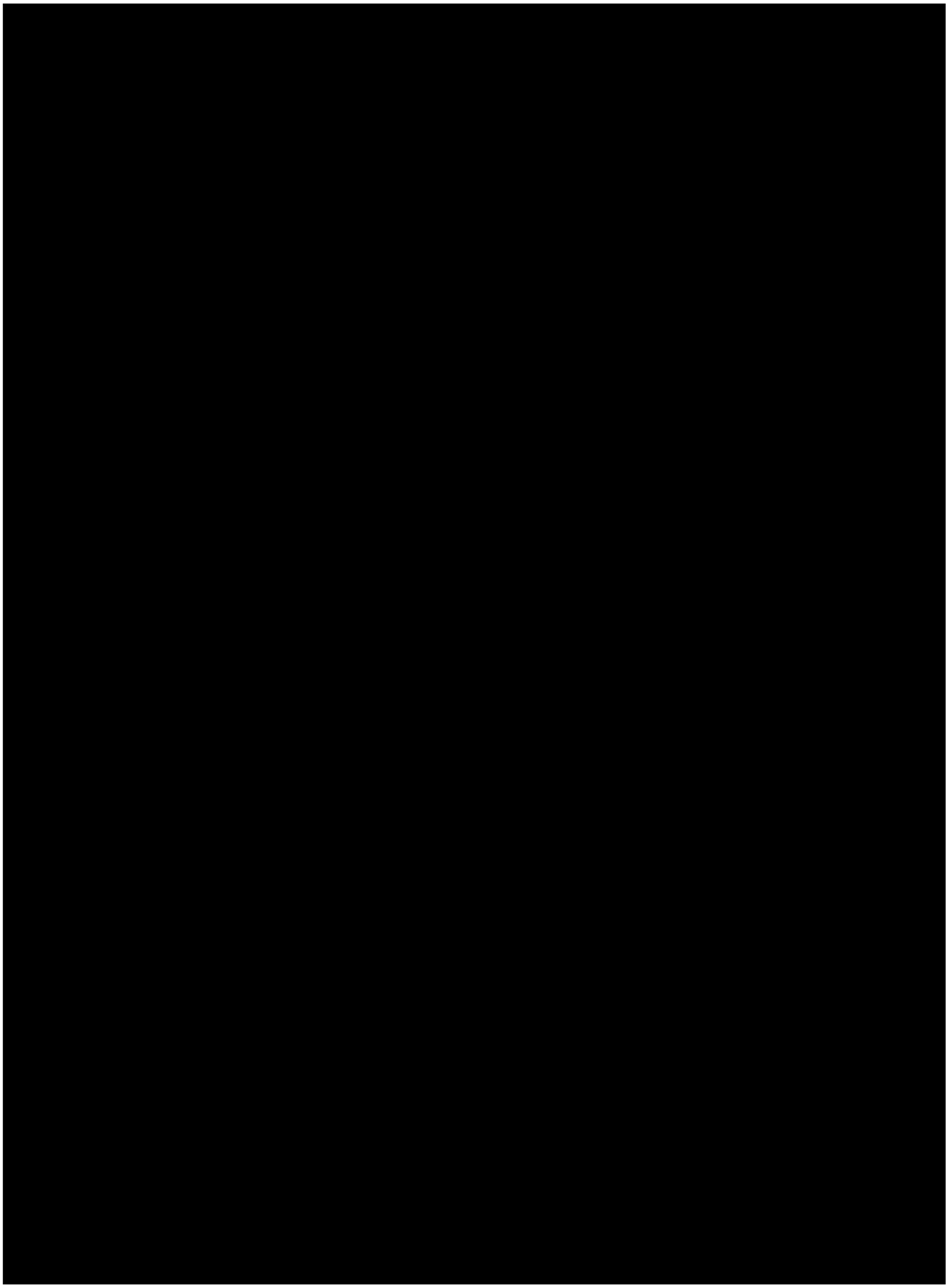

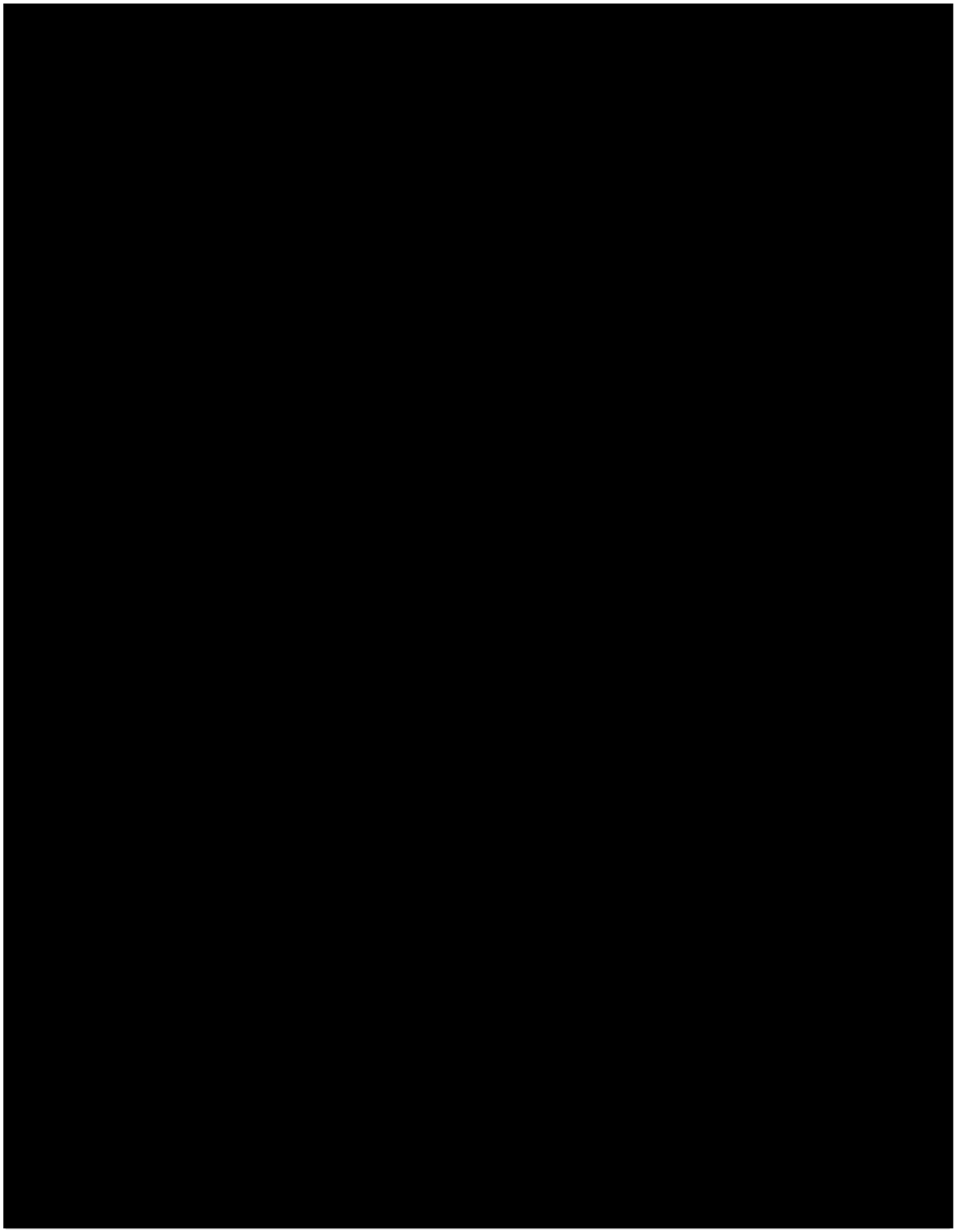

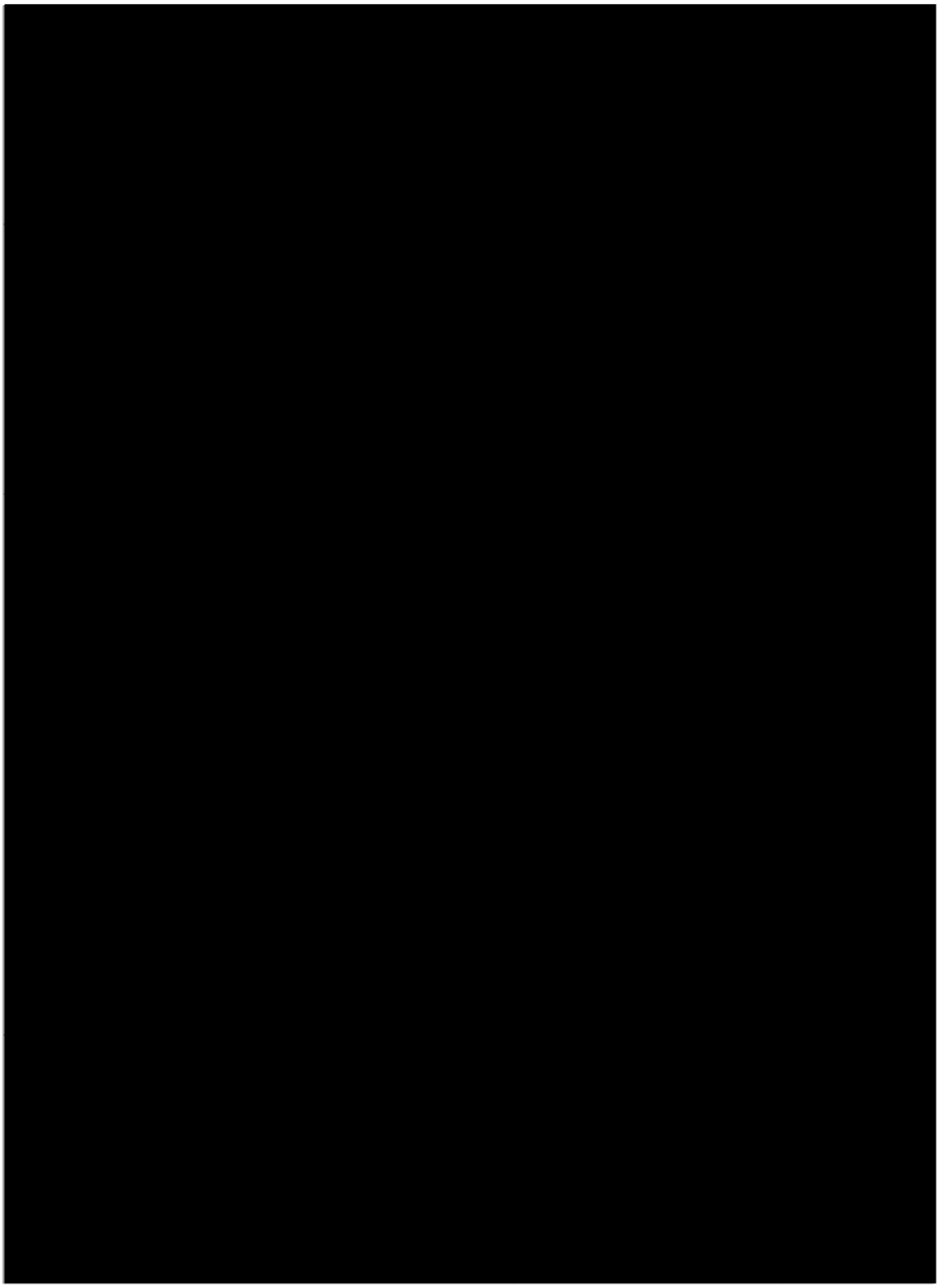

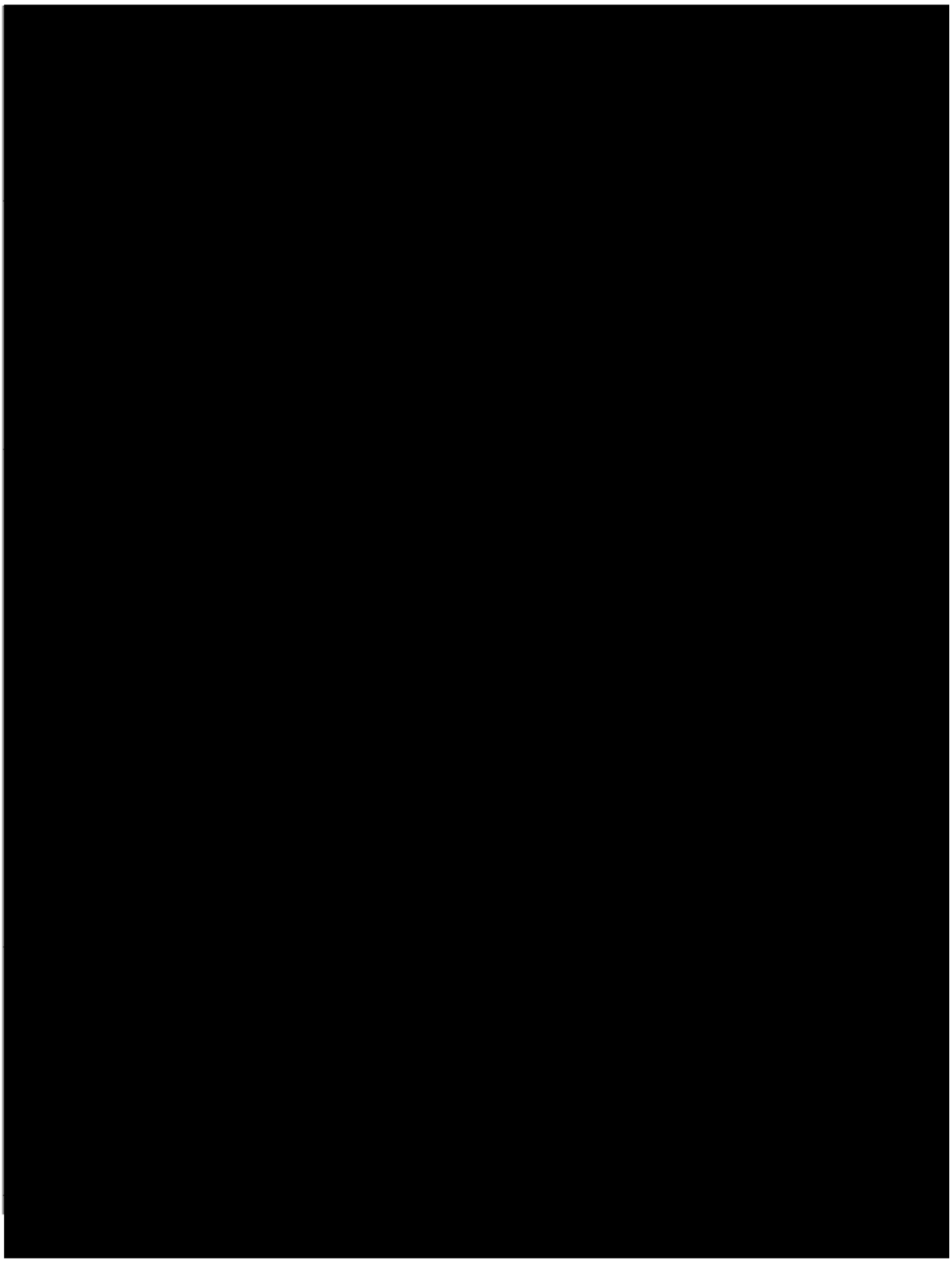

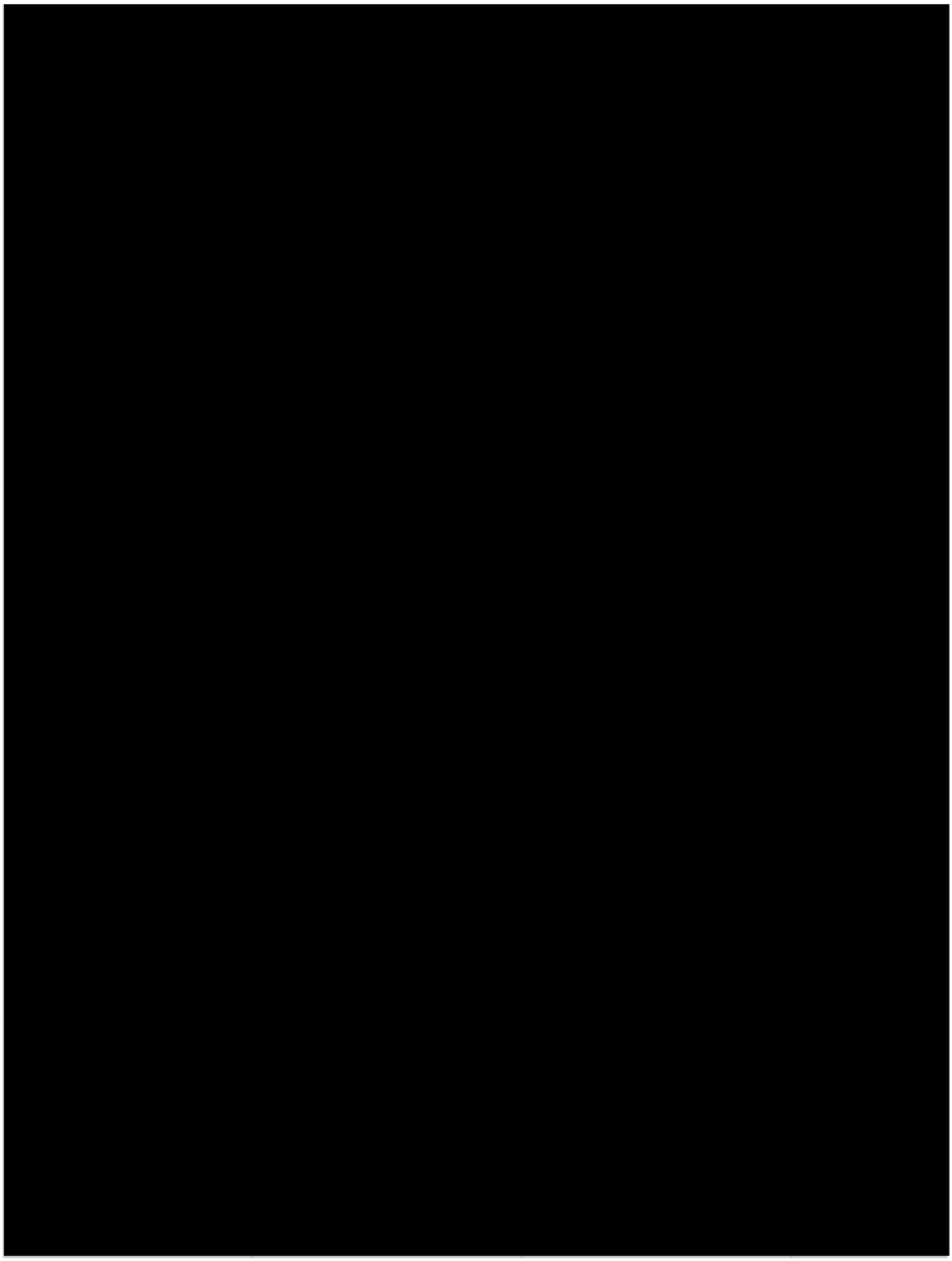

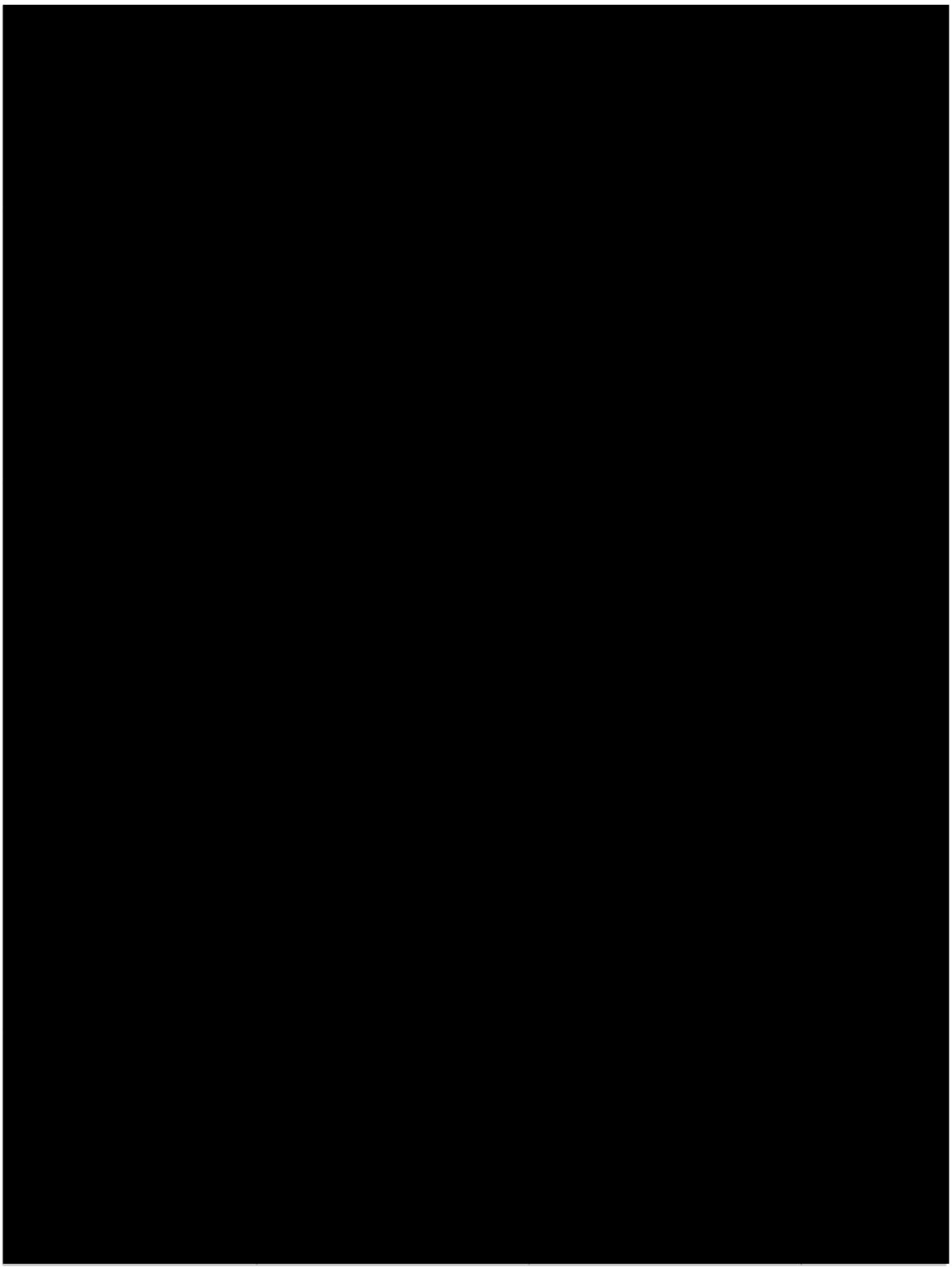

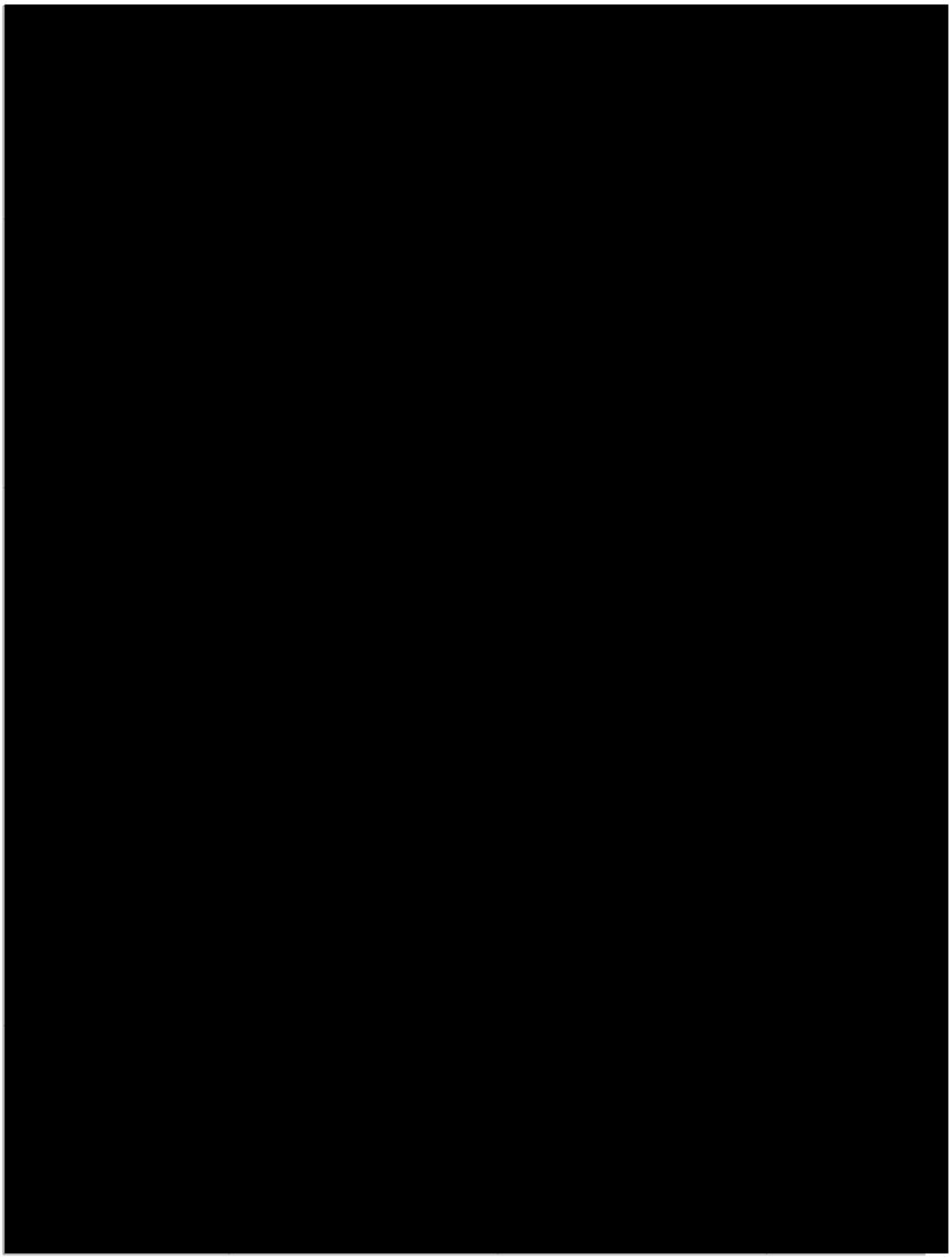

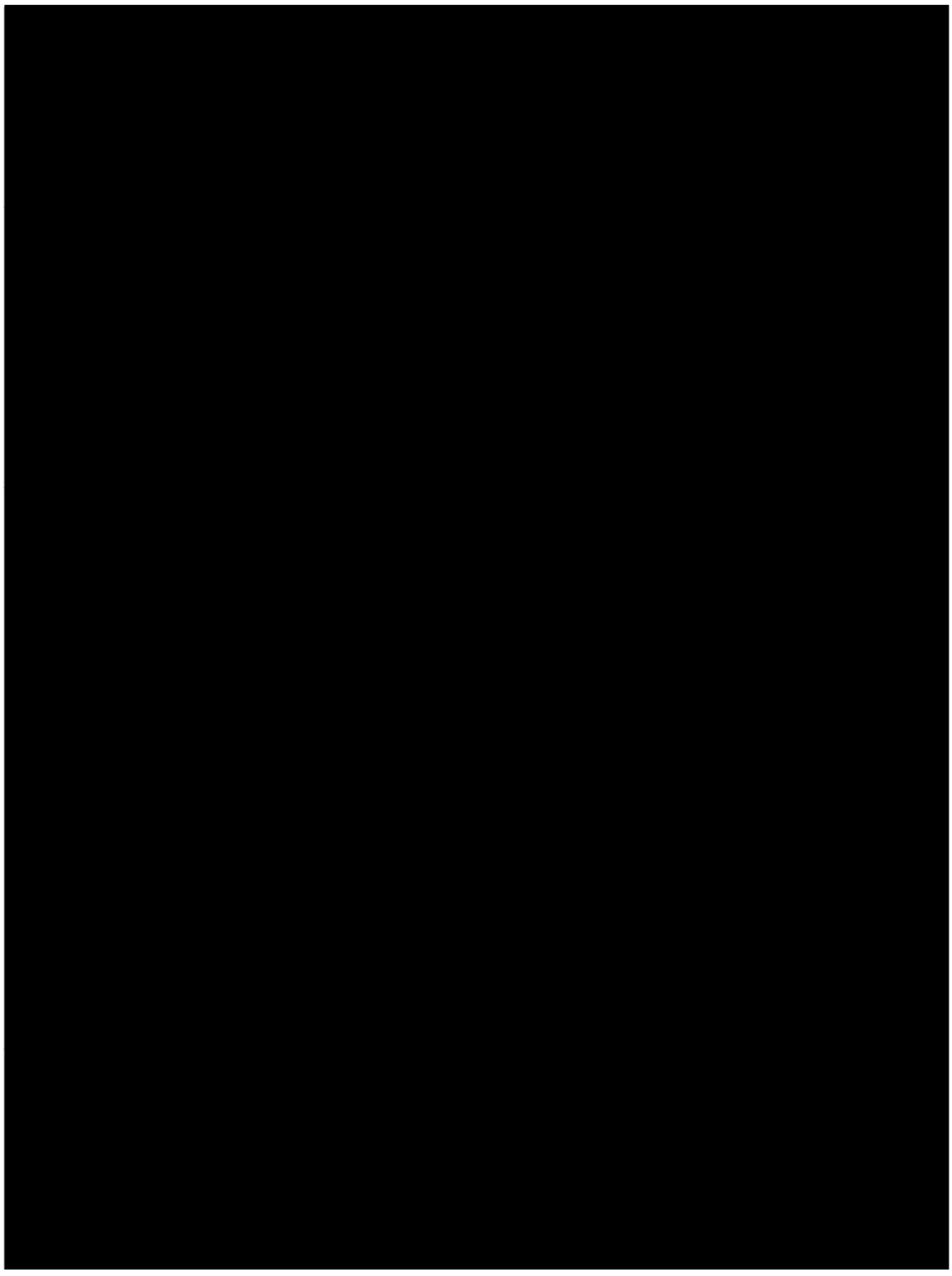

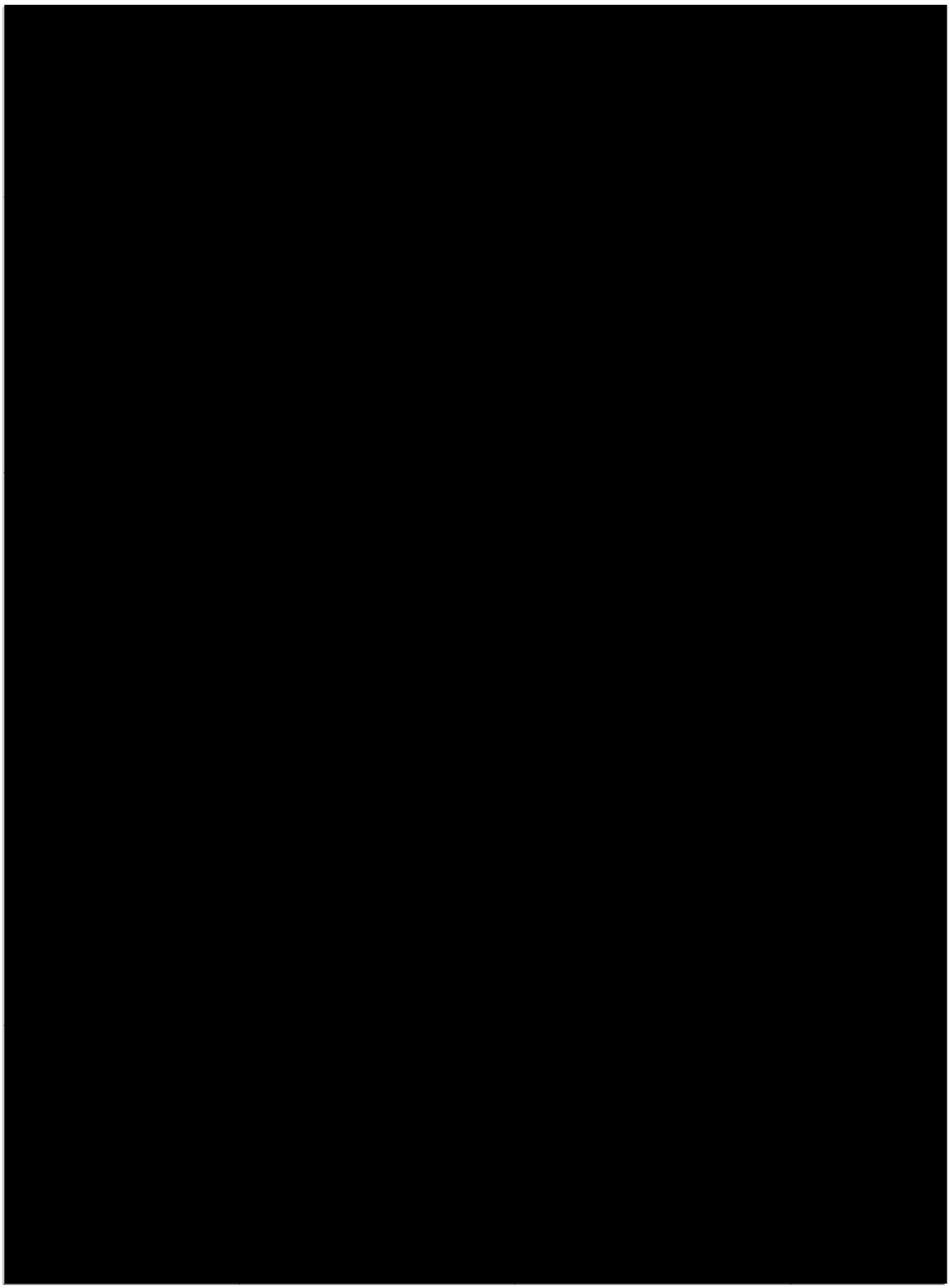

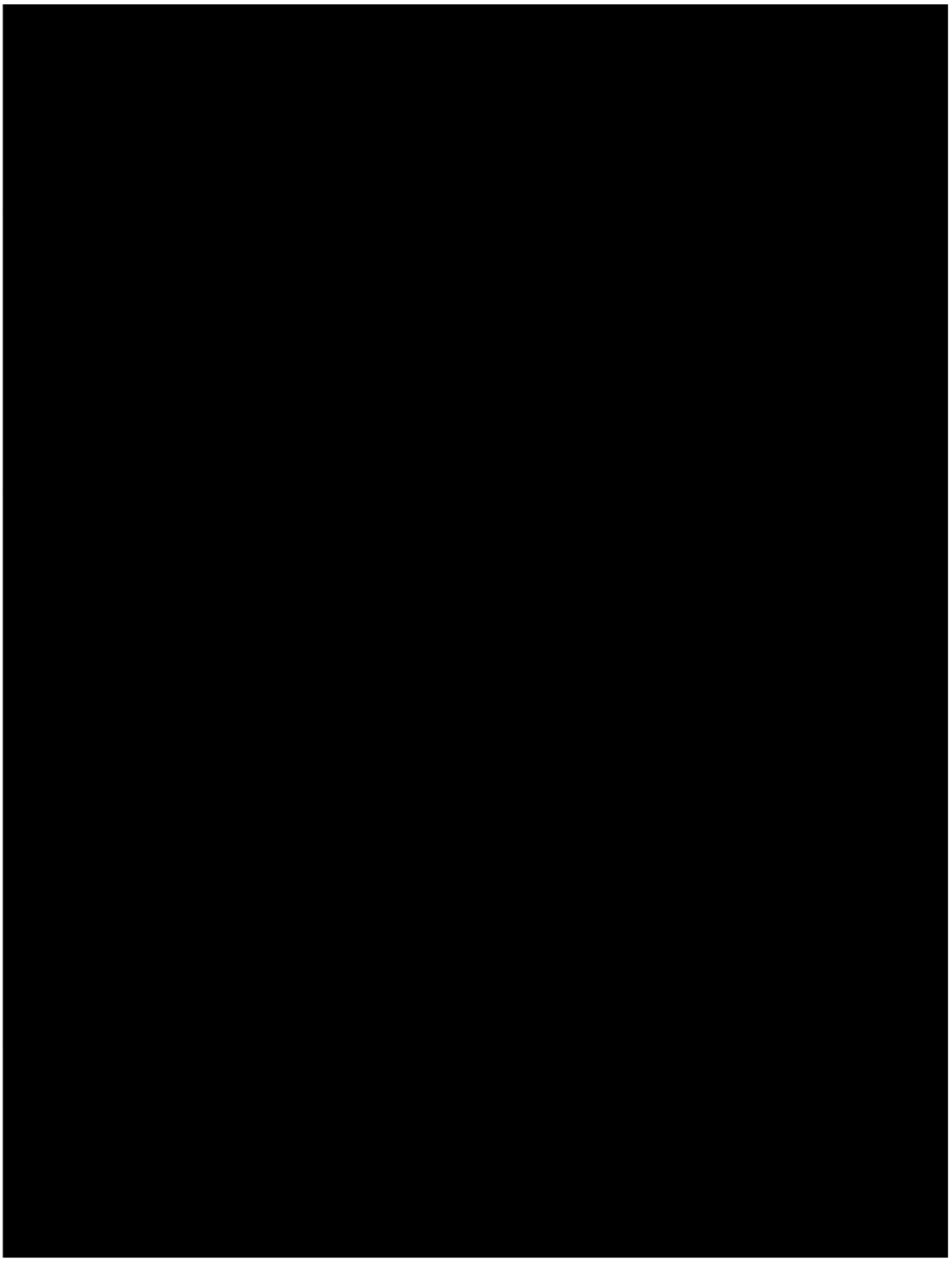

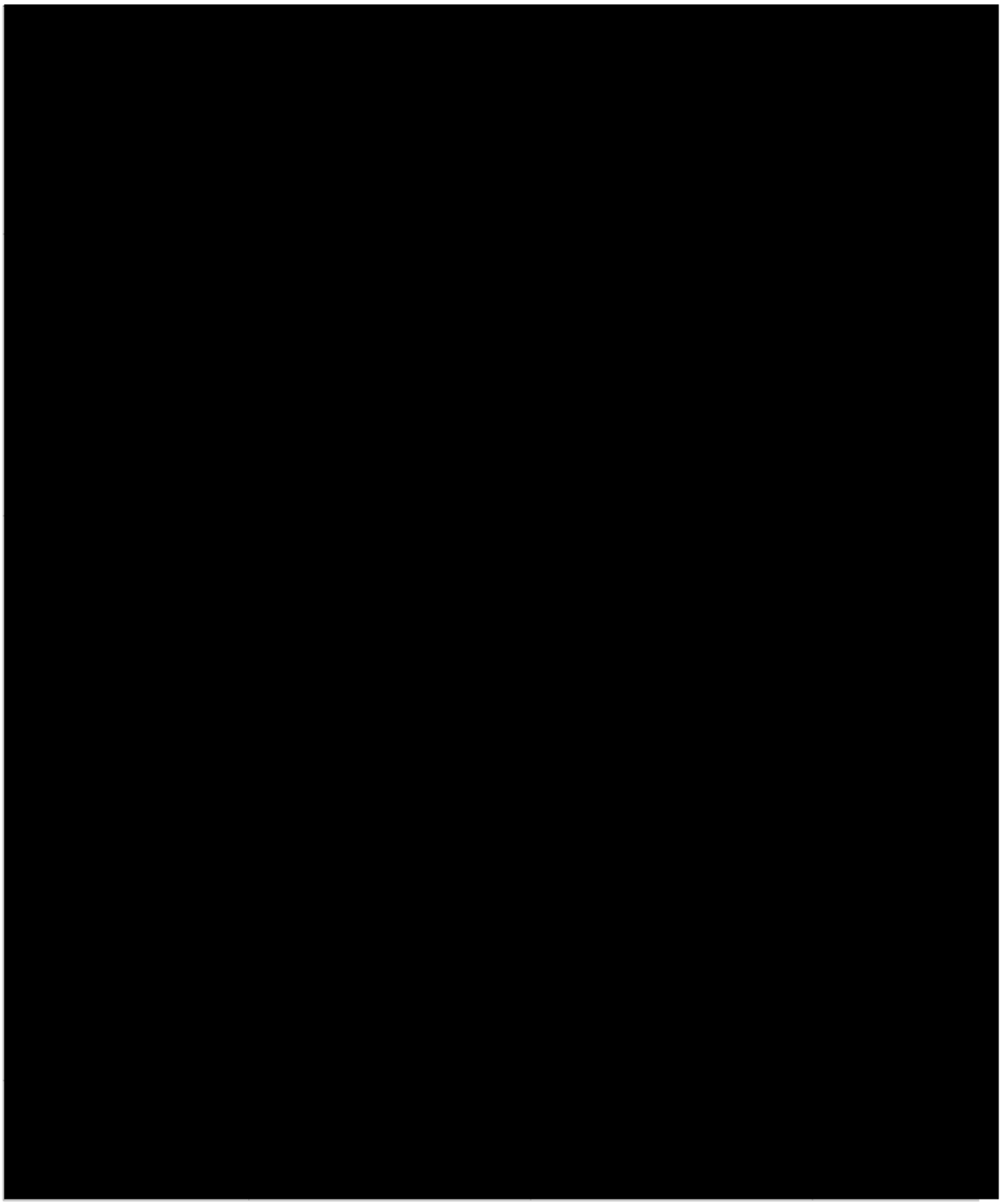

11

CHAPTER 3: DESIGN AND ANALYSIS OF A LOW-COST POTENTIOSTAT COMBINED WITH MICROBIAL ELECTROCHEMICAL SENSORS FOR THE ACCURATE MEASUREMENT OF VOLATILE FATTY ACIDS

This Chapter was submitted as **Paper II** – "Design and analysis of a low-cost potentiostat combined with microbial electrochemical sensors for the accurate measurement of volatile fatty acids" to the journal Applied Energy.

To facilitate MESe in both laboratory research as well as in-situ in-field measurements, a cost-effective prototype potentiostat is required as a key component of the MESe system. Potentiostats are electronic devices used for electrochemical analysis. A potentiostat is used in conjunction with a reference electrode to control the applied cell potential of an electrochemical cell allowing dynamic changes depending on electrolyte characteristics. The potentiostat is important to provide stable biofilm conditions for the measuring device despite dynamic fluctuations in the measurement electrolyte. To use a laboratory grade potentiostat in the field could be impractical and may require significant capital to implement. The knowledge gap identified in Chapter 2 highlighted a need for an affordable potentiostat that is functionally comparable to laboratory potentiostats. Accordingly, Chapter 3 strategically aimed to describe a low-cost alternative potentiostat design in the form of a methods paper. This then formed an essential component of the current laboratory potentiostat used in the later experiments of the thesis, as well as a potential reference point for future research and in-field applications.

Additionally, Chapter 3 introduces concepts required to build the potentiostat, and identifies the key subcircuits used to control potential with a reference electrode for feedback. Finally, Chapter 3 discusses why a potentiostat is used in electrochemical cells and why such a low-cost potentiostat is needed while identifying parameters that should be carefully considered depending on the application. Further information on specific component operation is presented in APPENDIX B.

3.1 Introduction

Biogas energy production via anaerobic digestion (AD) often relies on manual sampling and analysis to determine the stability and efficiency of the process. Volatile fatty acids (VFA) are commonly recognised as a sensitive stability indicator of AD (McCabe, Hamawand, Harris, Baillie, & Yusaf, 2014), but detailed diagnostic-level measurements of VFA typically require skilled personnel and relatively expensive measurement equipment. Conventional methods, including gas chromatography (Boe & Angelidaki, 2012), spectrophotometry (Falk, Reichling, Andersen, & Benz, 2015), and titration (T. Schmidt, McCabe, Harris, & Lee, 2018), are typically conducted offline. Novel approaches such as microbial electrochemical technologies (METs) have been recently identified as an alternative (Chapter 2).

Low-cost potentiostats are often built around a low-cost microcontroller, allowing for flexibility in experimental parameters. Important parameters include electric potential range, voltage sweep boundaries, timestamped values, and can add extra functionality such as wireless networking (Anshori et al., 2022; Meloni, 2016). Arduino's integrated development environment compatible microcontrollers are commonly used, although direct use of onboard peripherals such as analog to digital converters can limit operating resolution and capabilities (Cordova-Huaman, Jauja-Ccana, & La Rosa-Toro, 2021; Meloni, 2016). This highlights that an accurate and precise low-cost potentiostat will require a combination of low-cost microcontroller and external components. Using common components and software for development will assist in reducing costs.

Microbial electrochemical sensors (MESe), a type of MET, have a strong relationship between VFA concentration and output signal (Jörg Kretzschmar, Böhme, Liebetrau, Mertig, & Harnisch, 2018). Microbial communities that form on an electrode within the MESe take up VFA (e.g. acetate) for microbial respiration while concomitantly donating electrons to an electrode (Logan, Rossi, Ragab, & Saikaly, 2019; Saratale et al., 2017). These donated electrons generate a current which can be measured. Measurement methods vary but can be typically separated into two groups; resistive (Hassanein, Witarsa, Lansing, Qiu, & Liang, 2020; Schievano et al., 2018); and potentiostat (Atci, Babauta, Sultana, & Beyenal, 2016; Scarabotti, Rago, Buhler, & Harnisch, 2021). The resistive method involves placing an external load (e.g. a resistor) between the external terminals of the anode and cathode (Tommasi, Salvador, & Quaglio, 2016; X. Zhang, Xia, Ivanov, Huang, & Logan, 2014) and, similar to chronoamperometry, the current is

determined by applying Ohm's Law to measured voltages. However, external resistance inherently increases cell resistance and thereby reduces cell performance (Korth & Harnisch, 2019), removes control of the electrochemical cell environment, and negatively affects microbial community growth (Pasternak et al., 2018; Vilajeliu-Pons et al., 2016).

To minimise the cell error due to electrolytic resistance and other parasitic characteristics, a potentiostat can be used in conjunction with a 3-electrode cell is used to provide a controllable and efficient electrochemical cell environment. In a 3-electrode cell such as an MESe, a potentiostat regulates an electrolytic cell's potential relative to a reference electrode (RE), thereby reducing or eliminating unwanted effects from the cell's resistance. Modelling of biofilm thermodynamics in MESe shows that control of the cell potential allows the biofilm to achieve maximum efficiency (Korth & Harnisch, 2019). The combination of an MESe and potentiostat enables accurate control of the cell potential concomitantly allowing high-resolution measurement with minimal input from the operator. This method correlates well with changes in acetate (CH_3COO^-) concentration with relatively quick response times (Jiang et al., 2019). Moreover, a potentiostat is often the primary method to obtain quantifiable data from an MESe (Guo et al., 2019; Jörg Kretzschmar et al., 2018) and demonstrates that a potentiostat could in general be considered integral to MET technologies such as MESe.

Whilst an MESe should be relatively simple and affordable, a potentiostat is often sophisticated (e.g., multichannel), tailored to highly controlled laboratory investigations, and relatively costly. Although smaller, single-channel potentiostats can be purchased, accessibility may still prove to be prohibitive and may hinder progress in research and industrial practice. In keeping with a simple and affordable MESe approach, the supporting measurement device should also be economical and simple to operate. Several potentiostat circuits have been produced using a microcontroller (µC) and common electronic components which have demonstrated accurate analysis at a relatively affordable cost (Dryden & Wheeler, 2015; Friedman et al., 2012; Hoilett et al., 2020; Meloni, 2016). However, there is often a trade-off whereby cheaper potentiostats reduce functionality, resolution, and application.

Commonly found in the literature for low-cost potentiostats are studies aimed at low-cost (≈$50 USD) teaching potentiostats (Anshori et al., 2022; Cordova-Huaman et al., 2021) rather than targeting robust potentiostats. Potentiostats in a teaching context can be simple and low-cost but also limited in resolution and accuracy, which may be tolerable in the

teaching context. Although teaching on potentiostats can provide valuable experience to students, a potentiostat can vary by operating principles and configuration. Therefore, it is important to include potentiostat fundamental principles and relevant validation, which is often not reported (Y. C. Li et al., 2018; Meloni, 2016). A potentiostat can also be designed for teaching (in terms of cost and availability) but not sacrifice resolution and accuracy of the potentiostat.

This paper focuses on the design of an affordable yet accurate potentiostat for use in conjunction with an MESe (3-electrode cell), as this combination provides a controllable and efficient electrochemical cell environment. The design expands on previously identified circuits to provide a flexible, accurate, and low-cost potentiostat, that provides local and external (laptop) data storage. The potentiostat presented in this paper was designed to perform current vs. time measurements (chronoamperometry) and can be reprogrammed depending on application. This paper describes the design and analyses the performance of the potentiostat designed around an ultralow-noise instrumentation amplifier (in-amp) with supporting circuits and components. Simulation of the current measurement circuit utilising transimpedance amplification is provided along with measurements of current generated from acetate respiration in an MESe application. This demonstrates that a relatively affordable but versatile potentiostat can be designed that incorporates high accuracy and a simple design. This work aims to facilitate access to affordable and accurate potentiostats that support increasing research in MESe monitoring of AD systems, but also more broadly in the development of MET processes.

3.2 Materials and methods

All chemicals used were of an analytical reagent grade. Anaerobic digester sludge used for inoculation during testing of an MESe application was sourced from a domestic wastewater treatment plant previously described by Kazadi Mbamba, Flores-Alsina, John Batstone, and Tait (2016). The inoculum was filtered prior to use with a 150 µm sieve to remove large organic and inorganic material. Media for testing was comprised of 50 mM phosphate buffer containing trace minerals and vitamins as described by (J. R. Kim, Min, & Logan, 2005).

3.2.1 Device

Input voltage noise and voltage noise density were selected as the primary selection criteria for the amplifiers used in the potentiostat design. These parameters were used to

select components to limit noise in the potentiostat as potentiostats typically have to measure very small currents (i.e. 10^{-6} Amps) and are highly susceptible to interference. Other amplifier parameters that were considered before selection included input bias current, input offset voltage drift, and continuous output current. The selection criteria considered optimal values depending on the parameter, cost, and availability. A summary of these key characteristics for amplifiers is presented in Appendix A, Table A1.

The power requirement for each potentiostat was approximately 1 W, with the input voltage range being 5 – 24 V. Voltage supply to mounted components was via on-board regulators that produced ±5 V. The design of the potential range for the potentiostat was selected based on the anticipated experimental operating window and desired component parameters. The operating potential range was selected as ±2.5 V, and a maximum measurement current of ±2 mA was selected based on the trans-impedance amplifier (TIA) resistor (1,000 Ω) and in-amp maximum output (35 mA). Although higher potentials and currents are possible, these values were also selected to limit noise and simultaneously maintain a high resolution and simplicity.

To control the cell potential, the µC communicates a 16-Bit value to the digital-to-analog converter (DAC) via the I^2C communication bus. The DAC output signal is buffered and conditioned before reaching the counter electrode terminal (CE_t). The resulting current (in order to overcome cell resistance relative to the RE) is combined with reduction current to complete the biofilm oxidation reaction. From the working electrode terminal (WE_t), the current flow is measured by the TIA and conditioning circuit, while the biofilm oxidation current is fed back through the potentiostat to the CE_t circuit (Section 3.3.1). An analogue-to-digital converter (ADC) after the TIA circuit converts the signal to an integer value which is communicated back via the I^2C bus to the µC for processing. The RE connects to the reference electrode terminal (RE_t) of the feedback circuit and can either be shorted to potentiostat common ground or combined with the differential input to the CE_t in-amp. Values are stored on an SD card by the µC for later retrieval. The design also incorporates a common data bus running RS485 (Modbus) and a parallel power bus enabling multiple potentiostats to be daisy-chained. Data is transferred from the Modbus master to a computer via Serial-USB.

An ATMEL328P – Arduino Pro-Mini was selected as the µC for simplicity, cost, and availability. Programming of the µC was performed using the Arduino integrated development environment (IDE) using C/C++ coding language. For simplicity, the

Arduino IDE consists of a large open-source library for connection to peripheral devices and communication protocols. By utilising the Arduino IDE, the µC program can easily be modified depending on requirements and data storage. The µC can be purchased for around 10 USD and is supplied through most electronic and online stores, making the µC cost-effective and available to everyone. Incorporated into the design is the AD8429 in-amp for current sensing in a TIA configuration. To control the CE_t positive and negative voltages, the MAX5541 DAC is used. Both the ADC and the DAC are 16-Bit precision. All buffering operational amplifiers (op-amps) are of type MC33178.

3.2.2 Device simulation

Before assembly of the circuit, the design of the potentiostat was first simulated in LTspice XVII to determine circuit response and evaluate component values (Figure 1). The circuit analysis was simulated on an ideal cell (Figure 1, R1), the DAC was substituted with an ideal voltage source (variable DC supply), and all other components set as designed. Output of the simulation designated "ADC" connected to the input of the ADC circuit. A voltage sweep of ±2.5 V (10 mV steps) was performed across resistor R1 (Figure 1) was performed and the response values were recorded. This simulated circuit was evaluated to ensure the potentiostats fundamental operation was as expected and correct before the addition of other components, such as an ADC and power regulators.

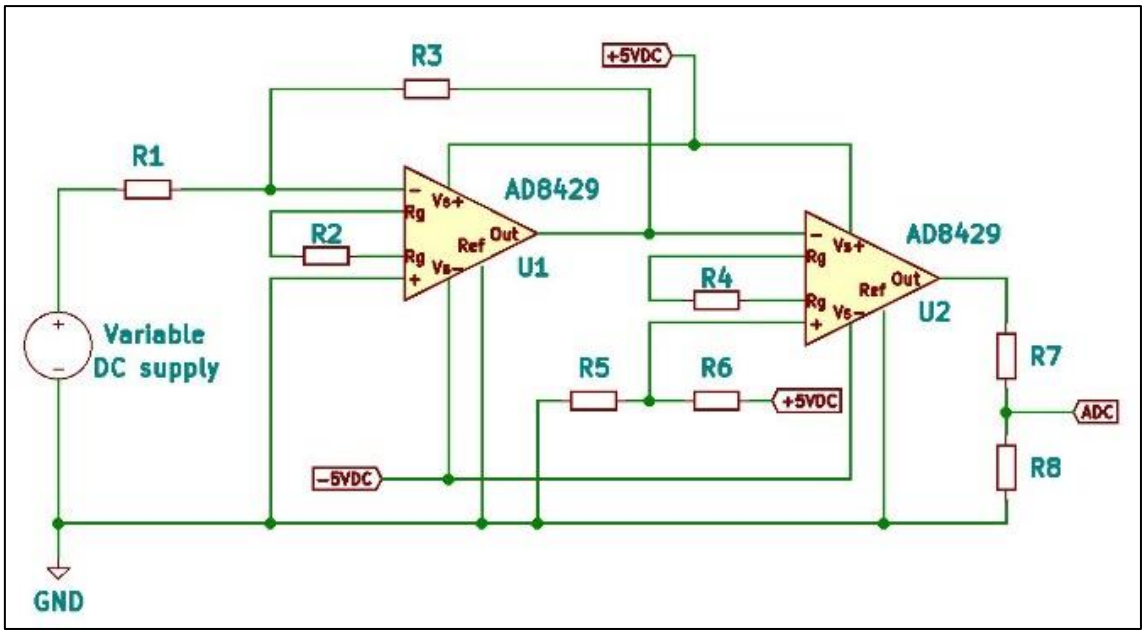

Figure 1 Simplified circuit for simulation showing incorporated TIA current sensing, where: U1 & U2 are in-amps; R1 – R8 are resistors; U1 & R3 form the TIA circuit; R2 & R4 are gain selecting resistors; U2 and supporting connections are used for conditioning the electrical signals.

The simulated circuit (Figure 1) has the electrolytic cell (as in an MESe application) represented by a fixed resistor (R1), noting that a real electrochemical cell would have additional complex resistance and capacitance (Kashyap et al., 2014; Trouillon & O'Hare, 2010). For simplicity, the simulation represented an ideal cell of fixed resistance which is later used for comparison with the physical potentiostat (Section 3.2.4).

3.2.3 Device evaluation

To evaluate the potentiostat design, the complete circuit was produced (Appendix A, Figure A1) on a printed circuit board and populated with components. In total, six potentiostats were assembled, and each test performed in triplicate. A 100 ±1% Ω, 0.25 W resistor was placed across the CE_t and WE_t (RE_t shorted to circuit ground). Firmware was uploaded to the µC to perform a voltage sweep at the resistor between the CE_t and WE_t. For this, the output values of the DAC were swept from 0 to 65,000 in increments of 1,000. The respective CE_t, WE_t, and TIA output values were recorded with a multimeter (Digitech QM1549), and the voltage was compared with the corresponding DAC value and ADC value (ADC_v) recorded on the SD card.

3.2.4 MESe verification

To further evaluate the response of the potentiostat in an application, it was connected to an MESe. Sodium Acetate (NaAc; 20 mM) was added and used as the sole carbon source in the tests. Initially, the cells were dosed with 10 mM NaAc but unfortunately, no measurable response was observed from the sensor. The NaAc concentration was increased to 20 mM (approximately 1,640 mg L^{-1}) and the cells were cleaned, fresh inoculum and media added, and the measurement restarted. Biofilms can tolerate high acetate concentrations (Schievano et al., 2018), so the concentration of 20 mM was selected, and this produced a biofilm and a current signal.

The cell was comprised of a 100 mL Schott bottle with a custom 3D-printed cap of acrylonitrile-butadiene-styrene (ABS) to hold 3 electrodes and to create a gas-tight seal, thereby maintaining anaerobic conditions. The cap design incorporated rubber o-rings to seal the cap on the bottle and around the electrodes protruding through the cap. The distance between the electrode holes (WE and CE) was 20 mm (center to center). The RE location was offset from the CE by 15 mm, and the WE by 11 mm (Appendix A, Figure A2). A small safety vent (2 mm diameter) was also placed in the cap as a safety measure for any gas overpressure and sealed with silicone grease. Once assembled the

cell was checked for water tightness by inserting all electrodes and seals, filling the bottle with water, and securing the cap. For this, the assembled cell setup was inverted and placed in a glass beaker and routinely checked for any droplets forming over 24 hours.

The RE consisted of a silver/silver chloride (Ag/AgCl) wire immersed in Potassium Chloride (3 M KCl) saturated with AgCl (Sigma-Aldrich 60137) and was housed in a glass tube with a CoralPor membrane (BASi MF-2042, USA). The constructed RE was calibrated against a standard Ag/AgCl electrode (BASi MF-2056, USA) to within ±10 mV.

The CE and the WE were both made from graphite rods (Morgan Advanced Materials), each with a diameter of 6.35 mm (1/4 ”) and were cut to 120 mm in length. Graphite electrodes were prepared by firstly rinsing with acetone and subsequently sanding with 1,200 grit sandpaper to produce a smooth uniform surface. The electrodes were then rinsed with deionised water (MilliQ), then acetone, and then dried with lint-free wipes to remove any loose debris from the electrode surface.

Three cells were constructed as above and were inoculated with anaerobic digester sludge sourced from a domestic wastewater treatment plant previously described by Kazadi Mbamba et al. (2016). The inoculum to media ratio and chronoamperometric settings are as previously described by Gimkiewicz and Harnisch (2013). After the initial inoculation period of 8 days, the buffer and NaAc mixture was exchanged every 4 days. After establishing sufficient current flow, the current values were measured for each feeding cycle (4 cycles). Testing was performed in an environmental chamber (CM Envirosystems, PAC-120-AH) maintained at 37 ± 0.5°C.

3.2.5 Data analysis and statistical methods

Descriptive statistics were calculated using the Microsoft Excel 365 (2021) Add-in Analysis ToolPak to determine the sample mean, standard deviation, and standard error of the mean (SEM). Linear regression analysis of each potentiostat’s ADC_v against TIA voltage, and CE_t voltage against DAC value were also performed in Microsoft Excel.

3.3 Theory

Microbial respiration is used by MESe to liberate electrons in an electrocatalytic oxidative process that produces electrons which are measured in the form of current or voltage (Okamoto et al., 2014). The current generated represents the oxidation of the electron donor (here being acetate) due to biofilm respiration. In the case of acetate respiration,

eight electrons are liberated per molecule of acetate oxidised (Eq. 1). According to Korth and Harnisch (2019), an acetate-derived electroactive biofilm used in an MESe is most thermodynamically efficient at 0.2 V. This will impact the desired design range of a potentiostat and can influence the type of RE to be used.

$$CH_3COO^- + 4H_2O \rightarrow 2HCO_3^- + 9H^+ + 8e^- \qquad (1)$$

3.3.1 Device circuit topology

This specific design topology (Figure 2) incorporates a TIA for current measurement, a RE circuit to allow automatic potential control, and a µC to allow for custom programming. Supporting components would also include operational amplifiers, an analog-to-digital converter, a digital-to-analog converter, data storage, and a communication network.

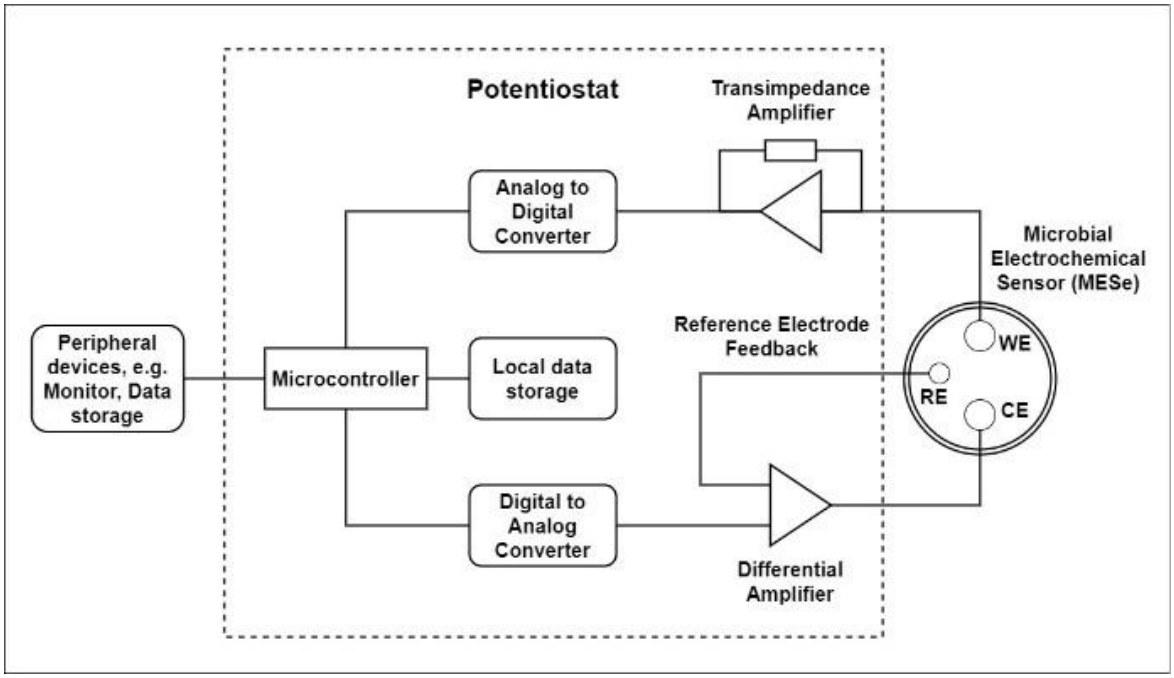

Figure 2 Potentiostat operational flow with lumped elements.

3.3.2 Component selection

For an MESe to operate in the field it would require integration into existing wastewater management infrastructure (e.g., an anaerobic digester) and would be exposed to harsh environments (e.g., corrosive gases, prolonged sun exposure, elevated ambient temperatures, electromagnetic noise, and humidity). Subsequently, the electronics used to operate the MESe could be exposed to similar harsh conditions and therefore, component selection needs to be robust and resilient to these conditions.

Electronic components are often sub-categorised depending on rated temperature range and class, which influences cost, availability, and applications. The components used in the current potentiostat design have been selected to provide a suitable range of operational environmental conditions, including temperature tolerance, noise immunity, appropriate resolution, and potential range. While the focus of this design is to be relatively low-cost wherever possible, it should be noted that there is often a trade-off between cost and performance.

3.3.3 Stability

The capacitance and resistance of an MESe measuring VFA would be variable, due to cell configuration and media changes. The capacitance and resistance of an MESe can be modelled using an equivalent circuit named the Randles circuit, which represents the combination of resistance due to the electrolyte (e.g. anaerobic digester liquid phase), charge/mass transfer resistance, double-layer capacitance, and Warberg diffusion (Chen, Patil, Brown, & Schröder, 2019; Kashyap et al., 2014; Trouillon & O'Hare, 2010), although in real-world applications these parameters constantly change in magnitude. Input capacitance is known to adversely affect the stability of in-amps and op-amps depending on magnitude (Texas Instruments, 2000). Capacitance and resistance are difficult to accurately and reliably determine in an application and negatively impact measurements if not properly compensated (e.g., RE) and if component selection is not appropriate.

3.3.4 Device operation

The potentiostat should be capable of meeting and/or exceeding the operational electrochemical potential to compensate for experimental conditions, such as cell geometry, electrode material, media conductivity, double-layer capacitance, and membrane diffusion resistance. To operate an MESe at the most thermodynamically efficient potential for VFA respiration/measurement, a minimum of ±0.2 V at the biofilm surface has been recommended (Korth & Harnisch, 2019), although additional range will be required to overcome cell resistance and capacitance. For example, a DAC (used to control the output potential) can require a reference voltage to function (in this case V_{ref} = 2.5 V), which limits the output range. The output from the DAC can be amplified to higher voltages but this will introduce additional unwanted noise and capacitance for each extra stage of the circuit, therefore it is best practice to use as little amplification as

possible for the application. Consequently, for a common 5 V circuit and for one stage of amplification the output potential would be ±2.5 V giving a differential range of 5 V. This would exceed the MESe recommended potential by more than 10 times, while enabling a broad range of applications.

Additionally, the current through an electrolytic cell and potentiostat needs to be sufficient to drive the reaction in Eq. 1, which is limited by the in-amps output and the TIA resistor selection. Current flow through the TIA resistor (Figure 1) is used to determine the relationship between the input potential, electrochemical cell resistance, and biofilm current, while the in-amp sets the maximum current.

The output measured at the point designated "ADC" in Figure 1, represents the signal into the ADC circuit. The ADC converts the signal to an integer that represents the current flow through the cell (Eq. 2). Current through a resistor representing the electrochemical cell (I_{cell}) can be represented using the output signal of the TIA in-amp and the virtual ground of the TIA circuit as follows (Eq. 2):

$$I_{cell} = -\left(2V_{out} - V_{off}\right)/R_{TIA} \qquad (2)$$

where V_{off} is the voltage generated from the voltage divider resistors R5 & R6 (Figure 1), V_{out} is the voltage to the ADC after the voltage divider R7 & R8 (Figure 1), and R_{TIA} is R3 (Figure 1).

3.4 Results and discussion

Affordability is a key consideration in the design of a proposed potentiostat for future MESe applications, including monitoring VFA in anaerobic digesters. The potentiostat reported in this work had a minimal estimated component cost of approximately 75 USD, which included peripherals added to facilitate data collection. Local data storage in the form of an SD card and reader was added, as well as RS485 communication for external data storage. Power supply was not included in the potentiostat cost, the aim being to provide installation flexibility by allowing power to be provided from any low-noise low voltage source (e.g. battery, USB, solar, etc). The cost of the unit compares well with other low-cost units (Dryden & Wheeler, 2015; Glasscott et al., 2019; Irving, Cecil, & Yates, 2021), but cost is highly dependent on potentiostat parameters such as range, resolution, or functionality. The potentiostat uses industrial communication standards (MODBUS RS485), data storage redundancy, and narrowed potentiostat parameters to

be more application-specific and aimed to facilitate the use of MESe in monitoring of anaerobic digesters for biogas energy production.

3.4.1 Circuit simulation

As expected, the voltage sweep produced a near-perfect linear response ($R^2 \approx 1.00$) (Appendix A, Figure A3). Over the applied voltage range, the simulated circuit voltages were mainly within the design specifications. However, the simulation showed the output to the ADC tended to deviate from the linear relationship at 2.25 V and at -2.25 V. These deviations indicated a possible limit of operation for the proposed design, which was then explored during testing on the fully assembled potentiostat. Simulation confirmed the circuit functionality and that the voltage output from the TIA op-amp behaved as predicted when the voltage applied remained between ±2.25 V. Commercially available potentiostats may substantially exceed this operational range, which can provide additional development scope. Although, MESe applications will often only require a potential of several hundred millivolts and are quite often operated between ±1 V (Guo et al., 2019; Jing, Liu, Deng, Chen, & Zhou, 2019; Jörg Kretzschmar et al., 2018), and higher voltages (e.g. ±10 V) may not necessarily be required for MESe. Overall, the simulation suggested predictable and sufficiently accurate behaviour for the potentiostat design.

3.4.2 Pseudo-cell testing

In order to determine the accuracy and linearity of the potentiostat, a voltage sweep across the resistor between CE_t and WE_t was performed (Figure 3). As expected, the recorded CE_t voltages showed a near-exact linear relationship against the DAC input value ($R^2 \approx 1.00$). Consequently, the output from the DAC was predictable and accurate across all six replicate potentiostats. Further analysis showed the standard error of the mean across all samples varied between 0.05 and 0.69 % and increased somewhat asymptotically towards a CE_t of zero volts. The asymptote appears to correspond with a DAC value of 32,767, where the circuit shaping split the CE_t output range between ±2.5 V.

The SEM reached a maximum of 0.69 % at 17.5 mV, corresponding to an absolute error of only 0.12 mV, the magnitude of which would be quite tolerable for MESe applications. However, it is possible that the error continued to grow in magnitude as the CE_t voltage approached zero; however, this was not investigated as the accuracy of the potentiostat

was deemed to be more than sufficient for the intended MESe application (e.g., AD monitoring).

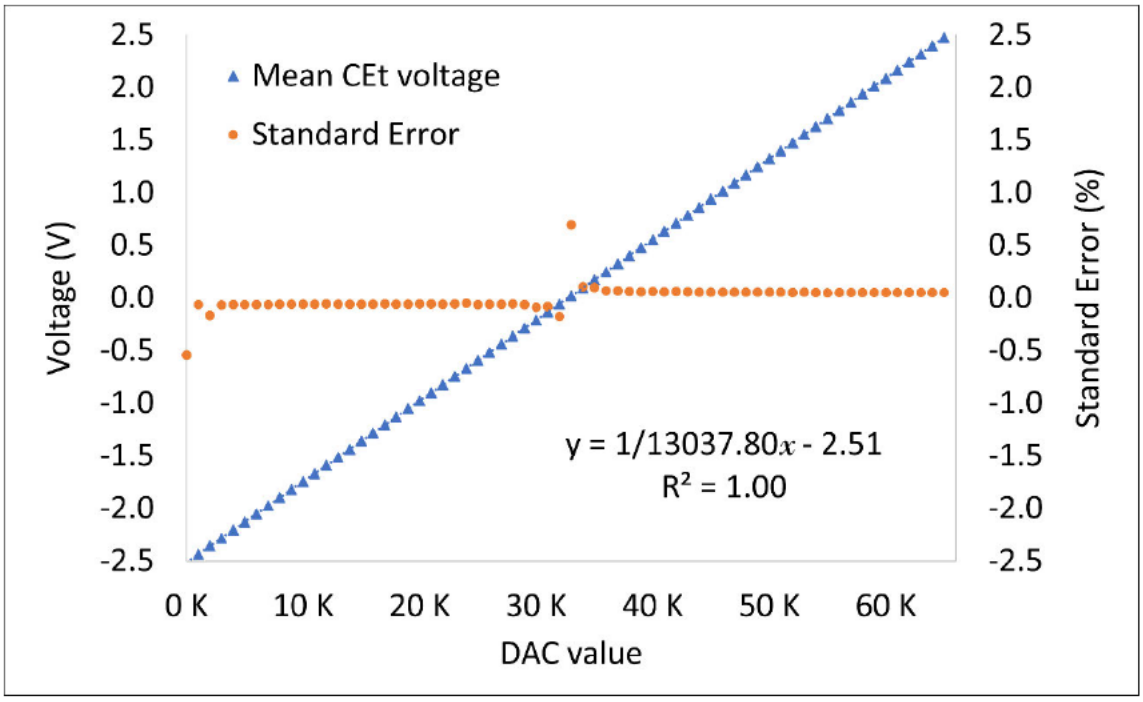

Figure 3 Defined 16-Bit DAC value with measured response CE_t voltage (▲) across all 6 potentiostats. Standard error of the mean (●) shows change around 16 bit DAC zero point (32767).

To further evaluate potentiostat performance and accuracy, the WE_t voltage and ADC_v recorded by the µC during the voltage sweep were investigated (Figure 4). Raw data of the ADC_v was analysed and the curve presented as a discontinuous line (Appendix A, Figure A4). The discontinuity was due to the electronic shaping performed by the input to the ADC circuit. Consequently, the ADC_v was modified (ADC_m) by subtracting 65,535 from any value over 32,767, allowing for regression analysis and plotting of a continuous curve (Figure 4). The modified integer value could be expressed as ±32,767 to represent the ADC_v (16-Bit). A linear regression fit to the mean ADC_m (Figure 4) provided a statistically good fit ($R^2 \approx 1.00$), with the SEM between 0.00 and 1.58 %. The SEM reached a maximum of 1.58 % at a WE_t voltage of 48 mV, and an approximate zero SEM was approached towards +2.1 V and -2.1 V. The SEM again showed asymptotic tendencies towards zero applied voltage, similar to the CE_t data. This could have been a cumulative error from the CE_t, albeit that SEM for ADC_m remained consistent with decreasing ADC_m values, creating a relative increase. This should result in a linear increase in error while the curve presents as logarithmic. In comparison, the CE_t error asymptote in Figure 3 appears to be from variance between the values. Unfortunately, the cause of this change in error for both cases was unclear.

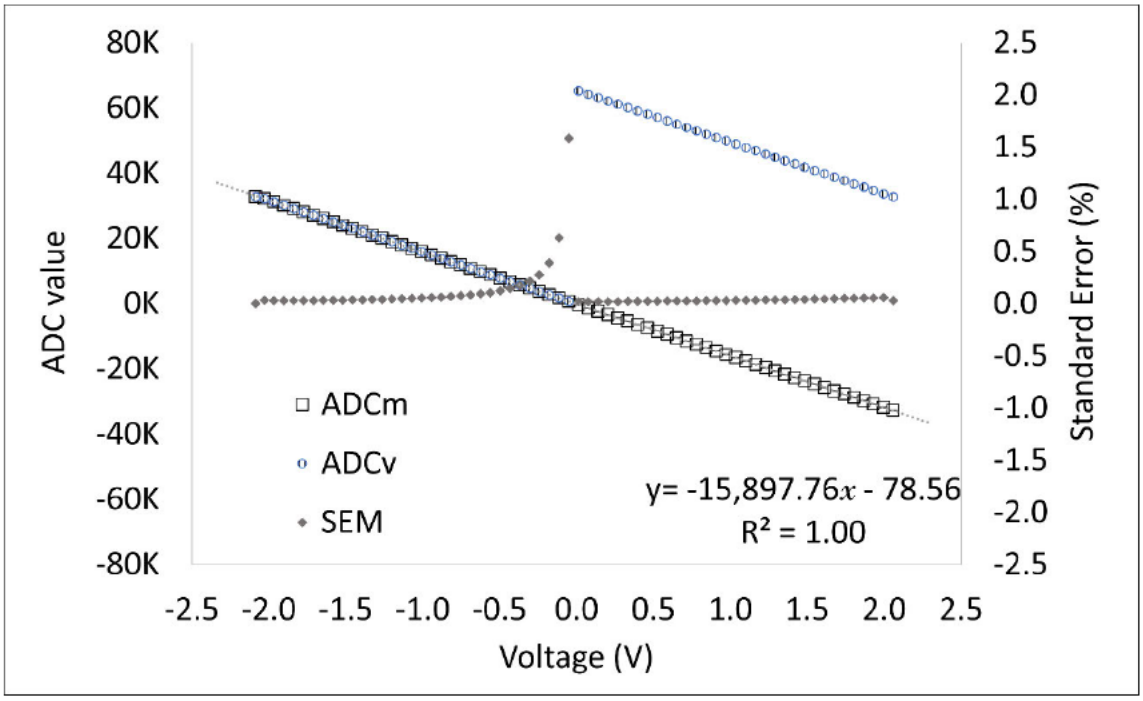

Figure 4 ADC_v in response to WE_t voltage measured across 6 replicate potentiostats. The mean value is presented for both the raw ADC_v (○) and the ADC_m (□), together with standard error of the mean (◆).

To present the distribution of the values, the standard deviation (std. dev.) was graphed in Figure 4, although, the values were visually indistinguishable from the data points. The relative std. dev. values ranged from 34.7 to 84.9 at an ADC_m (±32,767) of 22,037 and -31,810 respectively. The highest std. dev. occurred close to the maximum WE_t voltage. In contrast, the highest relative std. dev. corresponds with values approaching the zero applied voltage of the potentiostat (also reflected in the SEM), with std. dev. of 6.7 % at an ADC_m of 698. The potentiostat was unable to produce WE_t voltages above 2.1 V or below -2.1 V, although the op-amp supply rails were ±5 V. However, the recorded values enabled the potentiostat to measure a range of ±2.0 mA which was within the design specifications for an MESe application.

High resolution of the potentiostat is crucial to have confidence in the values being reported. The designed current resolution was calculated based on the range of the 16-Bit ADC and voltage range (5 V), resulting in a resolution of 76 nA. By using Ohm's law in combination with the linear regression fit of the data in Figure 4, a relationship with the resistor current was formulated. Potentiostat resolution was better than expected, with an accuracy of 63 nA, corresponding to the maximum range produced from the assembled potentiostat (4.2 V). This enables a user to have a degree of certainty in the values being reported, especially when measuring very small signals, such as are typical of MESe.

Via the pseudo-cell (resistor), the potentiostat demonstrated appropriate accuracy across a range of relevant and tested voltages. As expected, the potentiostat also showed strong linearity in the measured values. Accordingly, the potentiostat design was deemed appropriate to provide adequate control of the cell potential as well as give accurate measurements of current for an MESe application.

3.4.3 Laboratory test with a microbial electrochemical sensor (MESe)

An MESe was assembled as described in Section 3.2.4. The output from the potentiostat (Figure 5) showed typical biofilm growth behaviour, with an initial lag phase with near-zero current generation typical of biofilm establishment, followed by a logarithmic/exponential increase in the current flow, followed by a stationary phase. The MESe (biofilm) started producing current after approximately 220 hours. Establishment of the primary biofilm was visually confirmed as a reddish-brownish tint (Figure 6) that formed on the anode, appearing similar to what is reported in the literature for *Geobacter spp*. biofilms (Ueki et al., 2018; Yadav & Patil, 2020); and which was reflected in the current generation observed with NaAc addition. In subsequent cycles of NaAc addition, the cell demonstrated a typical current curve with the initial peak in current (due to addition of NaAc) was followed by a stable current output, and finally, substrate-limited decline in current generation (Figure 5). Between days 10 and day 25, peak values were recorded between 0.080 - 0.093 mA cm^{-2} and the mean current output was 0.068 mA cm^{-2}. Although, these values are somewhat lower than other values reported in the literature (Jörg Kretzschmar et al., 2018); this could have been due to non-sterile conditions, which possibly promoting bacterial growth in the electrolyte consuming NaAc in the bulk liquid phase rather than by biofilm at the electrode (Figure 6). This highlights the need for a high resolution and accurate potentiostat under such conditions, as measured currents may be relatively small. The potentiostat provided a high-resolution measurement of current fluctuations that were produced from the MESe biofilm with reproducible peaks in current being measured. Furthermore, the measured values were comparable with what is observed with other potentiostats measuring NaAc respiration at a fixed applied potential (Jin, Li, Zhao, Angelidaki, & Zhang, 2017).

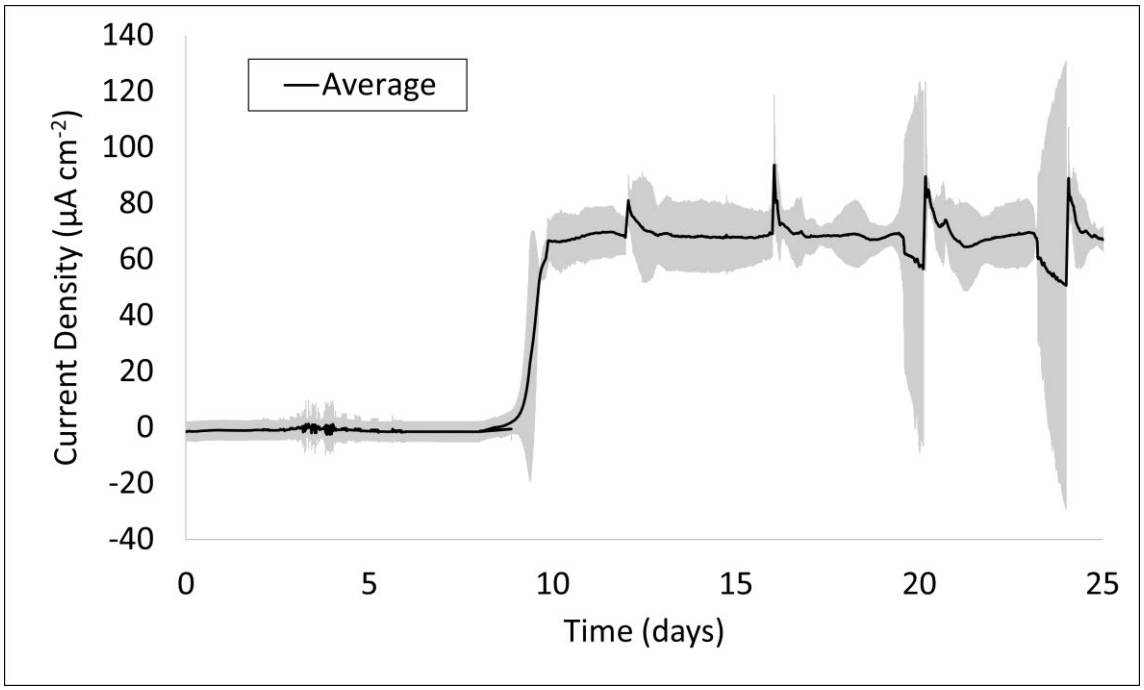

Figure 5 Average signal output from biofilms (n=3) over 25 days (600 hours). Grey shaded area represents the standard deviation in replicate measurements.

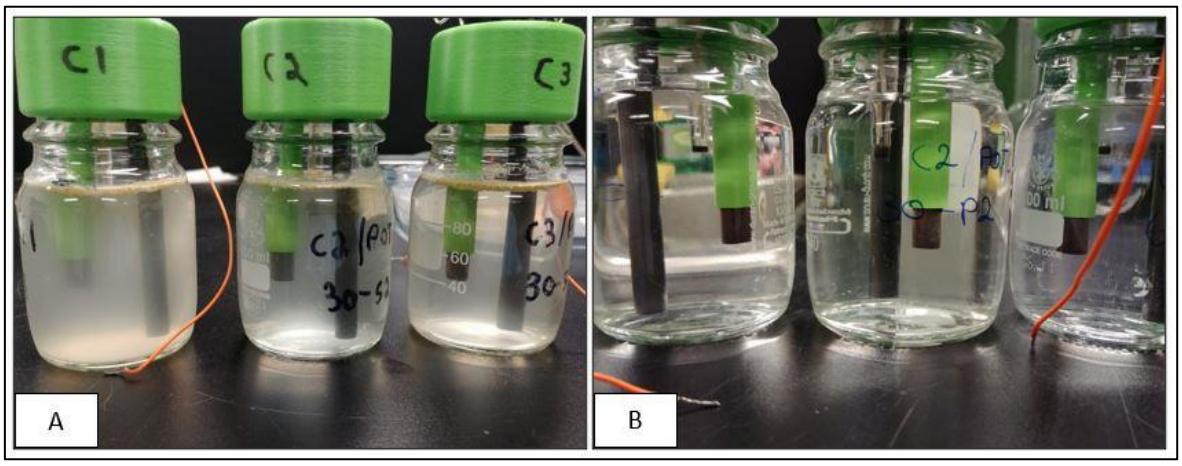

Figure 6 Electrolytic Cells; (A) before and (B) after media exchange

The current measurement of this potentiostat was lower than single chambered cells reported in the literature. For example, J. Kretzschmar, Koch, Liebetrau, Mertig, and Harnisch (2017) investigated MESe for sodium acetate measurement, and their sensor produced 0.569 ±0.013 mA cm^{-2} which is much higher in the current study; although, the authors do identify the sensor response being highly dependent on prior acetate exposure (J. Kretzschmar et al., 2017).

Moreover, the current study investigated a primary biofilm, which is known to produce lower current densities than secondary biofilms (Baudler, Riedl, & Schroder, 2014; Y. Liu, Harnisch, Fricke, Sietmann, & Schroder, 2008). The cell output in the current study

was comparable to what has been observed in microbial electrochemical cells with a membrane (Jiang et al., 2019; G. Q. Zhang et al., 2019). A novel submersible sensor reportedly measured approximately 0.025 to 0.075 mA (Jiang et al., 2019). While H. Sun, Zhang, et al. (2019) reported a microbial cell producing a maximum of 0.1 mA cm^{-2} and a similar current response to NaAc as observed in the current work. A comparable response was also reported from a microbial electrochemical cell using a fixed applied voltage, which reached between 0.1 – 0.15 mA cm^{-2} for a comparable NaAc concentration (Jin et al., 2017).

Overall, the potentiostat described here was able to measure the biofilm response due to NaAc addition, and although lower current densities were observed than previously reported, the potentiostat was functional, including for an MESe application. Further studies using this potentiostat design and other NaAc concentrations, could provide an additional data for comparison with the available literature.

3.5 Conclusion

Volatile fatty acids are a known indicator of AD stability. Previous MESe output signals demonstrated a correlation with VFA concentration and thus potential to be used applied to monitor AD. However, simple surrogate methods to a potentiostat, such as an external resistor to measure the current from an MESe was considered inadequate because of expected impacts on microbial communities and behaviour. Accordingly, a potentiostat is likely required to control the cell potential for electrochemical applications in general, and also for stable cell environment and biofilm growth in MESe applications.

Currently, a relatively low-cost and accurate potentiostat is lacking and this was a key need to enable MESe applications for more timely measurement of VFA in AD.

A potentiostat design was presented and tested for use in electrochemical analysis, developed based on the key considerations of affordability, simplicity, and robust measurements. A simulated circuit evaluation confirmed that the initial circuit design behaved as expected. Once assembled, the potentiostat showed good linearity when using a pseudo-cell (resistor), and the observed operation was within the desired potentiostat performance specifications.

When connected to a microbial electrochemical cell for a practical evaluation of an MESe application, the potentiostat operated as expected and produced accurate results that were comparable to literature values in terms of peak currents for the substrate. The

microcontroller used in the design is programmable using C/C++ coding language, and thus allows flexibility to be customised for various applications.

Overall, it was concluded that the presented potentiostat design can be built and can provide accurate and precise measurements while being simple and affordable, as are especially important for prospective MESe applications. This would be important to improved response times for VFA measurements in AD. Future improvements of the design could attempt to increase current generation for measurement, as well as making the design robust for application in harsh environments.

3.6 References

Anshori, I., Mufiddin, G. F., Ramadhan, I. F., Ariasena, E., Harimurti, S., Yunkins, H., & Kurniawan, C. (2022). Design of smartphone-controlled low-cost potentiostat for cyclic voltammetry analysis based on ESP32 microcontroller. *Sensing and Bio-Sensing Research, 36*. doi:10.1016/j.sbsr.2022.100490

Atci, E., Babauta, J. T., Sultana, S. T., & Beyenal, H. (2016). Microbiosensor for the detection of acetate in electrode-respiring biofilms. *Biosens Bioelectron, 81*, 517-523. doi:10.1016/j.bios.2016.03.027

Baudler, A., Riedl, S., & Schroder, U. (2014). Long-term performance of primary and secondary electroactive biofilms using layered corrugated carbon electrodes. *Frontiers in Energy Research, 2*. doi:10.3389/fenrg.2014.00030

Boe, K., & Angelidaki, I. (2012). Pilot-scale application of an online VFA sensor for monitoring and control of a manure digester. *Water Sci Technol, 66*(11), 2496-2503. doi:10.2166/wst.2012.498

Chen, S., Patil, S. A., Brown, R. K., & Schröder, U. (2019). Strategies for optimizing the power output of microbial fuel cells: Transitioning from fundamental studies to practical implementation. *Applied Energy, 233-234*, 15-28. doi:10.1016/j.apenergy.2018.10.015

Cordova-Huaman, A. V., Jauja-Ccana, V. R., & La Rosa-Toro, A. (2021). Low-cost smartphone-controlled potentiostat based on Arduino for teaching electrochemistry fundamentals and applications. *Heliyon, 7*(2), e06259. doi:10.1016/j.heliyon.2021.e06259

Dryden, M. D., & Wheeler, A. R. (2015). DStat: A Versatile, Open-Source Potentiostat for Electroanalysis and Integration. *PLoS One, 10*(10), e0140349. doi:10.1371/journal.pone.0140349

Falk, H. M., Reichling, P., Andersen, C., & Benz, R. (2015). Online monitoring of concentration and dynamics of volatile fatty acids in anaerobic digestion processes with mid-infrared spectroscopy. *Bioprocess Biosyst Eng, 38*(2), 237-249. doi:10.1007/s00449-014-1263-9

Friedman, E. S., Rosenbaum, M. A., Lee, A. W., Lipson, D. A., Land, B. R., & Angenent, L. T. (2012). A cost-effective and field-ready potentiostat that poises subsurface electrodes to monitor bacterial respiration. *Biosens Bioelectron, 32*(1), 309-313. doi:10.1016/j.bios.2011.12.013

Gimkiewicz, C., & Harnisch, F. (2013). Waste water derived electroactive microbial biofilms: growth, maintenance, and basic characterization. *J Vis Exp*(82), 50800. doi:10.3791/50800

Glasscott, M. W., Verber, M. D., Hall, J. R., Pendergast, A. D., McKinney, C. J., & Dick, J. E. (2019). SweepStat: A build-it-yourself, two-electrode potentiostat for macroelectrode and ultramicroelectrode studies. *J Chem Educ, 97*(1), 265-270. doi:10.1021/acs.jchemed.9b00893

Guo, X. G., Jia, J. B., Dong, H., Wang, Q. Y., Xu, T., Fu, B. Y., . . . Zhang, X. Y. (2019). Hydrothermal synthesis of Fe-Mn bimetallic nanocatalysts as high-efficiency cathode catalysts for microbial fuel cells. *J Power Sources, 414*, 444-452. doi:10.1016/j.jpowsour.2019.01.024

Hassanein, A., Witarsa, F., Lansing, S., Qiu, L., & Liang, Y. (2020). Bio-electrochemical enhancement of hydrogen and methane production in a combined anaerobic digester (AD) and microbial electrolysis cell (MEC) from dairy manure. *Sustainability, 12*(20). doi:10.3390/su12208491

Hoilett, O. S., Walker, J. F., Balash, B. M., Jaras, N. J., Boppana, S., & Linnes, J. C. (2020). KickStat: A coin-sized potentiostat for high-resolution electrochemical analysis. *Sensors (Basel), 20*(8). doi:10.3390/s20082407

Irving, P., Cecil, R., & Yates, M. Z. (2021). MYSTAT: A compact potentiostat/galvanostat for general electrochemistry measurements. *Hardwarex, 9*. doi:10.1016/j.ohx.2020.e00163

Jiang, Y., Chu, N., & Zeng, R. J. (2019). Submersible probe type microbial electrochemical sensor for volatile fatty acids monitoring in the anaerobic digestion process. *J Clean Prod, 232*, 1371-1378. doi:10.1016/j.jclepro.2019.06.041

Jin, X., Li, X., Zhao, N., Angelidaki, I., & Zhang, Y. (2017). Bio-electrolytic sensor for rapid monitoring of volatile fatty acids in anaerobic digestion process. *Water Res, 111*, 74-80. doi:10.1016/j.watres.2016.12.045

Jing, X., Liu, X., Deng, C., Chen, S., & Zhou, S. (2019). Chemical signals stimulate Geobacter soli biofilm formation and electroactivity. *Biosens Bioelectron, 127*, 1-9. doi:10.1016/j.bios.2018.11.051

Kashyap, D., Dwivedi, P. K., Pandey, J. K., Kim, Y. H., Kim, G. M., Sharma, A., & Goel, S. (2014). Application of electrochemical impedance spectroscopy in bio-fuel cell characterization: A review. *Int J Hydrogen Energ, 39*(35), 20159-20170. doi:10.1016/j.ijhydene.2014.10.003

Kazadi Mbamba, C., Flores-Alsina, X., John Batstone, D., & Tait, S. (2016). Validation of a plant-wide phosphorus modelling approach with minerals precipitation in a full-scale WWTP. *Water Res, 100*, 169-183. doi:10.1016/j.watres.2016.05.003

Kim, J. R., Min, B., & Logan, B. E. (2005). Evaluation of procedures to acclimate a microbial fuel cell for electricity production. *Appl Microbiol Biotechnol, 68*(1), 23-30. doi:10.1007/s00253-004-1845-6

Korth, B., & Harnisch, F. (2019). Spotlight on the energy harvest of electroactive microorganisms: The impact of the applied anode potential. *Front Microbiol, 10*, 1352. doi:10.3389/fmicb.2019.01352

Kretzschmar, J., Böhme, P., Liebetrau, J., Mertig, M., & Harnisch, F. (2018). Microbial electrochemical sensors for anaerobic digestion process control - Performance of electroactive biofilms under real conditions. *Chem Eng Technol, 41*(4), 687-695. doi:10.1002/ceat.201700539

Kretzschmar, J., Koch, C., Liebetrau, J., Mertig, M., & Harnisch, F. (2017). Electroactive biofilms as sensor for volatile fatty acids: Cross sensitivity, response dynamics, latency and stability. *Sensors and Actuators B-Chemical, 241*, 466-472. doi:10.1016/j.snb.2016.10.097

Li, Y. C., Melenbrink, E. L., Cordonier, G. J., Boggs, C., Khan, A., Isaac, M. K., . . . Mallouk, T. E. (2018). An easily fabricated low-cost potentiostat coupled with user-friendly software for introducing students to electrochemical reactions and electroanalytical techniques. *Journal of Chemical Education, 95*(9), 1658-1661. doi:10.1021/acs.jchemed.8b00340

Liu, Y., Harnisch, F., Fricke, K., Sietmann, R., & Schroder, U. (2008). Improvement of the anodic bioelectrocatalytic activity of mixed culture biofilms by a simple consecutive electrochemical selection procedure. *Biosens Bioelectron, 24*(4), 1012-1017. doi:10.1016/j.bios.2008.08.001

Logan, B. E., Rossi, R., Ragab, A. a., & Saikaly, P. E. (2019). *Electroactive microorganisms in bioelectrochemical systems* (1740-1526). Retrieved from

McCabe, B. K., Hamawand, I., Harris, P., Baillie, C., & Yusaf, T. (2014). A case study for biogas generation from covered anaerobic ponds treating abattoir wastewater: Investigation of pond performance and potential biogas production. *Applied Energy, 114*, 798-808. doi:10.1016/j.apenergy.2013.10.020

Meloni, G. N. (2016). Building a microcontroller based potentiostat: A inexpensive and versatile platform for teaching electrochemistry and instrumentation. *J Chem Educ, 93*(7), 1320-1322. doi:10.1021/acs.jchemed.5b00961

Okamoto, A., Saito, K., Inoue, K., Nealson, K. H., Hashimoto, K., & Nakamura, R. (2014). Uptake of self-secreted flavins as bound cofactors for extracellular electron transfer in Geobacter species. *Energy Environ. Sci., 7*(4), 1357-1361. doi:10.1039/c3ee43674h

Pasternak, G., Greenman, J., & Ieropoulos, I. (2018). Dynamic evolution of anodic biofilm when maturing under different external resistive loads in microbial fuel cells. Electrochemical perspective. *J Power Sources, 400*, 392-401. doi:10.1016/j.jpowsour.2018.08.031

Saratale, R. G., Saratale, G. D., Pugazhendhi, A., Zhen, G., Kumar, G., Kadier, A., & Sivagurunathan, P. (2017). Microbiome involved in microbial electrochemical systems (MESs): A review. *Chemosph, 177*, 176-188. doi:10.1016/j.chemosphere.2017.02.143

Scarabotti, F., Rago, L., Buhler, K., & Harnisch, F. (2021). The electrode potential determines the yield coefficients of early-stage Geobacter sulfurreducens biofilm anodes. *Bioelectrochemistry, 140*, 107752. doi:10.1016/j.bioelechem.2021.107752

Schievano, A., Colombo, A., Cossettini, A., Goglio, A., D'Ardes, V., Trasatti, S., & Cristiani, P. (2018). Single-chamber microbial fuel cells as on-line shock-sensors for volatile fatty acids in anaerobic digesters. *Waste Manag, 71*, 785-791. doi:10.1016/j.wasman.2017.06.012

Schmidt, T., McCabe, B. K., Harris, P. W., & Lee, S. (2018). Effect of trace element addition and increasing organic loading rates on the anaerobic digestion of cattle slaughterhouse wastewater. *Bioresour Technol, 264*, 51-57. doi:10.1016/j.biortech.2018.05.050

Sun, H., Zhang, Y., Wu, S., Dong, R., & Angelidaki, I. (2019). Innovative operation of microbial fuel cell-based biosensor for selective monitoring of acetate during anaerobic digestion. *Sci Total Environ, 655*, 1439-1447. doi:10.1016/j.scitotenv.2018.11.336

Texas Instruments. (2000). *Effect of Parasitic Capacitance in Op Amp Circuits*. Retrieved from https://www.ti.com/lit/an/sloa013a/sloa013a.pdf

Tommasi, T., Salvador, G. P., & Quaglio, M. (2016). New insights in microbial fuel cells: novel solid phase anolyte. *Sci Rep, 6*, 29091. doi:10.1038/srep29091

Trouillon, R., & O'Hare, D. (2010). Comparison of glassy carbon and boron doped diamond electrodes: Resistance to biofouling. *Electrochimica Acta, 55*(22), 6586-6595. doi:10.1016/j.electacta.2010.06.016

Ueki, T., Nevin, K. P., Woodard, T. L., Aklujkar, M. A., Holmes, D. E., & Lovley, D. R. (2018). Construction of a Geobacter strain with exceptional growth on cathodes. *Front Microbiol, 9*, 1512. doi:10.3389/fmicb.2018.01512

Vilajeliu-Pons, A., Baneras, L., Puig, S., Molognoni, D., Vila-Rovira, A., Hernandez-Del Amo, E., . . . Colprim, J. (2016). External resistances applied to MFC affect core microbiome and swine manure treatment efficiencies. *PLoS One, 11*(10), e0164044. doi:10.1371/journal.pone.0164044

Yadav, S., & Patil, S. A. (2020). Microbial electroactive biofilms dominated by Geoalkalibacter spp. from a highly saline-alkaline environment. *NPJ Biofilms Microbiomes, 6*(1), 38. doi:10.1038/s41522-020-00147-7

Zhang, G. Q., Zhou, Y. F., & Yang, F. L. (2019). Hydrogen production from microbial fuel cells-ammonia electrolysis cell coupled system fed with landfill leachate using Mo2C/N-doped graphene nanocomposite as HER catalyst. *Electrochimica Acta, 299*, 672-681. doi:10.1016/j.electacta.2019.01.055

Zhang, X., Xia, X., Ivanov, I., Huang, X., & Logan, B. E. (2014). Enhanced activated carbon cathode performance for microbial fuel cell by blending carbon black. *Environ Sci Technol, 48*(3), 2075-2081. doi:10.1021/es405029y

CHAPTER 4: LONG-TERM BIOFILM GROWTH IN A MICROBIAL ELECTROCHEMICAL SENSOR AND THE EFFECT ON TRANSDUCED SIGNAL

This Chapter was written up as **Paper III** titled "Long-term biofilm growth in a microbial electrochemical sensor and the effect on transduced signal", to be submitted to the Journal of Environmental Chemical Engineering (IF 5.90).

Utilising the potentiostat developed in Chapter 3, this Chapter investigates the long-term growth of biofilms, as this would be important for reliable MESe applications. This paper addresses the knowledge gap from Chapter 2, which identified microbial electrochemical sensors (MESe) need to be capable of operating for extended periods and the implications this would have on transduced signal. Experiments evaluated performance in terms of current density, coulombic efficiency (CE_f) and substrate (acetate) utilization. For an MESe to be adopted it must have minimal maintenance requirements, and minimal signal drift, degradation, and variability over time.

Chapter 4 investigates long-term electroactive biofilm growth. Biofilms are at the interface of electrolyte and electrode in an electrochemical cell, which influences sensor operation. This Chapter investigates biofilm behaviour that would be undesirable for a sensor, such as signal drift, biofilm efficiency, and signal trends.

This is a highly active area of research, with studies into novel materials and construction methods. Although, there are still questions about reliability and accuracy of biofilm response long-term, and more importantly how researchers can control performance as the biofilm grows and responds to stimuli.

4.1 Introduction

Monitoring the AD of high-strength wastewater such as slaughterhouse wastewater can be problematic due to wastewater characteristics (Abdelfattah, Hossain, & Cheng, 2020; Bustillo-Lecompte & Mehrvar, 2015). The inconsistency of wastewater sources can introduce instability to the AD process (H. Sun, Ni, Angelidaki, Dong, & Wu, 2019). There is a need for improved monitoring options for AD processes to ensure their reliable performance is maintained (Mauky et al., 2017). Monitoring of AD stability can be achieved by measuring VFAs, which can provide earlier information on the AD process than pH or total alkalinity alone (Chapter 2). AD stability can be masked when using

other methods due to the slaughterhouse wastewater's high alkalinity (H. Sun, Ni, et al., 2019). Typically, VFA measurements are conducted in a laboratory, and analytical methods can be costly, some can take several hours, and most require manual sampling and sample processing of the digestate (Chapter 2). Among technologies being explored as an alternative to traditional methods are MESe, which may provide cost-effective online measurements of VFAs (Chapter 2).

However, unlike traditional physico-chemical sensing methods, microbial sensors rely on a signal generated through electroactive biofilm respiration. As a result, biofilm ageing effects are important for the development of robust MESe. There are several stages in the formation of a biofilm, including adsorption, adhesion, maturation, and ageing (Huang et al., 2019). During biofilm growth, recalcitrant layers form below actively growing and oxidizing outermost layers (Steidl, Lampa-Pastirk, & Reguera, 2016). The microorganisms closer to the bonded surface (in this case the electrode) are then isolated from nutrients and substrate, which can lead to cell death and shedding of the biofilm (Huang et al., 2019). As a biofilm matures, the thickness increases and this can subsequently affect electron transport (Renslow et al., 2013; D. Sun et al., 2016), charge production (Engel et al., 2019), and even electron transfer method (e.g., direct, mediated, nanowires) (Grobbler et al., 2018; Steidl et al., 2016). Biofilm ageing could have an impact on electrochemical cell power density to varied extents, even with identical conditions (Logan et al., 2019). This suggests that an ageing MESe may produce a varying response, and may become disproportionate to the analyte concentration, making future re-calibration more challenging and potentially less reliable.

While several MFC studies cover experimental periods from several weeks to several months, few studies have directly addressed long-term MESe response. This is particularly important as AD is a continual process that can operate for years and would require consistent and reliable monitoring over extended periods. Sensor operation in the field long-term (e.g., >6 months) would be a reasonable expectation, because replacing a sensor regularly would be both impractical and cost-prohibitive. However, biofilm development mechanisms are not well understood in the context of long-term MESe output (Jing et al., 2019; Scarabotti et al., 2021). For example, Engel et al. (2019) investigated the behaviour of a mixed biofilm in a bioelectrochemical system lasting 44 days and reported a mixed culture biofilm developing and changing depending on the growth period and substrate.

An MESe for sensing needs to have high correlation to the desired analyte and produce consistent, reproducible output over a long period (e.g., >12 months). B. H. Kim, Chang, Gil, Park, and Kim (2003) found good correlations between coulombs and biological oxygen demand (BOD) concentration in an MFC which had shown stable operation for 5 years. Over 4 months, Martin, Savadogo, Guiot, and Tartakovsky (2010) conducted a study into power density, pH, temperature, and substrate concentration effects and reported stable operation, but provided limited exploration into ageing effects. It is unclear how biofilm stability is identified and what effects are imposed due to biofilm ageing over extended periods (e.g., output magnitude, response time). MESe make use of electroactive biofilms to transduce analyte concentration through respiration, and as these biofilms are likely susceptible to ageing effects (Logan et al., 2019), the MESe output may also be affected by biofilm ageing.

The literature is varied regarding long-term biofilm characteristics, such as biofilm performance, feeding regimes, fluctuations in output, and the impact these might have on measurements. Biofilms are capable of acclimatising to changing conditions (Jing et al., 2019; Jörg Kretzschmar et al., 2018; Logan et al., 2019), and this can impact signal response. For an MESe to be an effective measurement device, the output must remain predictably stable (i.e., produce consistent response magnitude and response time). Laboratory investigations often rely on implied stability, but with an ageing biofilm, the measured current density is likely to be susceptible to change.

This study investigates, for the first time, the long-term growth and performance of biofilms within an MESe, to determine effects due to ageing. Current measurement and charge density are used to evaluate differences that arise due to temporal changes. Coulombic efficiency and substrate (acetate) utilisation are also tracked as additional key metrics of performance. Finally, limitations on cell charge production are identified and the impact these may have on the sensor output signal is discussed.

4.2 Materials and methods

4.2.1 Inoculum and media

To reduce duplication the inoculum, media, and carbon source are described in Section 3.2.4. The inoculum was filtered with a 150 µm sieve to remove large organic/inorganic material. All chemicals used were analytical reagent grade. Deionized water used in the experiment was from an Elix Essential 10 (MilliQ, Merck).

4.2.2 Microbial electrochemical cell

To reduce duplication the cell construction is described in Chapter 3, Section 3.2.4. The cap design (Appendix A, Figure A2) incorporated rubber o-rings to seal around electrodes and between the cap and bottle to maintain gastight anaerobic conditions. Current output from the cell was measured and timestamped with a potentiostat constructed in-house (Chapter 3).

A resistor (100 ±0.1% ohm) was soldered between the WE_t and the CE_t before the experiment to ensure the recorded values were within the expected values. A voltage sweep (±2.5 V) was performed using the potentiostat DAC (16 bit). During the sweep a multimeter (Digitech QM1549) was used to measure the voltage drop across the resistor. The results were compared to simulated and calculated values (Chapter 3), regression was performed on the resulting data ($r^2 = 0.99$) (Appendix C Figure C1) and the standard error of the mean in replicates found to be acceptable at < 1.0 %. Experimental conditions. The potentiostat was arranged in a 3-electrode configuration consisting of working, counter, and reference electrodes.

The cell was handled in an anaerobic chamber containing high purity nitrogen gas to exchange the media. The buffer was sparged with the same nitrogen gas for a minimum of 20 min at approximately 1 mL min^{-1} prior to use.

Experiments were performed in an environmental chamber (CM Envirosystems, PAC-120-AH) maintained at 37 ± 0.5°C. The working electrode (anode) potential was poised at 0.2 V vs Ag/AgCl (3 M KCL) for the duration of the experiment. The cells were operated in batch mode over 36 and 92 days for the short-term biofilms and long-term biofilms, respectively (See below).

4.2.3 Primary and secondary biofilm generation

Six primary biofilms were individually grown by combining 10 mL of inoculum and 90 mL of fresh media containing 20 mM sodium acetate (NaAc) into six separate 100 mL Schott bottles. The cell/inoculum mixture was placed in an environmental chamber and connected to a potentiostat. After 8 days with no additional input, the cells were disconnected from the potentiostat and removed from the environmental chamber, placed in the anaerobic chamber, the cap with electrodes removed and the electrodes rinsed with deionized water, making sure not to disturb the biofilm. After rinsing, the cap and

electrodes were secured on a clean bottle containing fresh media solution (100 mL) with 20 mM NaAc. This was repeated every 4 days until the biofilm was harvested.

The secondary biofilm production procedure was similar, for short-term (ST) and long-term (LT) biofilm groups (36-days, 92-days, respectively). For this, the primary biofilms were subjected to an 8-day period with no additional input before harvesting. The established primary biofilms were harvested in an anaerobic chamber, where the cap was removed, the electrodes rinsed with deionized water, and the biofilm scraped off the WE with a spatula. This biofilm sample was then placed in a 50 mL tube containing 20 mL of media without NaAc, and this was repeated for each cell in the anaerobic chamber. All samples of the biofilm from replicate cells were combined in the same sample tube. The tube was placed on a vortex mixer (Velp Scientifica, ZX3) for 2 min to disperse the biofilm. The electrodes were then thoroughly cleaned, and re-prepared as described above and re-assembled.

An aliquot of the dispersed primary biofilm sample (5 mL) was then added to each clean cell, and media solution containing 20 mM NaAc added to make the total volume up to 100 mL. This procedure was carried out in the anaerobic chamber. After this, the assembled cells were placed in the environmental chamber and reconnected to their respective potentiostats.

A reduced timeframe for establishment is typical for a secondary biofilm as well documented (Chapter 2)(Baudler et al., 2014), so a shorter establishment period was selected in the current work. Accordingly, after 4 days with no additional input (for biofilm establishment), the cell media of the secondary biofilms was exchanged every subsequent 4 days, and the signal output allowed to reach consistency.

4.2.4 Sodium acetate trial

To determine the stability of each cell, a sequence of NaAc concentrations (20, 50, 100, 150, and 200 mM) was added to each replicate cell at 4-day intervals. The timestamped current values were recorded over each interval and downloaded to a laptop for later analysis. After 4 days at the respective NaAc dose, each cell was disconnected and removed for cleaning and analysis. For this, fresh media (without NaAc) was added to each cell up to the total volume of 100 mL in the anaerobic chamber, the cell was moved into the environmental chamber and connected to the potentiostat and run for a 4-days

"rest period" between dosing to re-establish a cell baseline before changing to the next NaAc concentration. Data collection for the 200 mM dose was allowed to continue without intervention for an additional 8 days, up to a total operational time of 12 days (See below).

4.2.5 Offline titration & pH

Alkalinity and VFA concentration were measured by two-point titration based on the Nordmann method (Nordmann, 1977) with a TitraLab 1000 (Hach). For this, an aliquot of 5 mL was taken from a cell and added to 50 mL of deionized water. The NaAc concentration was then determined using 0.1 N H_2SO_4 with titration points at pH 5 and 4.3, with the results expressed in terms of equivalent CH_3COOH mg L^{-1} (acetic acid).

pH in the cell electrolytes was measured using a pH3110 meter (WTW). The mean pH of the replicate secondary biofilm groups was investigated for three media change cycles before NaAc was dosed and until the third media exchange after the NaAc trial.

4.2.6 Coulombic efficiency calculations

Coulombic efficiency (CE_f) was calculated using a formula described elsewhere (Gimkiewicz & Harnisch, 2013; H. Liu & Logan, 2004) (Eq. 2):

$$CE_f(\%) = \left({\int_0^t Iidt} \Big/ {Q_{th}} \right) \times 100 \qquad (2)$$

Where $\int_0^t idt$ is the integral of current over the period of measurement or actual charge produced (i.e. total charge); $Q_{th} = \Delta cVzF$, is the theoretically possible charge; $\Delta c = c_0 - c_1$ is the difference in the initial acetate concentration (c_0) the final acetate concentration (c_1) as measured by titration (and converted to molar equivalent); V is the volume of the medium; z is the number of electrons released per mole of substrate during the reaction (in this case 8); and F is Faraday's constant (F = 96,485.34 C/mol, electric charge of one mole of electrons).

4.2.7 Data analysis and statistical methods

All replicates were conducted independently. Statistics and regression were calculated using Microsoft Excel 365 (2021). Unless otherwise stated, ANOVA significance testing was performed at an alpha value of 0.05. The error values and error bars presented in figures below are calculated sample standard deviations (σ) for replicates.

For the purpose of this paper the definition of ‘stability’ is identified as the extent of reproducibility in the overall magnitude of a signal, or the total charge produced by replicate cells.

4.3 Results & discussion

4.3.1 Primary biofilm establishment and maturation

All cells with primary biofilms started producing charge within the initial 8-days period, and after the first media exchange were producing similar peak currents and total Coulombs. The short-term primary biofilms (ST_p) and the long-term primary biofilms (LT_p) started producing current at approximately the same time. Both primary biofilm groups continued similar stable current production throughout the initial 28-day period (Figure 7a), with no significant difference in current density between the ST_p and LT_p ($p = 0.26$) for the last feeding cycle. The biofilms were not significantly different in terms of charge production during the initial growth stage and presented consistent output with no unusual behaviour.

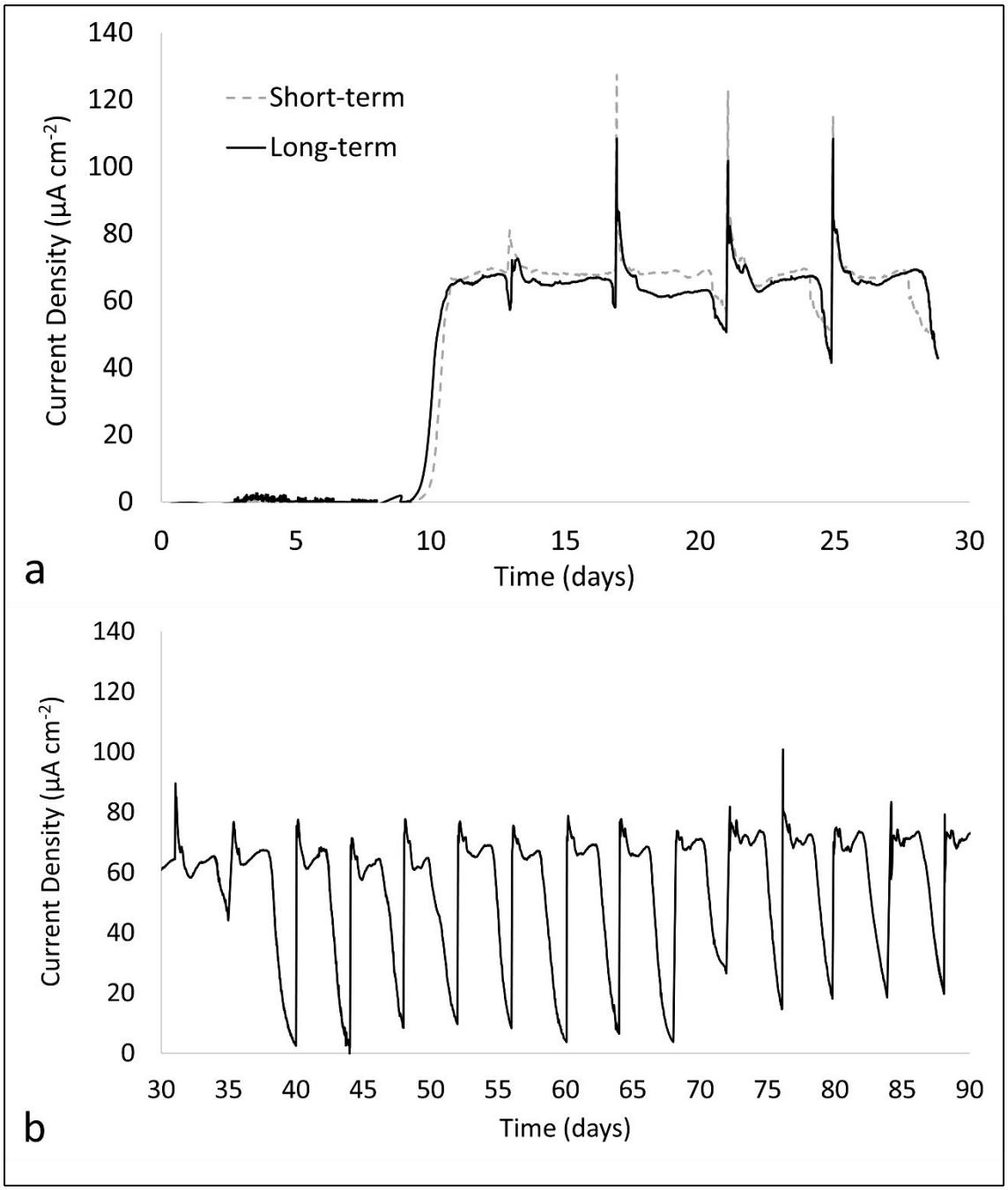

Figure 7 Mean current density produced by the short-term primary (ST_p) biofilms (n = 3) and long-term primary (LT_p) biofilms (n = 3) during the initial establishment and growth period (a); and current density for long-term primary biofilm (LT_p) operation showing consistent output[1](b)

A comparison was made between the last cycle of ST_p and LT_p before harvesting, to determine if there was any significant change in current production. In terms of stability, the replicate ST_p cells showed good repeatability in values before harvesting. The LT_p group continued to produce relatively stable results from day 30 onwards (Figure 10b)

[1] *LT_p (day 0-72 (n = 3), day 72-76 (n = 2), day 76-84 (n = 3), day 84-88 (n = 2), day 88-90 (n = 3)).*

until the biofilm was harvested and produced a similar total charge compared to the initial day 12 to day 28 period of operation. During its last media exchange cycle, the LT_p biofilm cells produced a slight but not significant ($p > 0.05$) reduction in output compared to day 28. This would suggest both primary biofilms were relatively stable.

4.3.2 Secondary biofilm behaviour before and after the NaAc dosing trial

Electrolyte pH can be used to indicate NaAc utilization. Accordingly, pH and alkalinity were used to investigate changes in the electrolyte for the short-term secondary biofilms (ST_s) and long-term secondary biofilms (LT_s) and compared with changes in charge production. For both ST_s and LT_s, the measured pH increased by approximately 5 - 6 %, and the mean carbonate alkalinity (g L^{-1} $CaCO_2$) increased by 18 %, as expected from NaAc utilization. After the NaAc trial, all cells performed similarly than prior to the trial. Specifically, increases in mean pH and alkalinity recorded post-trial showed an approximate 6 % and 18 % increase respectively for both groups (ST_s & LT_s). The mean total coulombs produced by the secondary biofilm groups during media exchange periods were also investigated before and after the NaAc trial (Figure 8). This was to also quantify any effect of the dosing trial on cell output and to assess whether the post-trial biofilms returned to their pre-trial behaviour in both the ST_s and LT_s biofilms. Pre-trial, the ST_s biofilms produced a mean charge density of 15.31 ± 2.89 C cm^{-2}, not significantly different from that of the LT_s biofilms at 17.71 ± 2.53 C cm^{-2}. The ST_s and LT_s biofilm post-trial produced a mean charge density of 15.47 ± 2.19 C cm^{-2} and 18.81 ± 2.50 C cm^{-2} respectively, which were also not statistically different between groups nor when compared to their respective pre-trial values. Both the pre- and post-trial data for both ST_s and LT_s biofilms presented as platykurtic (Kurtosis < 1), which indicates that both biofilm groups pre- and post-trial were less likely to produce outliers. This also suggests broad data peaks across the probability distribution, which indicates the values are a good representation of the population. These values show good stability pre- and post-trial. Specifically, the standard deviation shows similar values across all groups (Figure 8), which could indicate the variability in the biofilms did not change with age. Current density values for the 3 media exchanges preceding and the 3 media exchanges proceeding the NaAc trial are presented to show the biofilm stability (Figure 9). Importantly, the LT_s biofilms were still producing significant current when stopped (Figure 9b). This would suggest that if the period between media exchanges was increased, the LT_s biofilms would most likely produce higher total charge density

compared to the ST_s biofilm. As conditions and operation of the cells were maintained, any differences between the groups were likely rather due to temporal effects on the biofilm.

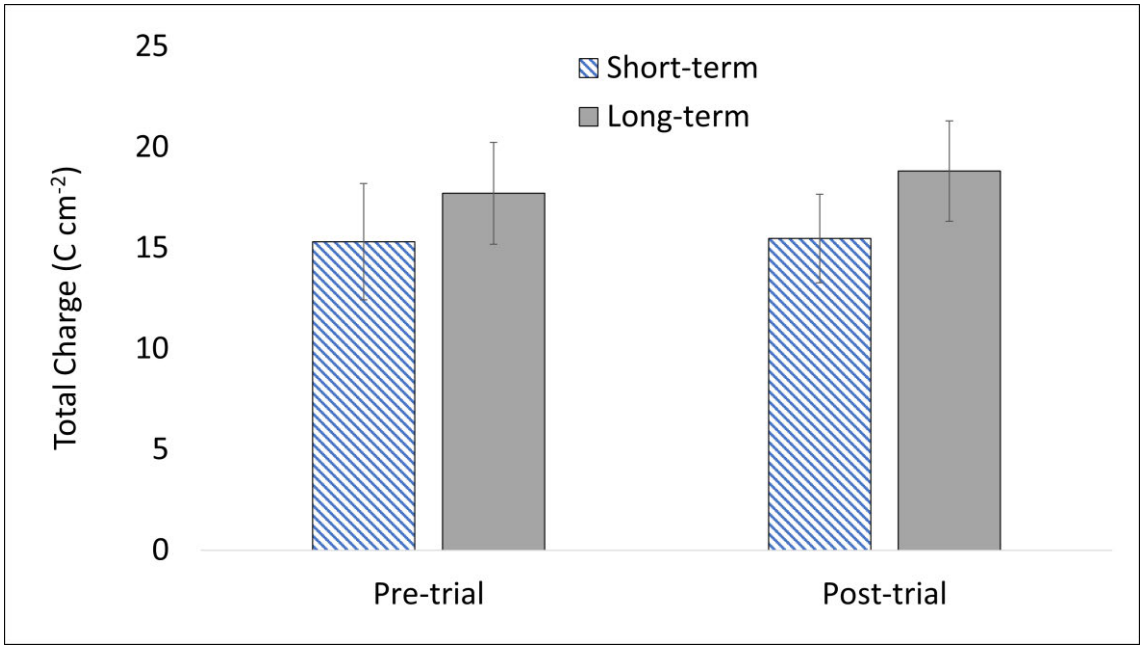

Figure 8 Pre- and post-trial mean total charge density produced by short-term[2] and long-term[3] secondary biofilms with standard deviation in replicates as error bars (σ)

[2] *ST_s (pre-trial day 0-8 (n = 2), day 8-12 (n = 3); post-trial day 0-12(n = 3)).*

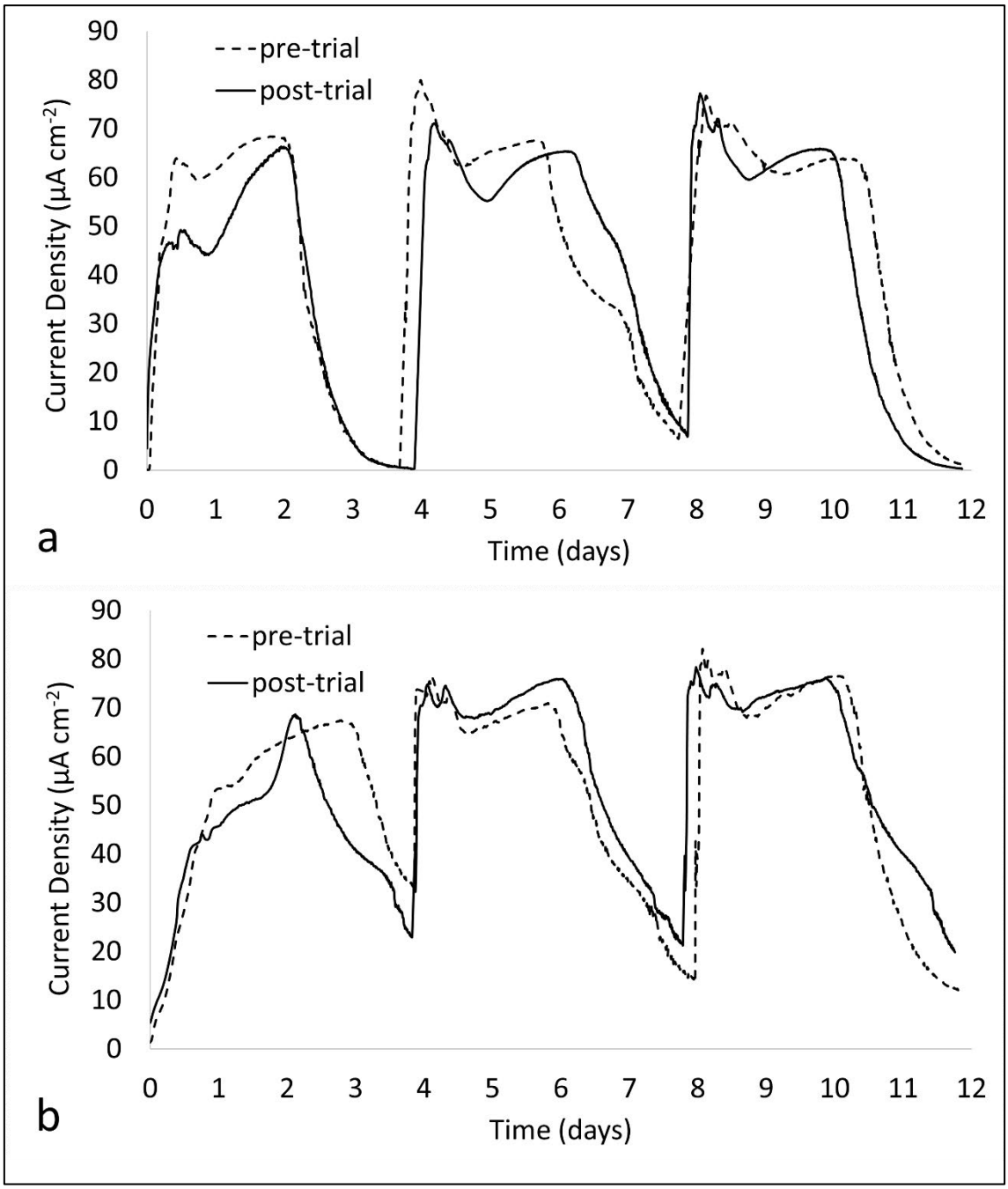

Figure 9 Data for the three media exchanges pre- and post-trial (mean) current response to 20 mM NaAc (a) Short-term secondary biofilm[2], (b) Long-term secondary biofilm[3].

4.4 Sodium acetate trials

Internal parameters, such as electrolyte, biofilm respiration, mass diffusion, etc in an MESe are charge-limiting steps that affect performance. To evaluate the cell performance, the NaAc utilization within the electrolyte was measured by titration and

[3] *LT_s (pre-trial day 0-8 (n = 3), day 8-12 (n = 2); post-trial day 0-12 (n = 3)).*

pH changes. During the NaAc trial, the ST_s biofilm showed a pH increase from 6 % to 18 % with an approximate positive linear trend (R^2 = 0.5) across the different acetate concentrations. The reason for the low R-value was the cell containing 150 mM NaAc experienced a smaller pH change compared to the 50, 100, and 200 mM. Without the lower response, the R^2 value is 0.97, which would indicate a linear response to increasing NaAc concentration and not a logarithmic as expected. The LT_s biofilm produced similar results but with slightly lower pH values, which increased from 6 % to 15 % and R^2 = 0.9.

Regression analysis on NaAc concentrations available (as added and confirmed by spot check titration analysis) and utilized (as measured by difference using titration analysis) was performed for both ST_s and LT_s (Figure 10). Linear trend lines showed good correlation with the data (R^2 = 0.99 and R^2 = 0.94, respectively). ANOVA of all concentrations showed a significant change between initial and final concentrations within each biofilm group ($p < 0.001$). This data also showed that NaAc was in excess at each of the tested concentrations, so that no biofilms were able to consume all available NaAc within the test period; except at the lowest NaAc concentration of 20 mM for which acetate available and utilized did not differ greatly. The ST_s biofilm utilized 76 % and 85 % of acetic acid for 20 and 50 mM NaAc, respectively, and similarly, the LT_s biofilm consumed 81 % and 80 % of acetic acid for 20 and 50 mM NaAc, respectively.

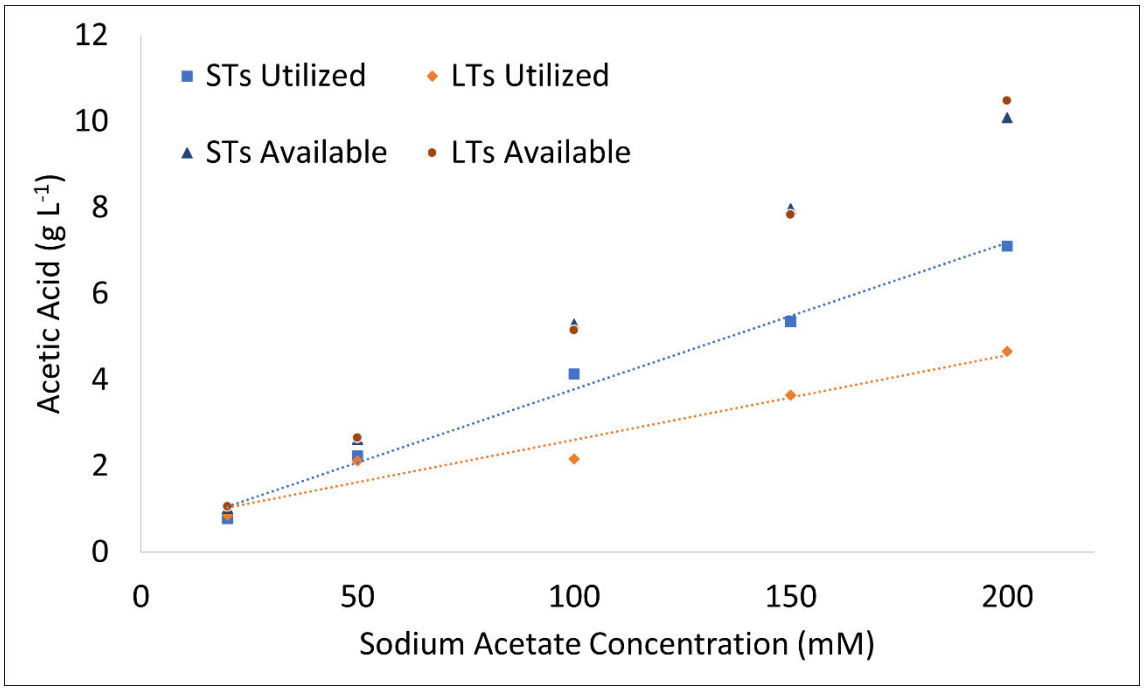

Figure 10 Biofilm utilization of NaAc in g L^{-1} of acetic acid. 200 mM values are from the extended period trial[4].

As the NaAc concentrations increased (>50 mM), a lower proportion of NaAc was utilised by the LT_s biofilms than by the ST_s biofilms, specifically with the ST_s biofilms consuming 47.8 % (at 100 mM), 31.9 % (at 150 mM), and 34.4 % (at 200 mM) more NaAc than the LT_s biofilms. This indicated an impact of biofilm ageing (Figure 10).

Total mean charge density produced during media exchange periods were also calculated and compared (Figure 11). These also showed a linear increasing trend with increasing dose for lower NaAc concentrations (≤ 100 mM NaAc). At higher doses (> 100 mM), a lower mean charge density was observed, possibly due to mass transport limitations or other reasons suggested further below. Both the ST_s and LT_s trials showed good linearity (R^2 = 0.98, 0.99) at ≤ 100 mM. ANOVA revealed that at ≤ 100 mM there was a significant difference in charge density between the ST_s and LT_s biofilms ($p < 0.001$). Variability in replicates (i.e. the error bars, Figure 11) was notably greater for ST_s than for LT_s (Figure 11), indicating that biofilm ageing can reduce variability in measured charge density.

[4] *ST_s (20 mM n = 3, 50 mM n = 2, 100 mM and 150 mM n = 3, 200 mM n = 2); LT_s (20 mM n = 2, 50 mM n = 3, 100 mM, 150 mM, and 200 mM n = 2).*

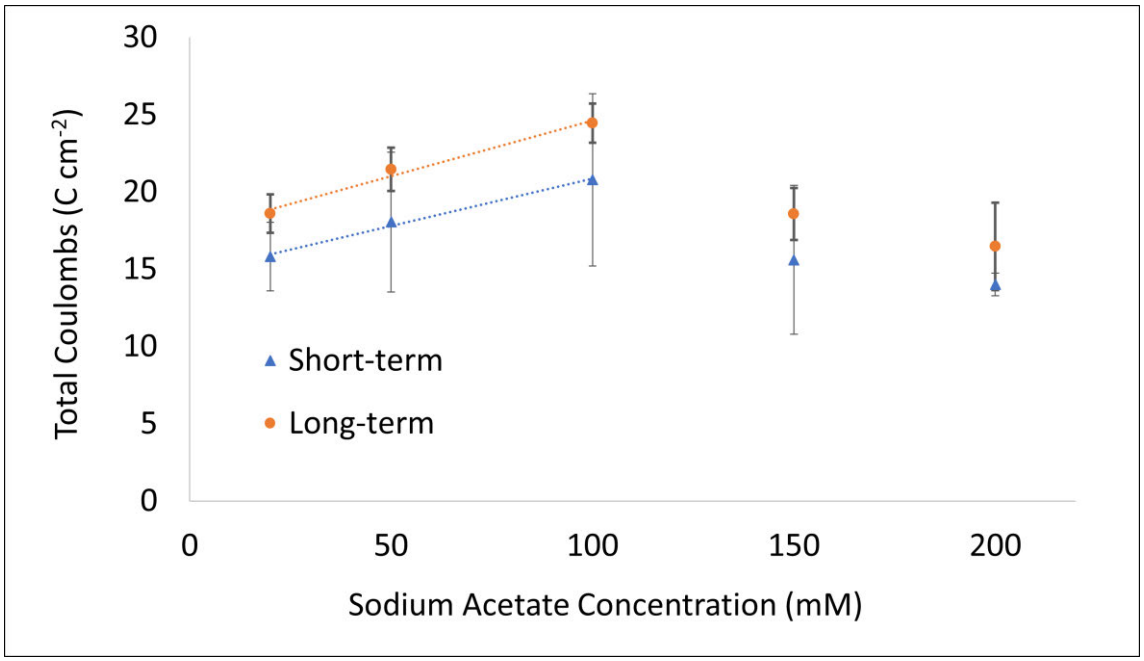

Figure 11 Mean charge density for NaAc trials. Reduced y-axis to show error bars[5].

To test for mass diffusion limitations and to evaluate continued biofilm charge production, the 200 mM dose test was continued for a further 8 days, and mean charge density subsequently recalculated for the 12-day test period. The corresponding value is shown in Figure 12, identified by 'A'. The ST_s and LT_s biofilm produced approximately 3.5 times higher cumulative charge over this extended period, compared to the charge produced over 4 days. This suggested an influence of mass transfer limitations; with the higher charge density observed after allowing the biofilms additional time to consume additional substrate.

The LT_s biofilms (4-day value) test showed a 15.0 % higher net charge density than the ST_s biofilms, whereas for the extended test (12-days) this discrepancy reduced to only 6.5 %. This suggested that, given enough time for the biofilms to consume enough NaAc, the resulting charge density may converge. However, an extended period of operation could become impractical for sensing or other applications and was evaluated in this case only to test mass transfer limitations and to demonstrate the capability of the biofilms.

[5] *ST_s (20 mM n = 3, 50 mM n = 2, 100 mM and 150 mM n = 3, 200 mM n = 2); LT_s (20 mM n = 2, 50mM n = 3, 100mM, 150mM, and 200mM n = 2).*

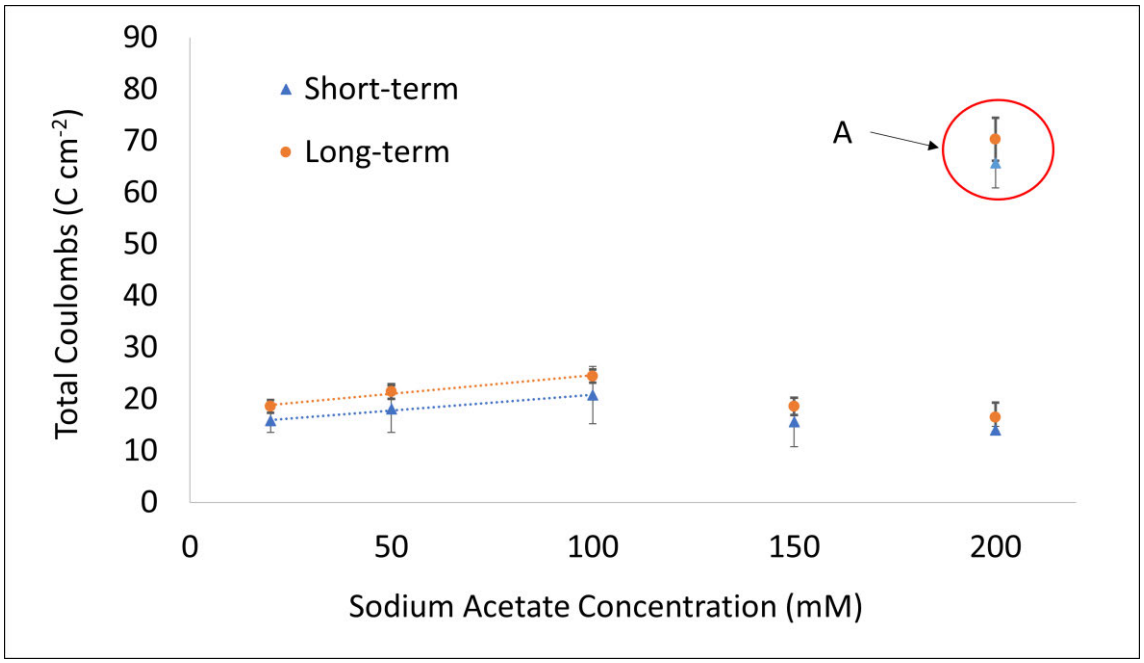

Figure 12 Mean charge density for NaAc trial. A indicates the 200 mM trial extended period (12-day) results[6].

4.4.1 Coulombic efficiency & limitations

Overall, a comparison between the substrate utilisation data (Figure 10) and the mean charge density data (Figure 12) suggested that the ST_s biofilms consumed more NaAc but produced a lower mean charge density, indicating a lower efficiency in the case of the ST_s than the LT_s. Possible causes for these could include:

- Biofilm community of the external inoculum used for primary inoculation may not have been dominant in electroactive bacteria (EAB) (Katuri et al., 2020), resulting in reduced performance of subsequent primary and secondary biofilms.
- The introduction of bacteria into the solution during the trial from non-sterile cell media and components, which could have consumed NaAc without producing electrons on the electrode.
- Biofilm respiration and/or mass diffusion limited electron production could have resulted in the biofilm becoming saturated with NaAc at higher levels.

While all three theories impact on NaAc utilization, mass diffusion limitations could be resolved by allowing sufficient time to pass as noted above.

[6] *ST_s (20mM n = 3, 50mM n = 2, 100mM and 150mM n = 3, 200mM n = 2); LT_s (20mM n = 2, 50mM n = 3, 100mM, 150mM, and 200mM n = 2).*

CE_f is a reliable indicator of energy conversion. As such, CE_f was determined in this paper to emphasize any differences that may have resulted from biofilm ageing, even if CE_f is uncommon in sensor applications. CE_f was also calculated to compare with the relevant literature. CE_f can also be impacted on by bacterial growth within the solution due to non-sterile conditions. Additionally, Eq. 2 does not consider mass transport limitations, biofilm NaAc exposure time, and assumes all NaAc is used to directly generate electrons at the working electrode. Therefore, true CE_f values would likely have been higher than the calculated values reported here. CE_f can also differ with cell geometry, electrode materials, and electrolytes. However, the CE_f values presented in this study were found to be similar (albeit on the low end of the range) to those reported by Batlle-Vilanova et al. (2017); Bian et al. (2018). Scarabotti et al. (2021) showed a much higher CE_f of approximately 30 % at a similar charge density of 20 C cm^{-2} to that in the current study.

The CE_f pre-trial to post-trial showed no statistically significant difference between the ST_s and LT_s biofilm groups (Figure 13). However, there was a relative increase in CE_f between ST_s and LT_s biofilms during each phase (pre, trial, post) of 16.7 %, 15.0 % (20mM only), and 18.6 % respectively; the mean CE_f across all concentrations of the trial was 15.4 %. The results across all phases show a trend of increased efficiency (Figure 13), and the LT_s biofilms outperforming the ST_s biofilms by 16.8 % (relative). This also indicated that biofilm ageing affected performance and output but did not cause a decline in charge efficiency.

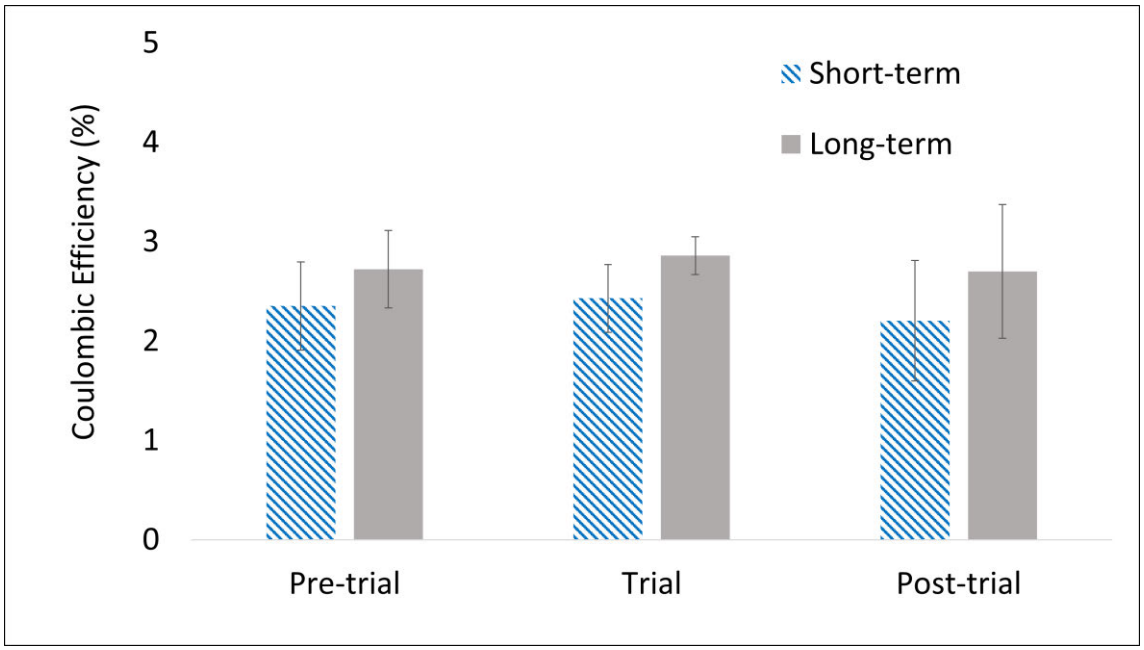

Figure 13 Coulombic efficiency of ST_s and LT_s biofilms during pre-trial[7], trial[8], and post-trial[9]. Trial values are from NaAc concentration of 20 mM only.

4.5 Conclusion

The biofilms that form in MESe are subject to ageing, which can affect performance. This study investigated the short-term and long-term performance of primary and secondary biofilms grown in MESe. Performance was compared in terms of NaAc utilization, CE_f, and current density. The results indicated no significant changes in ST_s and LT_s when comparing performance before and after the dedicated acetate dosing trial. Consequently, no lasting effects from the trial were observed and the biofilms fully recovered, despite receiving acetate doses up to 200 mM during the trial.

Performance of the LT_s showed a marginal improvement over the ST_s biofilm in terms of measured mean charge density, and a marginally higher CE_f for LT_s. The LT_s therefore performed better than the younger ST_s biofilm, which is a positive indicator for MESe applications.

Several influences were identified which could have affected the biofilm's output at higher acetate doses, with mass transport limitations considered plausible. Specifically,

[7] *ST_s (day 0-8 (n = 2), day 8-12 (n = 3)); LT_s (day 0-8 (n = 3), day 8-12 (n = 2)).*

[8] *ST_s (20 mM n = 3, 50 mM n = 2, 100 mM and 150 mM n = 3, 200 mM n = 2); LT_s (20 mM n = 2, 50 mM n = 3, 100 mM, 150 mM, and 200 mM n = 2).*

[9] *ST_s (day 0-12 (n = 3)), LT_s (day 0-12 (n = 3)).*

given enough time to consume a significant proportion of the acetate provided, charge density may converge, albeit excessive wait-times would be impractical for MESe applications.

Future investigations could identify micro-organisms that are more stable and consistent for MESe applications over the long-term, although this may be challenging in the typical non-sterile environment. Additionally, MESe future investigations could focus on biofilm response times to minimise data collation and analysis periods.

4.6 References

Abdelfattah, A., Hossain, M. I., & Cheng, L. (2020). High-strength wastewater treatment using microbial biofilm reactor: a critical review. *World J Microbiol Biotechnol, 36*(5), 75. doi:10.1007/s11274-020-02853-y

Batlle-Vilanova, P., Ganigue, R., Ramio-Pujol, S., Baneras, L., Jimenez, G., Hidalgo, M., . . . Puig, S. (2017). Microbial electrosynthesis of butyrate from carbon dioxide: Production and extraction. *Bioelectrochemistry, 117*, 57-64. doi:10.1016/j.bioelechem.2017.06.004

Baudler, A., Riedl, S., & Schroder, U. (2014). Long-term performance of primary and secondary electroactive biofilms using layered corrugated carbon electrodes. *Frontiers in Energy Research, 2*. doi:10.3389/fenrg.2014.00030

Bian, B., Shi, D., Cai, X., Hu, M., Guo, Q., Zhang, C., . . . Yang, J. (2018). 3D printed porous carbon anode for enhanced power generation in microbial fuel cell. *Nano Energy, 44*, 174-180. doi:10.1016/j.nanoen.2017.11.070

Bustillo-Lecompte, C. F., & Mehrvar, M. (2015). Slaughterhouse wastewater characteristics, treatment, and management in the meat processing industry: A review on trends and advances. *J Environ Manage, 161*, 287-302. doi:10.1016/j.jenvman.2015.07.008

Engel, C., Schattenberg, F., Dohnt, K., Schroder, U., Muller, S., & Krull, R. (2019). Long-term behavior of defined mixed cultures of Geobacter sulfurreducens and Shewanella oneidensis in bioelectrochemical systems. *Front Bioeng Biotechnol, 7*, 60. doi:10.3389/fbioe.2019.00060

Gimkiewicz, C., & Harnisch, F. (2013). Waste water derived electroactive microbial biofilms: growth, maintenance, and basic characterization. *J Vis Exp*(82), 50800. doi:10.3791/50800

Grobbler, C., Virdis, B., Nouwens, A., Harnisch, F., Rabaey, K., & Bond, P. L. (2018). Effect of the anode potential on the physiology and proteome of Shewanella oneidensis MR-1. *Bioelectrochemistry, 119*, 172-179. doi:10.1016/j.bioelechem.2017.10.001

Huang, H., Peng, C., Peng, P., Lin, Y., Zhang, X., & Ren, H. (2019). Towards the biofilm characterization and regulation in biological wastewater treatment. *Appl Microbiol Biotechnol, 103*(3), 1115-1129. doi:10.1007/s00253-018-9511-6

Jing, X., Liu, X., Deng, C., Chen, S., & Zhou, S. (2019). Chemical signals stimulate Geobacter soli biofilm formation and electroactivity. *Biosens Bioelectron, 127*, 1-9. doi:10.1016/j.bios.2018.11.051

Katuri, K. P., Kamireddy, S., Kavanagh, P., Muhammad, A., Conghaile, P. O., Kumar, A., . . . Leech, D. (2020). Electroactive biofilms on surface functionalized anodes:

The anode respiring behavior of a novel electroactive bacterium, Desulfuromonas acetexigens. *Water Res, 185*, 116284. doi:10.1016/j.watres.2020.116284

Kim, B. H., Chang, I. S., Gil, G. C., Park, H. S., & Kim, H. J. (2003). Novel BOD (biological oxygen demand) sensor using mediator-less microbial fuel cell. *Biotechnol Lett, 25*(7), 541-545. doi:10.1023/a:1022891231369

Kretzschmar, J., Böhme, P., Liebetrau, J., Mertig, M., & Harnisch, F. (2018). Microbial electrochemical sensors for anaerobic digestion process control - Performance of electroactive biofilms under real conditions. *Chem Eng Technol, 41*(4), 687-695. doi:10.1002/ceat.201700539

Liu, H., & Logan, B. E. (2004). Electricity generation using an air-cathode single chamber microbial fuel cell in the presence and absence of a proton exchange membrane. *Environ Sci Technol, 38*(14), 4040-4046. doi:10.1021/es0499344

Logan, B. E., Rossi, R., Ragab, A. a., & Saikaly, P. E. (2019). *Electroactive microorganisms in bioelectrochemical systems* (1740-1526). Retrieved from

Martin, E., Savadogo, O., Guiot, S. R., & Tartakovsky, B. (2010). The influence of operational conditions on the performance of a microbial fuel cell seeded with mesophilic anaerobic sludge. *Biochemical Engineering Journal, 51*(3), 132-139. doi:10.1016/j.bej.2010.06.006

Mauky, E., Weinrich, S., Jacobi, H. F., Nagele, H. J., Liebetrau, J., & Nelles, M. (2017). Demand-driven biogas production by flexible feeding in full-scale - Process stability and flexibility potentials. *Anaerobe, 46*, 86-95. doi:10.1016/j.anaerobe.2017.03.010

Nordmann, W. (1977). Die Überwachung der Schlammfaulung. *KA-Informationen für das Betriebspersonal, Beilage zur Korrespondenz Abwasser, 3*(77), 77.

Renslow, R. S., Babauta, J. T., Dohnalkova, A. C., Boyanov, M. I., Kemner, K. M., Majors, P. D., . . . Beyenal, H. (2013). Metabolic spatial variability in electrode-respiring Geobacter sulfurreducens biofilms. *Energy and Environmental Science, 6*(6), 1827-1836. doi:10.1039/c3ee40203g

Scarabotti, F., Rago, L., Buhler, K., & Harnisch, F. (2021). The electrode potential determines the yield coefficients of early-stage Geobacter sulfurreducens biofilm anodes. *Bioelectrochemistry, 140*, 107752. doi:10.1016/j.bioelechem.2021.107752

Steidl, R. J., Lampa-Pastirk, S., & Reguera, G. (2016). Mechanistic stratification in electroactive biofilms of Geobacter sulfurreducens mediated by pilus nanowires. *Nature Communications, 7*, 12217. doi:10.1038/ncomms12217

Sun, D., Chen, J., Huang, H., Liu, W., Ye, Y., & Cheng, S. (2016). The effect of biofilm thickness on electrochemical activity of Geobacter sulfurreducens. *International Journal of Hydrogen Energy, 41*(37), 16523-16528. doi:10.1016/j.ijhydene.2016.04.163

Sun, H., Ni, P., Angelidaki, I., Dong, R., & Wu, S. (2019). Exploring stability indicators for efficient monitoring of anaerobic digestion of pig manure under perturbations. *Waste Manag, 91*, 139-146. doi:10.1016/j.wasman.2019.05.008

CHAPTER 5: EFFECT OF CONDUCTIVITY AND PEAK CURRENT RESPONSE TIMES AS A MEASURE OF LONG-TERM STABILITY AND ACCURACY OF MICROBIAL ELECTROCHEMICAL SENSOR BIOFILMS

This Chapter was written in the form of **Paper IV** titled "Effect of conductivity and peak response times as a measure of long-term stability and accuracy of microbial electrochemical sensor biofilms", to be submitted to the journal Biotechnology and Bioengineering (IF 4.53).

Chapter 5 investigates the use of microbial electrochemical sensor (MESe) output response time as a function of electrolyte conductivity. In Chapter 2 a knowledge gap identified in order to meet increasing demands imposed by high-rate and flexible feeding anaerobic digesters an online response from MESe would be required. Previous studies identified sensor response times were as low as 10 minutes with higher accuracy obtained after several hours (Jiang et al., 2019). Chapter 4 identified that long-term MESe biofilms output would change over time. This Chapter investigates the behaviour of biofilms over time and the effect of common salts (NaCl and NH_4Cl) on biofilm response, with a focus on response time to address the knowledge gap.

5.1 Introduction

Volatile fatty acids (VFA) are formed during anaerobic digestion (AD) and are an indicator of process stability during biogas production. In highly buffered digestate an accumulation of VFA can occur before traditional sensors (e.g., pH) register a change. If not detected, VFA may accumulate as a symptom of process instability, and approach the buffer equivalence point whereby a large change in pH can occur, resulting in process failure. Sensors such as MESe could provide an alternative solution to current VFA measurement, although measurement response times are equivalent or longer than current methods. Timely monitoring of the process is especially important in high-rate or on demand anaerobic digesters (Mauky et al., 2017; Ülgüdür, Ergüder, Uludağ-Demirer, & Demirer, 2019). This highlights a need to investigate ways of improving MESe response times before the technology can be recognised as a comparable alternative (Jin et al., 2017; J. Kretzschmar et al., 2017).

An MESe determines VFA concentration by measuring and correlating peak current density, and as current density can be manipulated by salt addition, this may also impact response times. G. Liu et al. (2014) investigated addition of NaCl to increase conductivity of the electrolyte and found increasing conductivity coincided with a reduction in current density. The same authors also found NaCl addition up to 5.84 g L^{-1} decreased coulombic efficiency (CE_f), which is a function of current density and analyte concentration (G. Liu et al., 2014). Jin et al. (2016) demonstrated NaCl concentrations up to 1.75 g L^{-1} in a three-chambered bioelectrochemical cell produced an increase in current density, while NaCl of 100 mM reduced current density. Similarly, Jin et al. (2017) investigated the addition of 0, 1.16, 2.33, and 4.67 g L^{-1} NaCl and reported an increase in the current density, but found an upper limit of 2.33 g L^{-1} NaCl above which no increase in current density was observed. These studies demonstrate the addition of NaCl improved current density and concomitantly increased conductivity. Although, it is not clear the effect of conductivity on cell resistance and thus signal response times.

Measurement of acetate concentration and peak current response times of biofilm communities has been shown to vary (Jiang et al., 2018; Logan et al., 2019), which is not ideal for a sensor. Jiang et al. (2018) investigated the response time by changing the cell volume from 25 mL to 5 mL and recorded response times of 36 minutes and 5 minutes respectively. While this achieved a reduction in response time it may pose engineering issues related to the physical characteristics of wastewater, such as blockages. Currently, MESe have shown response times of approximately 5 minutes (Jiang et al., 2019), this could be considered a step toward a robust sensor with online response times. Although Jiang et al. (2019) identified more accurate results were obtained after several hours. Five minutes is relatively quick for low concentrations of acetate, however, improvements to response times are required before the current technology could be considered a rapid measurement.

Sodium chloride (NaCl) and ammonium chloride (NH_4Cl) can increase conductivity in solution resulting in improved electron transport (Kuntke et al., 2011; Lefebvre, Tan, Kharkwal, & Ng, 2012), high concentrations are also inhibitory to microorganisms and are commonly present in waste water (Foglia et al., 2020; McCabe et al., 2020; Pitk, Palatsi, Kaparaju, Fernandez, & Vilu, 2014; Thomas Schmidt et al., 2018). NH_4Cl can be moderately inhibitory to microorganisms at concentrations between 1.5 – 3.0 g L^{-1} while higher concentrations > 3.0 g L^{-1} produce strong inhibitory effects (Appels, Baeyens,

Degrève, & Dewil, 2008), while low concentrations of 2-3 g L^{-1} do not show any inhibitory effect (Jörg Kretzschmar et al., 2018). Kuntke et al. (2011) investigated the effect of NH_4Cl addition up to 4 g L^{-1} on MFC performance and reported no adverse effects on the cell's performance. However, Kuntke et al. (2011) noted that operational time decreased due to higher current density but times were not reported. Jörg Kretzschmar et al. (2018) reported bioelectrochemical type cells dosed with NH_4Cl produced similar current density to those dosed with NaCl and suggest that inhibited cells could recover to original activity. This demonstrates the addition of NH_4Cl in an MFC had no lasting effect on the biofilm or cell performance and could be investigated to reduce measurement response times.

Sensor stability is key for accurate measurement and, over time, a sensor that varies due to high salt concentration could require re-calibration. The effect of salts and other inhibitory conditions within wastewater will affect the sensor's response, therefore a key requirement for long-term sensor operation is to identify effects from known compounds within the wastewater. This paper explores the effect of NaCl and NH_4Cl on a low-cost MESe by measuring response time and peak current to determine electrolyte conductivity effects, long-term stability, and output signal accuracy.

5.2 Materials and methods

5.2.1 Electrochemical cell construction

To reduce duplication the cell construction is described in Chapter 3, Section 3.2.4.

5.2.2 Inoculum and media

To reduce duplication the primary source of inoculum, media, and carbon source are described in Section 3.2.4. Inoculum was sourced from established biofilms that were actively running, the cells were routinely dosed with 20 mM sodium acetate (NaAc) as substrate. Biofilm samples were combined in a single 50 mL tube which was subsequently filled to 50 mL with media solution. The biofilm was dispersed using a vortex mixer (Velp Scientifica, ZX3) for 2 minutes. A 5 mL aliquot was taken to inoculate each cell.

Conductivity was measured using a conductivity meter (ATI Orion, model 170). The NH_4Cl and NaCl solutions were a combination of media (buffer) and weighed salt concentration. Spot checks were performed on the solution for pH to ensure the media was maintained at pH 7. The NH_4Cl and NaCl dosing solutions were made within 24

hours prior to dosing to ensure the pH was maintained and solution was free from bacterial growth.

5.2.3 Experimental design

Experiments were performed in an environmental chamber (CM Envirosystems, PAC-120-AH) maintained at 37 ± 0.5 °C. The working electrode (anode) potential was poised at 0.2 V vs Ag/AgCl (3M KCl) for the duration of the experiment. NaCl and NH_4Cl were added using a modified pipette tip with a 50 mm syringe tip and injected through the cap vent hole. After injection the vent hole was resealed.

The potentiostat used for measurements was as described in chapter 3, with the exception of the microcontroller. Due to supply issues with the Arduino Pro Mini the microcontroller was swapped out for a Raspberry Pi Pico. The same firmware used in chapter 3 was uploaded to the Pico to collect measurement. The remaining hardware containing the fundamental components of the potentiostat was exactly as described in chapter 3. Calibration of the potentiostat before the experiment was conducted as outlined in Chapter 4, Section 4.2.2.

The biofilm trials were comprised of 9 separate cells consisting of 1 control; 4 cells of varying concentrations of NaCl, the remaining 4 cells were dosed with varying concentrations of NH_4Cl. Each cell was subjected to 3 dosing events of the respective salt (Figure 14). Individual dosing regimens were designated a trial with sequential numerical ordering of each trial (e.g., trial 1, trial 2, trial 3). These trials were later used to identify each set of data.

5.2.4 Biofilm establishment

The biofilm feeding regime was split into 2 periods as phosphate buffer solutions are known to affect current production in electroactive biofilms (Torres, Kato Marcus, & Rittmann, 2008). Continual biofilm growth and feeding regime consisted of fixed batch feed for a period of 7-days. After an initial biofilm establishment period (4 days) the cell lid was removed with the electrodes, electrodes were rinsed with deionized water and transplanted to a new cell containing 90 mL of fresh media. After assembly, the cells were placed into an environmental chamber and connected to the respective potentiostat. After 3 days without any additional input, an additional 10 mL of solution containing media and NaAc was added to the cell for a final volume of 100 mL at a concentration of 20 mM NaAc. Cell operation was then allowed to continue without interruption for a further

4 days and current was measured and recorded for the entire duration of each cycle (7-days) (Figure 14).

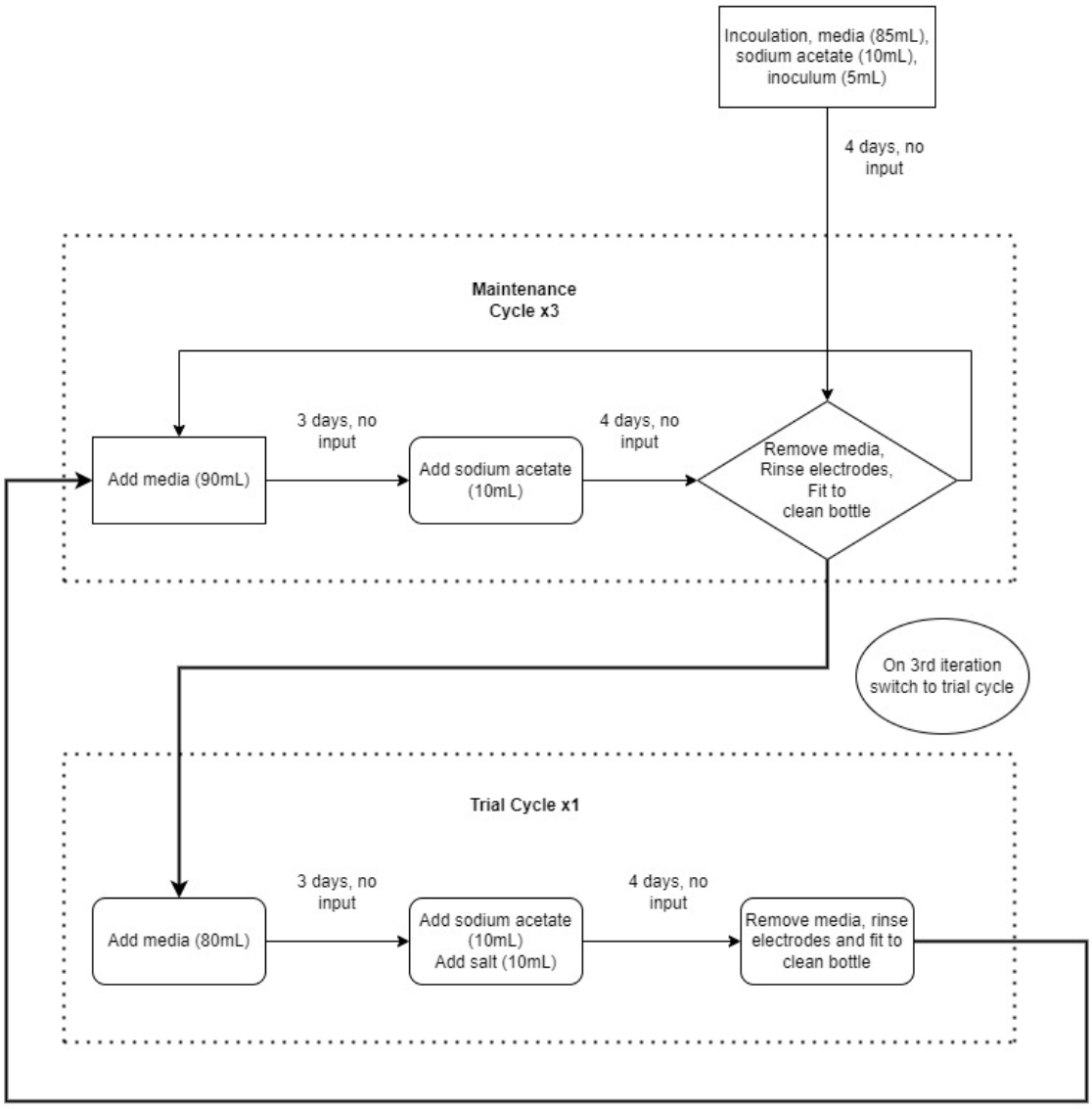

Figure 14 Experimental flow for inoculation and dosing of a microbial electrochemical sensor

During the trial the media solution volumes were changed, only 80 mL of media was added to each cell for the initial 3-days to allow for 10 mL NaAc solution and 10 mL salt solution. This was followed by the same process as described above, 3 days with no addition, followed by 4 days with acetate and analyte addition. A period of 21 days separated the trials where three cycles were conducted of 7-day batch feeding before and after salt addition to stabilize the biofilm and ensure there were no residual effects.

5.2.5 Response time measurement

MESe response time was measured between a lower (5%) and upper (95%) limit of the peak current density value for each cell. Calculations were based on the method used by

Jiang et al. (2018), which utilised modified upper and lower limits to determine the response time. The calculated values were used to determine the closest actual recorded value within the initial current response. The measured values for analysis are identified as peak current density, which represents 95% of the maximum peak current density, and peak time (PT) which represents the time taken in minutes from 5% of the maximum peak current density to 95% of the maximum peak current density. The subscript represents the trial sequence number in order. From here on in peak current density shall simply be referred to as "current".

5.2.6 Data analysis and statistical methods

All replicates were conducted independently. Statistics and regression were calculated using Microsoft Excel 365 (2022). Unless otherwise stated, ANOVA significance testing was performed at an alpha value of 0.05. Following the ANOVA the Student's *t*-test was performed to identify any significant difference between the trials. The *t*-test was performed with equal variances and a mean difference of zero, the two tail P value was used for analysis.

5.3 Results and discussion

5.3.1 Measured cell conductivity

To investigate the effect of conductivity on biofilm response NH_4Cl and NaCl were added to the cell. Typical conductivities for NaCl and NH_4Cl are approximately 13 mS cm^{-1} and 18 mS cm^{-1} at concentrations of 1 % respectively (Instrumentation; SmartMeasurement). The conductivity in the NaCl samples increased linearly with concentration as expected (Figure 15a). Although conductivity due to NH_4Cl increased linearly, the values were significantly lower than expected (Figure 15b). The lower values were most likely the result of narrower concentration range, or, less likely, the ammonium ion was consumed by the biofilm and/or bacteria in the solution. Although the conductivity was not affected to the same degree as with NaCl, it does present the effect of lower conductivity on biofilm response.

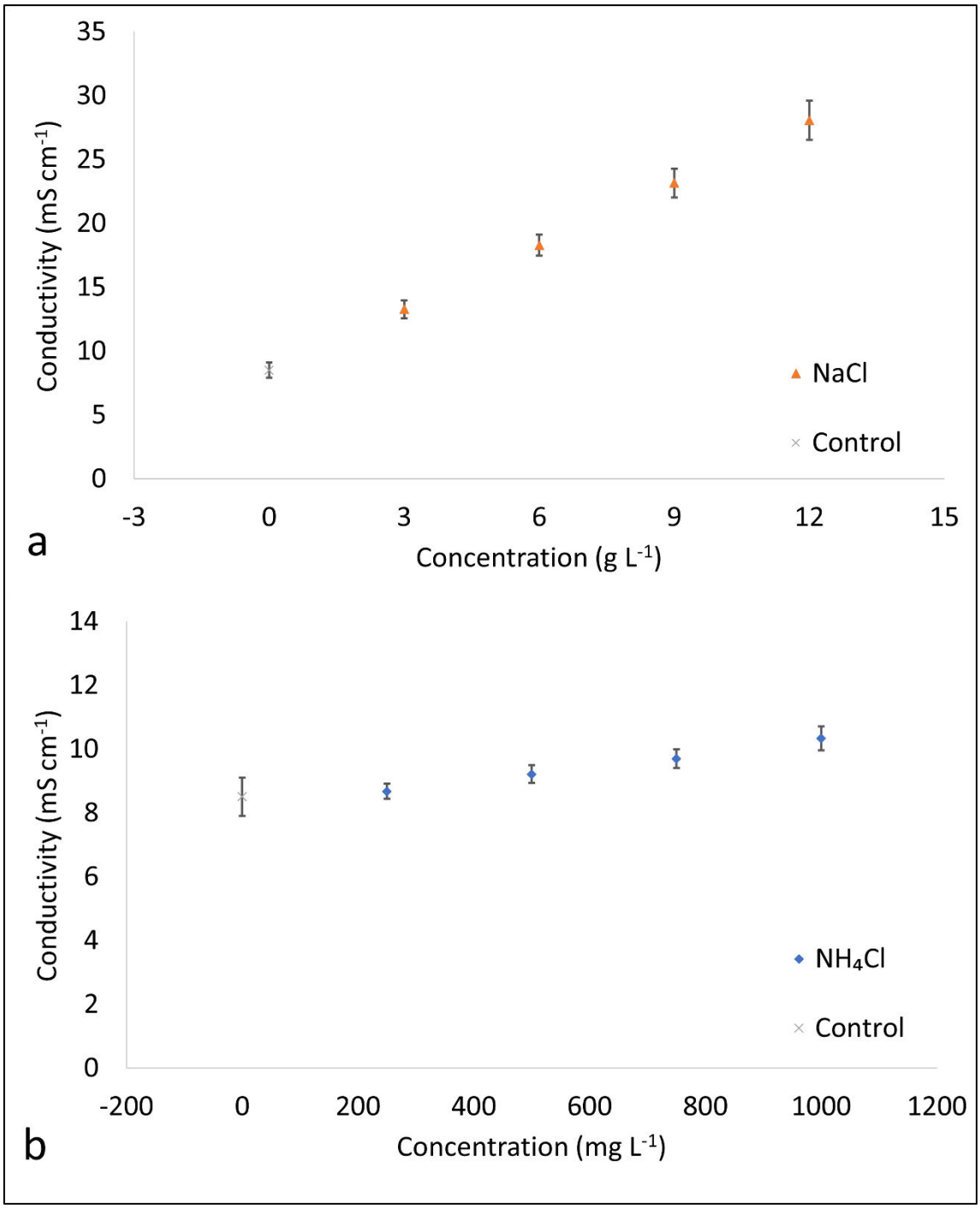

Figure 15 Conductivity of the media (control) and dosed solution a) NaCl conductivity, b) NH_4Cl conductivity

5.3.2 Impact of NaCl on peak current density

MESe require an output that is stable and reproducible to produce reliable and accurate measurement. Peak current density was used to determine the effect of NaCl in MESe, as described in Section 5.2.5. Biofilm signal response due to the addition of NaCl was varied when compared with the control biofilm (Figure 16). In terms of current there was significant (p = 0.03) change within each trial ($PkC_{1\text{-}3}$), and significant (p < 0.001)

different between each trial group. Further investigation of the differences in the values was justified to determine the context of the changes. Although, lower current was measured compared to other studies (H. Sun, Zhang, et al., 2019), results are diverse depending on setup (Logan et al., 2019) and are considered appropriate for this setup.

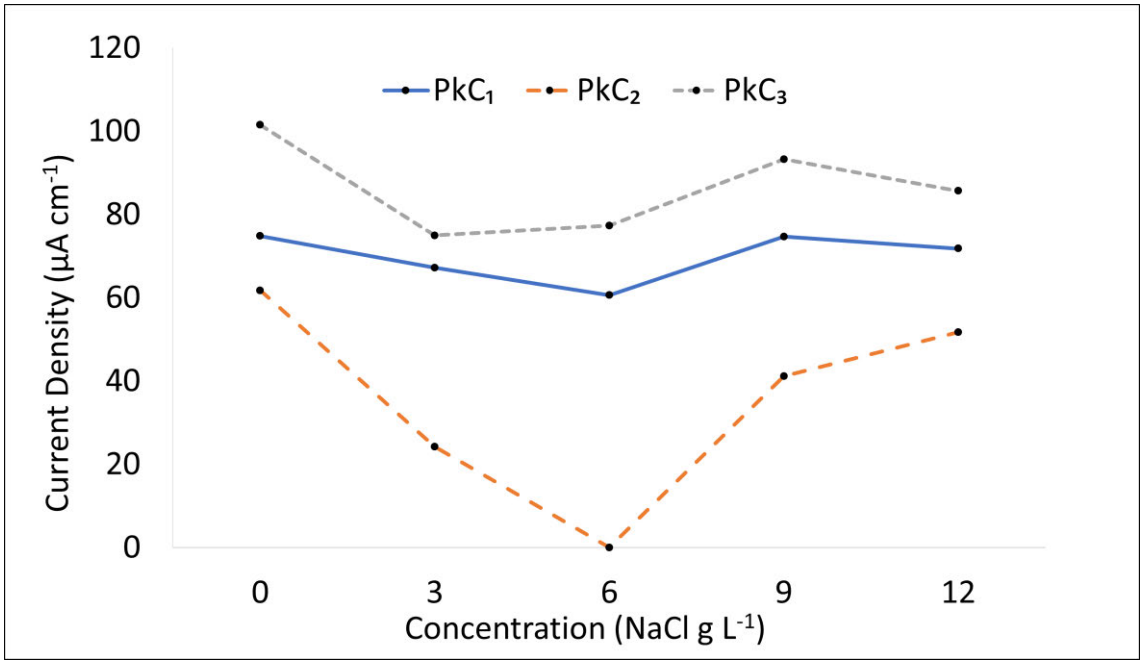

Figure 16 Current response to NaCl addition

Initial current values (PkC_1) were relatively consistent across all concentrations with 67±7 µA cm^{-2}. NaCl addition affected no significant variation in current across the group. This indicated that the biofilms were stable and there were no significant effects from NaCl addition. However, the second trial (PkC_2) showed a significant drop in current across all NaCl concentrations and was significantly lower than the first trial (PkC_1). Across all concentrations the second trial current values were lower compared with the control. No trend was observed between different concentrations, although 3 & 6 g L^{-1} NaCl were noticeably lower than 9 & 12 g L^{-1} NaCl. The significant drop in peak current from PkC_1 to PkC_2 does suggest a delayed inhibition of the cells, as no significant drop in current was observed for PkC_1. The response from 6 g L^{-1} for PkC_2 is remarkable as lower and higher concentrations did not see similar levels of current loss, inhibition was the likely cause but may not have been the only influencing factor. Poor electrical connection to the cell could have contribute to loss of current. A poor connection would create a high resistance and thus lower current flow, the subsequent trial reconnected the cell resulting in improved performance. Interestingly, this may be demonstrating the ability of the biofilm to remain active despite being unable to donate electrons through

the electrode, as previously identified (H. Sun, Zhang, et al., 2019; X. Zhang, Prevoteau, Louro, Paquete, & Rabaey, 2018). The final trial (PkC_3) produced significantly higher current compared with the trials PkC_1 and PkC_2. As found in trials PkC_1 and PkC_2, current values in PkC_3 were lower than the control. Similarly, PkC_3 NaCl concentrations of 3 & 6 g L^{-1} current values were noticeably lower than 0, 9 & 12 g L^{-1}.

The lower current density produced by 3 & 6 g L^{-1} NaCl in the second and third trials indicate that lower concentrations of NaCl would impact biofilm current but may not be the only variable in effect (e.g. ageing). The results reveal the biofilm current response was impacted across all concentrations of NaCl and indicates biofilms are likely to underperform in terms of current compared with NaCl-free media. This was inconsistent with other studies (Jörg Kretzschmar et al., 2018; G. Liu et al., 2014; Mohan & Das, 2009), which identified biofilm salt tolerance. However, Mohan and Das (2009) reported poor performance at high salinity (6 g L^{-1} NaCl). This demonstrates cell setup and biofilm maturity contribute to the effect of salinity on MESe output (Logan et al., 2019; Mohan & Das, 2009). The current response from all biofilms followed the control with each trial, with initially good current production (albeit low), followed by a large reduction, and finally PkC_3 there was an increase above initial (PkC_1) current values. Peak current was negatively impacted by NaCl in trial 2, which indicates acute inhibition with no correlation between concentrations. The final trial (PkC_3) shows recovery and increased efficiency. This highlights an insensitivity of current and response time to salt concentration (and thus conductivity) but shows by comparing biofilm groups as time-sequence, there is considerable effect of biofilm ageing. This indicates biofilm signal response time is more likely affected by acclimation and ageing.

5.3.3 Impact of NaCl on response times

There was no significant difference in response times (p = 0.95) between the concentrations (3, 6, 9, 12 g L^{-1}) in each trial (Figure 17). However, there was significant change in response times between each trial group ($PT_{1\text{-}3}$) (p = 0.046), the response times were further analysed and compared. Response times for each trial as percentage of control cell are presented in Table 1. Mostly response times were below the control with the exception of 6 g L^{-1}. Although there was no significant difference between the concentrations, the 6 g L^{-1} response time was much longer than other concentrations, which may indicate inhibition due to the presence of NaCl.

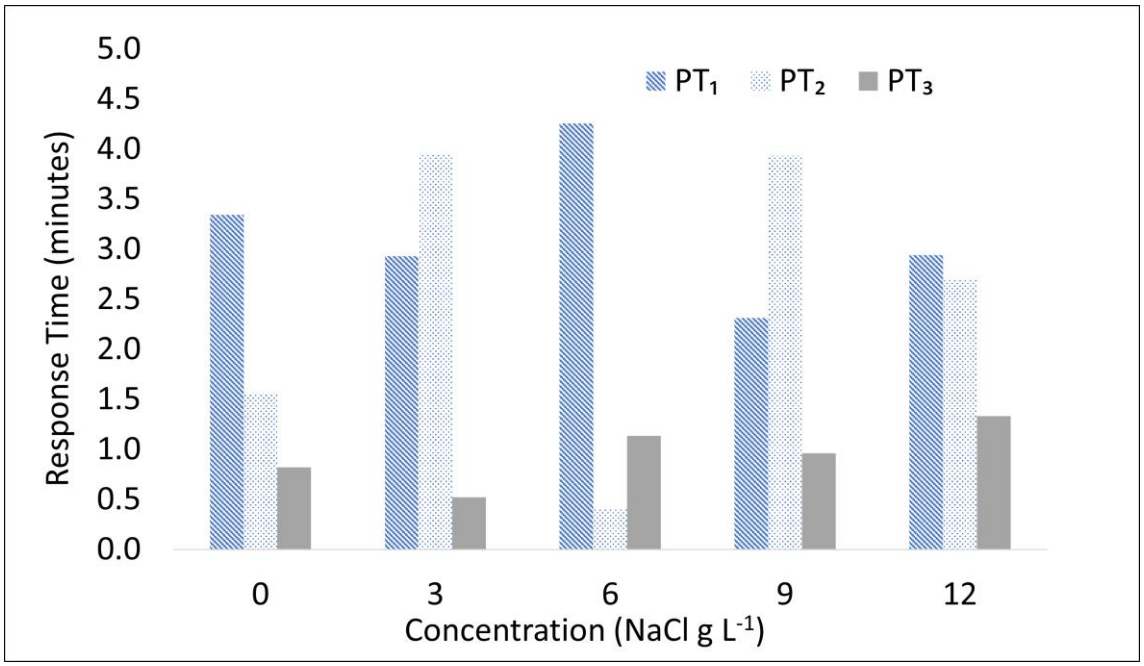

Figure 17 Effect of NaCl addition on response times for each trial.

Trial 2 generally showed longer response times compared to the control. During the second trial (PT_2) (approximately 56 days), the cell containing 6 g L^{-1} recorded a large decrease in response time, which corresponds with a large drop in peak current. The decrease in response time was likely due to inhibition but ageing may also play a role as later trials show improvement. In contrast, the 9 and 3 g L^{-1} NaCl biofilms responded to dosing with an increase in response time for the same period (PT_2). By the third trial there had been a significant reduction in response times compared to initial response times (PT_1), although the times were consistent with the control (Figure 17). The recorded response times demonstrated no relationship to NaCl concentration, with response times more representative of biofilms acclimation and ageing effects. Ageing was suspected to contribute to response as there was 21 days in between each trial, and in total 88 days had passed by the third trial. The first two trials (Figure 17) indicate high variability in response times, which may indicate a period of acclimation as later biofilms (Trial 3) coalesce.

Table 1 NaCl trial results compared to control

NaCl (g L^{-1})	Trial 1 (%)		Trial 2 (%)		Trial 3 (%)	
	PkC_1	PT_1	PkC_2	PT_2	PkC_3	PT_3
3	-10	-12	-61	153	-26	-37
6	-19	27	-100	-74	-24	39
9	0	-31	-33	152	-8	17
12	-4	-12	-16	73	-16	62

5.3.4 Impact of NH_4Cl on peak current density

To further evaluate the effect of electrolyte conductivity on biofilms for acetate measurement, dosing of NH_4Cl was investigated (Figure 18). A relatively small positive trend in current density for PkC_4 across all concentrations was observed. Improved performance from NH_4Cl have been investigated previously and show a positive trend (Zhao, Angelidaki, & Zhang, 2018). However, this is dependent on substrate concentration, without sufficiently high concentration of substrate MESe current output may decline (Tice & Kim, 2014).

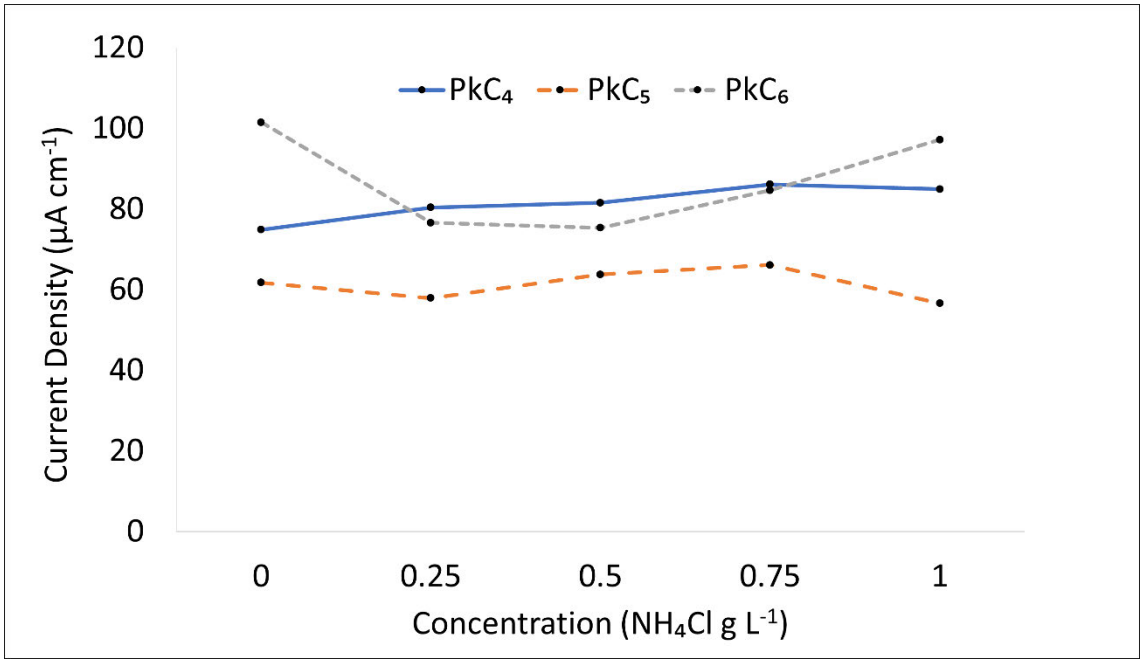

Figure 18 Current response to NH_4Cl addition

PkC_5 showed significantly reduced current compared to the other trials (Section 5.3.2), which may indicate acute inhibition, although, the control recorded similar values. There was no significant change in peak current during the second trial and peak values were uniform (61±5 µA cm^{-2}) across all concentrations. When comparing PkC_5 with the fourth

trial the biofilm response follows a similar trend across all concentrations, albeit significantly lower current. Biofilms for PkC_6 were similar to PkC_4 values, except at 1 g L^{-1}. There was depression of all values, which was in contrast to the previous trials (PkC_4 and PkC_5) and shown in Table 2. This would suggest the NH_4Cl had a direct impact on biofilm growth rather than through increased conductivity. The results indicate that NH_4Cl had insignificant impact (p = 0.66) on peak current. The control and 1 g L^{-1} biofilms were more variable, while lower concentrations show better stability and more consistent results. The addition of NH_4Cl may produce a more stable biofilm and therefore a more stable MESe output, however, the reduction in current response would require further investigation to test correlation to different acetate concentrations.

5.3.5 Impact of NH_4Cl on response times

Through the subsequent trials the response times were progressively and significantly shorter (p = 0.003). However, response times in each trial from addition of NH_4Cl showed no significant improvement (p = 0.69). Biofilms in the fourth trial (PT_4) demonstrated an improvement compared to the control. Although there was insufficient evidence that NH_4Cl dosing reduced biofilm response time, biofilms in PT_4 produced between approximately 20-50 % shorter response times (Figure 19). The fifth trial (PT_5) showed similar reduction in response times compared to the control (Table 2). Only the higher concentration of 1 g L^{-1} showed longer response time, while the remaining concentrations recorded a reduction in response time between approximately 40-50 %. Unfortunately, further analysis of this reduction was unable to be investigated due to the restrictions of the experiment. In the final trial (PT_6) the response times were similar across all concentrations and no clear trend relating reduced response time with increasing concentration. The final trial was consistent with the control across all concentrations and showed reduced response times when compared with the previous trial.

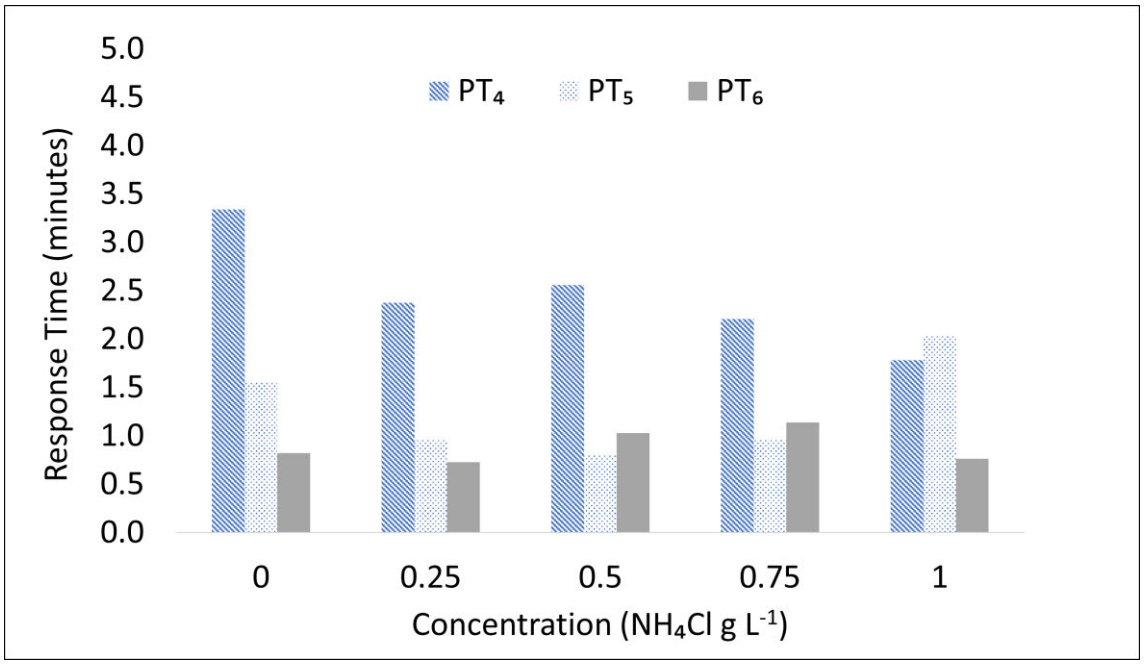

Figure 19 NH_4Cl response times for each trial.

Initially, NH_4Cl reduced the response times, although, concomitantly there was a reduction in biofilm current density. Subsequent trials indicated biofilm acclimation to NH_4Cl and slightly less variation in response time. The impact on response time from NH_4Cl in lower concentrations was more pronounced by the second trial, where the response in the second trial was comparable to the third trial. The lower concentrations continued the trend with lower response times in the third trial and only a small increase in time from the previous trial. This indicates that by the second trial (at approximately 60 days) the biofilms response time to NH_4Cl was at a minimum and further reduction may not be possible. Although response time reached a minimum the current density did not show the same trend, this indicates the biofilm respiration was limited but was able to acclimate to NH_4Cl.

Table 2 NH_4Cl trial results compared to the control

NH_4Cl ($g\ L^{-1}$)	Trial 4 (%)		Trial 5 (%)		Trial 6 (%)	
	PkC_4	PT_4	PkC_5	PT_5	PkC_6	PT_6
0.25	7	-29	-6	-39	-25	-11
0.5	9	-23	3	-48	-26	25
0.75	15	-34	7	-38	-17	39
1	13	-47	-8	31	-4	-7

Short-term (approximately 26-56 days, PT_4 and PT_5) biofilm demonstrated a reduction in response times at low NH_4Cl concentrations. However, there was insufficient evidence that NH_4Cl impacted the biofilm response time for each trial. Although, between the trials showed a significant reduction in response times and less variation. Any affect from NH_4Cl was limited and ageing appears to be the dominant effect on biofilm signal, with longer-term (>80 days) producing significantly shorter response times, similar to the control.

Biofilm response time is relative to current, and MESe current output the main indicator of acetate concentration. A biofilm that is unable to produce a specific current for a given VFA concentration would result in misinterpretation of the signal. For example, if the current is expected to be 80 μA cm^{-2} for a given concentration, and the cell is unable to reach this peak it could be misinterpreted as a lower concentration. This also affects response time as the cell can produce the lower peak in less time, similarly, when reduced current production is observed response times increase. This does suggest that response time of the cells was more influenced by NaCl or NH_4Cl inhibition/acclimation than conductivity changes by these salts. Short-term (approximately 60 days) the MESe output current and response time was negatively affected, after which the MESe is able to recovery and improve above the initial current/time response.

5.4 Conclusion

MESe are being investigated as a novel alternative to current VFA measurement methods. Current MESe can take 10-30 minutes to produce a measurement, which may not be quick enough for some high-rate anaerobic digesters (Ülgüdür et al., 2019). High-rate and on-demand digesters require timely measurement (Mauky et al., 2017), therefore MESe response times need to be improved to keep up with demand. MESe output signal is influenced by external and internal electrical resistance. By influencing the electrolyte physico-chemical properties, the internal resistance of an MESe can be lowered improving performance and stability. Increased conductivity can reduce the internal resistance of an MESe but little is known about the conductivity effects on MESe response times. This study investigates salts commonly found in anaerobic digestate (NH_4Cl and NaCl) and their conductivity effects in relation to biofilm peak current density. Addition of NaCl and NH_4Cl insignificantly impacted response times. While NaCl-dosed biofilms produced higher variation initially, the final trial results indicated

biofilms had acclimated to the NaCl. There was a general trend to lower response times, although, this was similar to the control biofilm and was more consistent with the effects of biofilm maturation/ageing. NH4Cl-dosed biofilms initially presented a reduction in response times at lower concentrations, but the NH4Cl biofilms showed similar response times to the control in the long-term (approximately 88 days) as was observed in the NaCl biofilms. It appears that all biofilms investigated were tolerant of the increased salinity and were able to acclimate long-term. Peak biofilm current is used to determine volatile fatty acid concentration in MESe. Consequently, this work demonstrates that sudden changes in NaCl or NH_4Cl can negatively impact biofilm peak current and response time, which in turn impacts MESe measurement accuracy. Initially, biofilms were able to produce a response time of approximately 3 minutes, and by the final trial, times were under 1 minute without any salt addition (i.e. control). Younger biofilms dosed with NaCl showed significant variability and reduced response times, while NH_4Cl dosed biofilms showed good stability short-term (approximately 26-56 days), although longer-term (approximately 88 days) all biofilms produced >50% reduction in response time. This study shows that biofilm response times will reduce over time despite changes in electrolyte salinity. This study found ageing is the dominant factor in biofilm response time. Salinity is likely to affect microbes directly and conductivity plays a lesser role in biofilm response time. Further investigation of the response times of MESe applied to pilot-scale anaerobic digesters may yield further insight short- and long-term.

5.5 References

Appels, L., Baeyens, J., Degrève, J., & Dewil, R. (2008). Principles and potential of the anaerobic digestion of waste-activated sludge. *Progress in Energy and Combustion Science, 34*(6), 755-781. doi:10.1016/j.pecs.2008.06.002

Foglia, A., Akyol, Ç., Frison, N., Katsou, E., Eusebi, A. L., & Fatone, F. (2020). Long-term operation of a pilot-scale anaerobic membrane bioreactor (AnMBR) treating high salinity low loaded municipal wastewater in real environment. *Separation and Purification Technology, 236*. doi:10.1016/j.seppur.2019.116279

Instrumentation, T. Conductivity chart of liquids. Retrieved from chrome-extension://efaidnbmnnnibpcajpcglclefindmkaj/https://www.traskinstrumentation.com/pdf/app_notes/Conductivity_Chart_of_Liquids.pdf

Jiang, Y., Chu, N., & Zeng, R. J. (2019). Submersible probe type microbial electrochemical sensor for volatile fatty acids monitoring in the anaerobic digestion process. *J Clean Prod, 232*, 1371-1378. doi:10.1016/j.jclepro.2019.06.041

Jiang, Y., Yang, X. F., Liang, P., Liu, P. P., & Huang, X. (2018). Microbial fuel cell sensors for water quality early warning systems: Fundamentals, signal resolution, optimization and future challenges. *Renewable & Sustainable Energy Reviews, 81*, 292-305. doi:10.1016/j.rser.2017.06.099

Jin, X., Angelidaki, I., & Zhang, Y. (2016). Microbial electrochemical monitoring of volatile fatty acids during anaerobic digestion. *Environ Sci Technol, 50*(8), 4422-4429. doi:10.1021/acs.est.5b05267

Jin, X., Li, X., Zhao, N., Angelidaki, I., & Zhang, Y. (2017). Bio-electrolytic sensor for rapid monitoring of volatile fatty acids in anaerobic digestion process. *Water Res, 111*, 74-80. doi:10.1016/j.watres.2016.12.045

Kretzschmar, J., Böhme, P., Liebetrau, J., Mertig, M., & Harnisch, F. (2018). Microbial electrochemical sensors for anaerobic digestion process control - Performance of electroactive biofilms under real conditions. *Chem Eng Technol, 41*(4), 687-695. doi:10.1002/ceat.201700539

Kretzschmar, J., Koch, C., Liebetrau, J., Mertig, M., & Harnisch, F. (2017). Electroactive biofilms as sensor for volatile fatty acids: Cross sensitivity, response dynamics, latency and stability. *Sensors and Actuators B-Chemical, 241*, 466-472. doi:10.1016/j.snb.2016.10.097

Kuntke, P., Geleji, M., Bruning, H., Zeeman, G., Hamelers, H. V., & Buisman, C. J. (2011). Effects of ammonium concentration and charge exchange on ammonium recovery from high strength wastewater using a microbial fuel cell. *Bioresour Technol, 102*(6), 4376-4382. doi:10.1016/j.biortech.2010.12.085

Lefebvre, O., Tan, Z., Kharkwal, S., & Ng, H. Y. (2012). Effect of increasing anodic NaCl concentration on microbial fuel cell performance. *Bioresour Technol, 112*, 336-340. doi:10.1016/j.biortech.2012.02.048

Liu, G., Yu, S., Luo, H., Zhang, R., Fu, S., & Luo, X. (2014). Effects of salinity anions on the anode performance in bioelectrochemical systems. *Desalination, 351*, 77-81. doi:10.1016/j.desal.2014.07.026

Logan, B. E., Rossi, R., Ragab, A. a., & Saikaly, P. E. (2019). *Electroactive microorganisms in bioelectrochemical systems* (1740-1526). Retrieved from

Mauky, E., Weinrich, S., Jacobi, H. F., Nagele, H. J., Liebetrau, J., & Nelles, M. (2017). Demand-driven biogas production by flexible feeding in full-scale - Process stability and flexibility potentials. *Anaerobe, 46*, 86-95. doi:10.1016/j.anaerobe.2017.03.010

McCabe, B. K., Harris, P., Antille, D. L., Schmidt, T., Lee, S., Hill, A., & Baillie, C. (2020). Toward profitable and sustainable bioresource management in the Australian red meat processing industry: A critical review and illustrative case study. *Critical Reviews in Environmental Science and Technology*, 1-25. doi:10.1080/10643389.2020.1712310

Mohan, Y., & Das, D. (2009). Effect of ionic strength, cation exchanger and inoculum age on the performance of microbial fuel cells. *International Journal of Hydrogen Energy, 34*(17), 7542-7546. doi:10.1016/j.ijhydene.2009.05.101

Pitk, P., Palatsi, J., Kaparaju, P., Fernandez, B., & Vilu, R. (2014). Mesophilic co-digestion of dairy manure and lipid rich solid slaughterhouse wastes: process efficiency, limitations and floating granules formation. *Bioresour Technol, 166*, 168-177. doi:10.1016/j.biortech.2014.05.033

Schmidt, T., McCabe, B., & Harris, P. (2018). Process monitoring and control for an anaerobic covered lagoon treating abattoir wastewater. *Chemical Engineering & Technology*. doi:10.1002/ceat.201700391

SmartMeasurement. Conductivity. Retrieved from https://www.smartmeasurement.com/calculators-utilities/conductivity/

Sun, H., Zhang, Y., Wu, S., Dong, R., & Angelidaki, I. (2019). Innovative operation of microbial fuel cell-based biosensor for selective monitoring of acetate during

anaerobic digestion. *Sci Total Environ, 655*, 1439-1447. doi:10.1016/j.scitotenv.2018.11.336

Tice, R. C., & Kim, Y. (2014). Influence of substrate concentration and feed frequency on ammonia inhibition in microbial fuel cells. *Journal of Power Sources, 271*, 360-365. doi:10.1016/j.jpowsour.2014.08.016

Torres, C. I., Kato Marcus, A., & Rittmann, B. E. (2008). Proton transport inside the biofilm limits electrical current generation by anode-respiring bacteria. *Biotechnol Bioeng, 100*(5), 872-881. doi:10.1002/bit.21821

Ülgüdür, N., Ergüder, T. H., Uludağ-Demirer, S., & Demirer, G. N. (2019). High-rate anaerobic treatment of digestate using fixed film reactors. *Environmental Pollution, 252*, 1622-1632. doi:10.1016/j.envpol.2019.06.115

Zhang, X., Prevoteau, A., Louro, R. O., Paquete, C. M., & Rabaey, K. (2018). Periodic polarization of electroactive biofilms increases current density and charge carriers concentration while modifying biofilm structure. *Biosens Bioelectron, 121*, 183-191. doi:10.1016/j.bios.2018.08.045

Zhao, N., Angelidaki, I., & Zhang, Y. (2018). Current as an indicator of ammonia concentration during wastewater treatment in an integrated microbial electrolysis cell - Nitrification system. *Electrochimica Acta, 281*, 266-273. doi:10.1016/j.electacta.2018.05.187

CHAPTER 6: DISCUSSION AND CONCLUSION

6.1 Thesis contribution

This thesis presented a literature review that identified knowledge gaps in current MESe technology. Overall, the thesis demonstrated that a cost-effective potentiostat capable of MESe measurement can be accurate and precise, and as biofilms age, their respiration will impact MESe output. The biofilm response shown in this thesis contributes to a more comprehensive understanding of MESe technology by presenting statistical analysis and electronic design while complementing and contributing to the ongoing research of microbial electrochemical technologies.

6.1.1 Literature background and gaps

Current investigations of the AD process are focusing on high-rate and on-demand digesters, which will require additional timelier monitoring. An intermediary in the AD process, VFA, when combined with total alkalinity (VFA:TA) plays a role as an indicator of stability. Microbial electrochemical sensors (MESe) are being explored for timely measurement of VFA, and show a good correlation to VFA concentration. To provide an in-depth background on microbial electrochemical technologies such as MESe and their application in anaerobic digestion, an exhaustive review of the literature was carried out.

Paper I identifies challenges and limitations of microbial electrochemical technology and highlights several knowledge gaps. A barrier to utilising MESe in application is the cost of a potentiostat. To investigate this barrier crucial design parameters in the design a cost-effective potentiostat were identified, and later applied in the production of a potentiostat. For an MESe to provide reliable measurements in-situ, the long-term output needs to provide a consistent relationship between MESe output to VFA concentration. Therefore, the performance and output correlation and the impact on long-term MESe behaviour was investigated. Additionally, the response time of MESe was identified as crucial in providing operators with timely VFA measurements, especially in high-rate digesters. Current biofilm response times can take several hours to produce accurate results, this presented a knowledge gap in understanding the impact of electrolyte electron mobility on response time, therefore, electrolyte conductivity on response times was investigated.

6.1.2 Designing a cost-effective potentiostat

Addressing a knowledge gap identified in **Paper I**, **Paper II** bridged the issue of addressing affordability and simplicity of an accurate potentiostat. To complement the potentiostat design a microcontroller and data storage was incorporated, automating data collection while allowing flexibility in an experimental setup. Being in the form of a Methods paper, **Paper II** aimed to enable researchers to reduce/eliminate barriers associated with costly laboratory equipment. Potentiostat design is complex and requires a detailed understanding of electronics, the investigation presented the information to the reader in an accessible language, while still detailing how accurate and consistent measurement can be achieved.

Paper II addressed the potentiostat associated cost barrier by detailing components and design parameters of a low-cost potentiostat. The potentiostat design achieved accurate measurements of a microbial electrochemical cell, and the paper was able to identify the key design parameters required for accurate measurements. A low-cost potentiostat was realised and by documenting the essential components and design aspects, the information could be presented and conveyed to those unfamiliar with potentiostats and their electrochemical applications.

While this design performed well there is more than one electronic circuit design to measure an electrochemical cell. This Chapter identified key aspects rather than a functional potentiostat circuit alone. This potentiostat was primarily designed to measure volatile fatty acid concentration during anaerobic digestion. The success of the potentiostat enabled subsequent investigations into long-term biofilm behaviour and the impact of conductivity on biofilm response times.

6.1.3 Long-term biofilm behaviour

Biofilms are susceptible to ageing effects due to their biological nature. In an MESe, it is crucial to understand the impact long-term biofilm growth has on output signal and VFA concentration. **Paper III** utilised the low-cost potentiostat developed in **Paper II** to investigate the long-term behaviour of biofilms grown for 36 and 92 days. The current density, coulombic efficiency, and acetate consumption was measured to determine biofilm performance. The recorded data was statistically analysed and showed the biofilms long-term impact on performance.

Paper III investigated short-term and long-term biofilm growth within a MESe to identify sensor behaviour long-term, a knowledge gap identified in **Paper I**. As a sensor of VFA concentration the MESe signal must be capable of producing a repeatable output, which can be measured by a potentiostat. The MESe output must follow the relationship between output signal and VFA concentration; if a change in this relationship were to occur the resulting output would no longer represent a known VFA concentration, and measurements would be misinterpreted. **Paper III** highlighted biofilm growth deviation, which may require additional sensor modification to maintain accurate operation. The investigation demonstrated long-term biofilm performance was positive, which could indicate typical biofilm behaviour. The findings indicate a trend in biofilm performance, where improved performance and less variation was observed as the biofilms age. This suggests for a MESe to measure VFA accurately a period of measurement in-situ may be required to allow a biofilm to mature and performance stabilise. This indicates further investigation is needed to determine if there is a period of time after which a biofilm could be considered stable and no further performance changes are observed.

6.1.4 Biofilm response times

Paper I identified that MESe would need to provide timely VFA measurements in AD to be an effective sensor. Conductivity is known to influence the speed of electron migration in the electrolyte of an MESe. However, the effect of increased conductivity on biofilm response time is poorly understood. Therefore, electrolyte conductivity was investigated in relation to biofilm peak current response times of MESe. In AD, salts such as NaCl and NH_4Cl are commonly found in wastewater. **Paper IV** investigated these salts by dosing MESe cells with NaCl and NH_4Cl and utilised the potentiostat developed in **Paper II** to investigate the effect on biofilm response time.

While no significant change in response time occurred across all concentrations, response times improved (shorter response time) with age. This was not surprising as **Paper III** investigated long-term effects and demonstrated improved performance in mature biofilms. Results from **paper IV** were varied and by the final trial all biofilms (both NaCl NH_4Cl) coalesced with the control demonstrating that **paper IV** biofilms were capable of acclimation and were only impacted short-term. This suggests there is further work in stabilising MESe measurements against fluctuations that can occur during the anaerobic digestion process.

6.1.5 Limitations

Several limitations throughout the thesis were identified and are discussed in the following section. Operation of the microcontroller and peripherals reached operational limitations, which required modification. Functionality of the potentiostat, code, and outputs were tested individually and operated as designed, however, when combined did not operate as expected. The phosphate buffer used in experiments was found to contribute to current production, this required modification to the experiment design.

Simulation and theory of operation can indicate how a circuit should operate, although in reality what happens may be to the contrary. Although, through testing and simulation of the circuit, data communication was unable to be fully tested. The potentiostat circuit relied on Modbus RS485 communication. The Modbus RS485 component required significant testing to ensure data communication timing and actual measurement could occur reliably. This presented limitations of the microcontroller, while the hardware (e.g., ADC, OPAMP's) was capable of operating, the microcontroller was at the limit of operating speed (16 MHz), often resulting in backup data being lost or inability to view experiment data in real-time. In preparation for the conductivity experiment (**Paper IV**) the microcontroller was swapped with a Raspberry Pi Pico (RP2040) that was capable of operating at 144 MHz as opposed to 16 MHz for the pro mini. This enabled consistent operation when collecting data from the potentiostats. There was no change in code or data acquisition and calibration using a 100 Ohm resistor was performed as previously described in **Paper II**.

The potentiostat that was produced was able to accurately and repeatably measure current response from a microbial electrochemical cell. However, the potentiostat design incorporated cyclic voltammetry sweeps in addition to the current measurements. The potentiostat was programmed to perform a sweep from -600 mV to 600 mV, although, the actual measured voltage (multimeter) was not as expected. The potentiostat was able to perform the sweep but the voltages recorded deviated significantly from expected values. Potentiostat design was compared with commercial units, fundamental concepts, and other circuits available in the literature, which identified the potentiostat produced in **Paper II** followed the same fundamental principles. The source of the problem was never found despite the circuit having all essential components. The PCB circuit was tested at key points for voltages which found the circuit to be performing as designed and within the designed voltages. The exact cause for the modified values was unable to be

determined, however the current measurements were very accurate. The current measurements had high resolution and no drift in values, and in most cases the error value was <0.2% at 7.6 µA. As an additional measure, pre-experiment calibration was performed on all experiments to ensure the recorded values were accurate.

During the initial electrochemical experiments (**Paper II** and **Paper III**) the phosphate buffer was found to be responsible for additional current production (Torres et al., 2008), which was not expected or revealed during the literature review. To account for the additional charge due to the media **Paper III** and **Paper IV** allowed for a brief period (2 days) before the experimental phase to allow for current production to reach approximately zero. This has implications for other studies as the reported values are likely impacted by the additional current. However, depending on the setup of the experiment, current production by the phosphate buffer may not be significant.

6.2 Future research

Further study into potentiostats used in electrochemistry may show further improvements in cost, accuracy, and field portability. Potentiostat design could focus on more bespoke designs as requirements are highly dependent on application, sensor materials, electrolyte composition and measured process. The use of a potentiostat in anaerobic digesters may be somewhat difficult due to the use of a reference electrode. Reference electrodes are known to become fouled due to the nature of high-strength wastewater. Further studies into biofouling of the reference electrode should be explored to limit interference and degradation of the electrode.

The microbial community will vary depending on the source of the wastewater (e.g., municipal waste, food waste, slaughterhouse waste, etc). The unique communities within these AD systems will not exhibit the same electrochemical characteristics to those studied herein. A MESe used in an AD system other than presented here may vary considerably in performance due to factors such as microbial community. This presents an opportunity to further study the influence of different applications on MESe behaviour.

More broadly there is a need to investigate biofilms stability with regards to ageing. While the papers presented in this thesis identify biofilm behaviour in fixed conditions, it is unclear how well the findings would translate to real-world and anaerobic digesters. Further investigations of the MESe biofilm could look to identify the key mechanisms for the biofilm growth cycle in relation to performance and ageing.

REFERENCES

Australian Government. (2020). *Australian Energy Update 2020*. Retrieved from https://www.energy.gov.au/sites/default/files/Australian%20Energy%20Statistics%202020%20Energy%20Update%20Report_0.pdf

Barchmann, T., Mauky, E., Dotzauer, M., Stur, M., Weinrich, S., Jacobi, H. F., . . . Nelles, M. (2016). Expanding the flexibility of biogas plants – substrate management, schedule synthesis and economic assessment. *LANDTECHNIK, 71*. doi:10.15150/lt.2016.3146

Call, T. P., Carey, T., Bombelli, P., Lea-Smith, D. J., Hooper, P., Howe, C. J., & Torrisi, F. (2017). Platinum-free, graphene based anodes and air cathodes for single chamber microbial fuel cells. *J Mater Chem A Mater, 5*(45), 23872-23886. doi:10.1039/c7ta06895f

Engel, C., Schattenberg, F., Dohnt, K., Schroder, U., Muller, S., & Krull, R. (2019). Long-term behavior of defined mixed cultures of Geobacter sulfurreducens and Shewanella oneidensis in bioelectrochemical systems. *Front Bioeng Biotechnol, 7*, 60. doi:10.3389/fbioe.2019.00060

Ertem, F. C., Martinez-Blanco, J., Finkbeiner, M., Neubauer, P., & Junne, S. (2016). Life cycle assessment of flexibly fed biogas processes for an improved demand-oriented biogas supply. *Bioresour Technol, 219*, 536-544. doi:10.1016/j.biortech.2016.07.123

Ivars-Barceló, F., Zuliani, A., Fallah, M., Mashkour, M., Rahimnejad, M., & Luque, R. (2018). Novel applications of microbial fuel cells in sensors and biosensors. *Applied Sciences, 8*(7). doi:10.3390/app8071184

Jiang, Y., Chu, N., & Zeng, R. J. (2019). Submersible probe type microbial electrochemical sensor for volatile fatty acids monitoring in the anaerobic digestion process. *J Clean Prod, 232*, 1371-1378. doi:10.1016/j.jclepro.2019.06.041

Jiang, Y., Yang, X. F., Liang, P., Liu, P. P., & Huang, X. (2018). Microbial fuel cell sensors for water quality early warning systems: Fundamentals, signal resolution, optimization and future challenges. *Renewable & Sustainable Energy Reviews, 81*, 292-305. doi:10.1016/j.rser.2017.06.099

Jin, X., Angelidaki, I., & Zhang, Y. (2016). Microbial electrochemical monitoring of volatile fatty acids during anaerobic digestion. *Environ Sci Technol, 50*(8), 4422-4429. doi:10.1021/acs.est.5b05267

Korth, B., & Harnisch, F. (2019). Spotlight on the energy harvest of electroactive microorganisms: The impact of the applied anode potential. *Front Microbiol, 10*, 1352. doi:10.3389/fmicb.2019.01352

Li, Z., Gadipelli, S., Li, H., Howard, C. A., Brett, D. J. L., Shearing, P. R., . . . Li, F. (2020). Tuning the interlayer spacing of graphene laminate films for efficient pore utilization towards compact capacitive energy storage. *Nature Energy, 5*(2), 160-168. doi:10.1038/s41560-020-0560-6

Liu, H., Cheng, S., & Logan, B. E. (2005). Production of electricity from acetate or butyrate using a single-chamber microbial fuel cell. *Environ Sci Technol, 39*(2), 658-662. doi:10.1021/es048927c

Mauky, E., Weinrich, S., Jacobi, H. F., Nagele, H. J., Liebetrau, J., & Nelles, M. (2017). Demand-driven biogas production by flexible feeding in full-scale - Process stability and flexibility potentials. *Anaerobe, 46*, 86-95. doi:10.1016/j.anaerobe.2017.03.010

Pasternak, G., Greenman, J., & Ieropoulos, I. (2018). Dynamic evolution of anodic biofilm when maturing under different external resistive loads in microbial fuel cells. Electrochemical perspective. *J Power Sources, 400*, 392-401. doi:10.1016/j.jpowsour.2018.08.031

Schmidt, T., McCabe, B., & Harris, P. (2018). Process monitoring and control for an anaerobic covered lagoon treating abattoir wastewater. *Chemical Engineering & Technology*. doi:10.1002/ceat.201700391

Schröder, U., Harnisch, F., & Angenent, L. T. (2015). Microbial electrochemistry and technology: terminology and classification. *Energy & Environmental Science, 8*(2), 513-519. doi:10.1039/c4ee03359k

Sun, H., Zhang, Y., Wu, S., Dong, R., & Angelidaki, I. (2019). Innovative operation of microbial fuel cell-based biosensor for selective monitoring of acetate during anaerobic digestion. *Sci Total Environ, 655*, 1439-1447. doi:10.1016/j.scitotenv.2018.11.336

Torres, C. I., Kato Marcus, A., & Rittmann, B. E. (2008). Proton transport inside the biofilm limits electrical current generation by anode-respiring bacteria. *Biotechnol Bioeng, 100*(5), 872-881. doi:10.1002/bit.21821

Turick, C. E., Shimpalee, S., Satjaritanun, P., Weidner, J., & Greenway, S. (2019). Convenient non-invasive electrochemical techniques to monitor microbial processes: current state and perspectives. *Appl Microbiol Biotechnol, 103*(20), 8327-8338. doi:10.1007/s00253-019-10091-y

Vilajeliu-Pons, A., Baneras, L., Puig, S., Molognoni, D., Vila-Rovira, A., Hernandez-Del Amo, E., . . . Colprim, J. (2016). External resistances applied to MFC affect core microbiome and swine manure treatment efficiencies. *PLoS One, 11*(10), e0164044. doi:10.1371/journal.pone.0164044

Wang, A., Sun, D., Cao, G., Wang, H., Ren, N., Wu, W. M., & Logan, B. E. (2011). Integrated hydrogen production process from cellulose by combining dark fermentation, microbial fuel cells, and a microbial electrolysis cell. *Bioresour Technol, 102*(5), 4137-4143. doi:10.1016/j.biortech.2010.10.137

Wang, J. (2000). *Analytical Electrochemistry* (Second Edition ed.). New York: Wiley-VCH.

Wang, W.-K., Tang, B., Liu, J., Shi, H., Xu, Q., & Zhao, G. (2019). Self-supported microbial carbon aerogel bioelectrocatalytic anode promoting extracellular electron transfer for efficient hydrogen evolution. *Electrochimica Acta, 303*, 268-274. doi:10.1016/j.electacta.2019.02.099

Wu, D., Li, L., Zhao, X., Peng, Y., Yang, P., & Peng, X. (2019). Anaerobic digestion: A review on process monitoring. *Renewable and Sustainable Energy Reviews, 103*, 1-12. doi:10.1016/j.rser.2018.12.039

Yu, L., Yuan, Y., Tang, J., & Zhou, S. (2017). Thermophilic Moorella thermoautotrophica-immobilized cathode enhanced microbial electrosynthesis of acetate and formate from CO2. *Bioelectrochemistry, 117*, 23-28. doi:10.1016/j.bioelechem.2017.05.001

Zhang, G. Q., Zhou, Y. F., & Yang, F. L. (2019). Hydrogen production from microbial fuel cells-ammonia electrolysis cell coupled system fed with landfill leachate using Mo2C/N-doped graphene nanocomposite as HER catalyst. *Electrochimica Acta, 299*, 672-681. doi:10.1016/j.electacta.2019.01.055

APPENDIX A

Table A1 Op-amp characteristics

Parameter	Unit	Amplifier Part Number						
		AD8429	**AD8221**	**MC33178**	**AD8220**	**AD8421**	**AD8428**	**AD8226**
Offset Voltage	µV	50	25	150	750	70	25	50
Input Offset Voltage Drift	nV/°C	300	300	150,000	10,000	900	300	1,000
Input Bias Current	pA	150,000	400	100,000	10	2,000	50,000	27,000
Supply Voltage	±V	18	18	15	18	15	18	18
Voltage Noise Density	nV/√Hz	1	8	8	14	3.2	1.5	24
Continuous Output Current	mA	35	18	80	15	65	30	13
Temperature Range	°C	-40 to +125	-40 to +85	-40 to +85	-40 to +85	-40 to +85	-40 to +85	-40 to +125
Slew Rate	V/µs	22	2	2	2	35	40	0.4

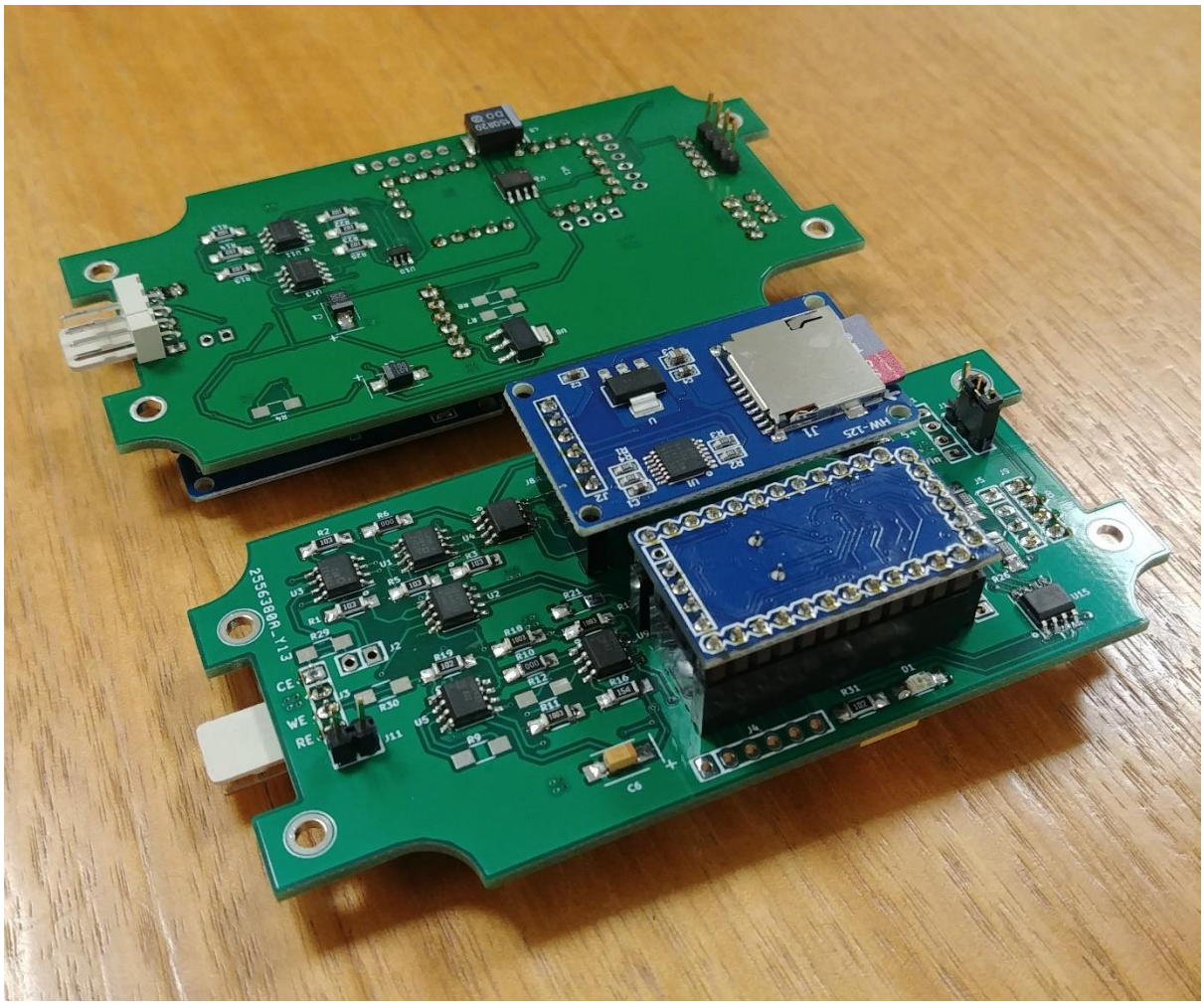

Figure A1 Fully assembled printed circuit board with micro SDcard/reader and micro-controller

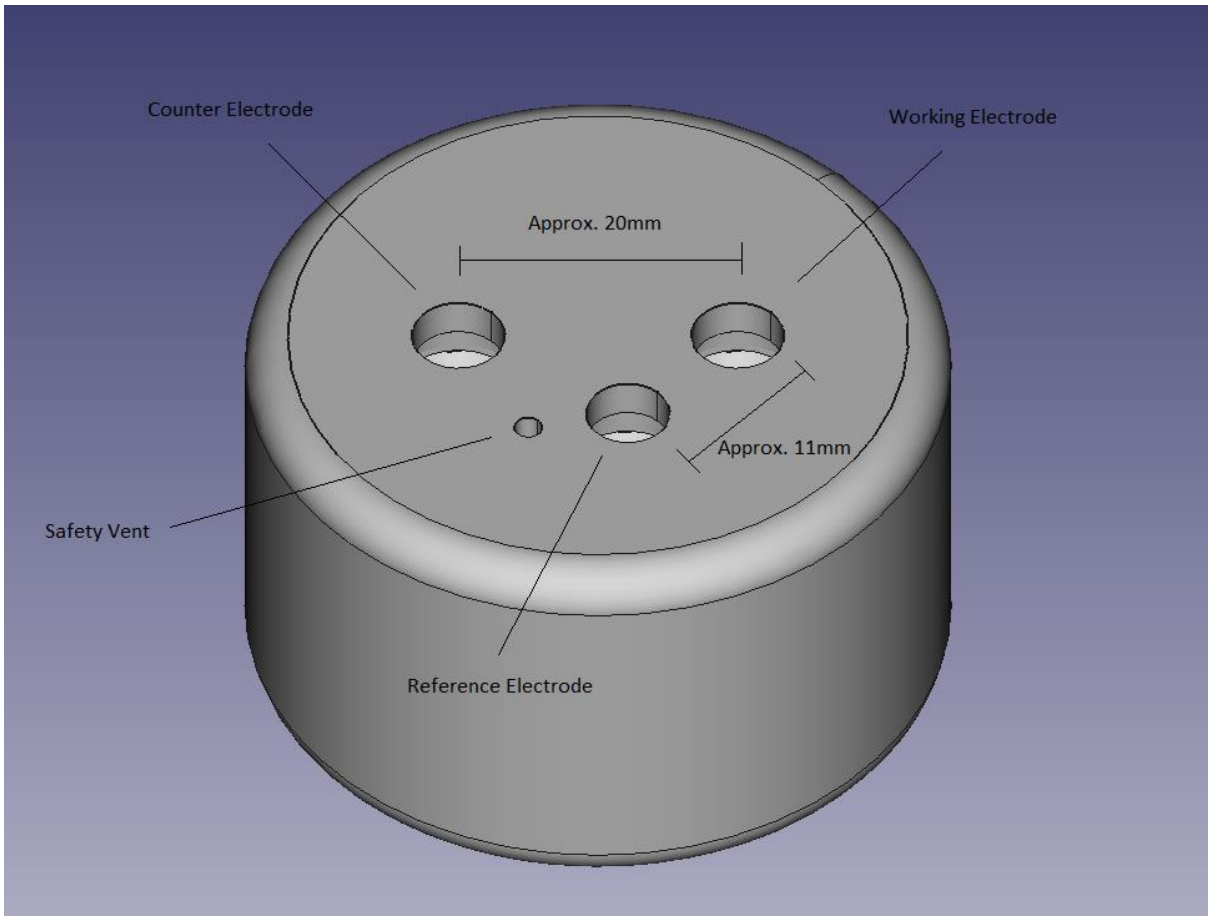

Figure A2 Schott bottle cap showing dimensions and locations for electrodes

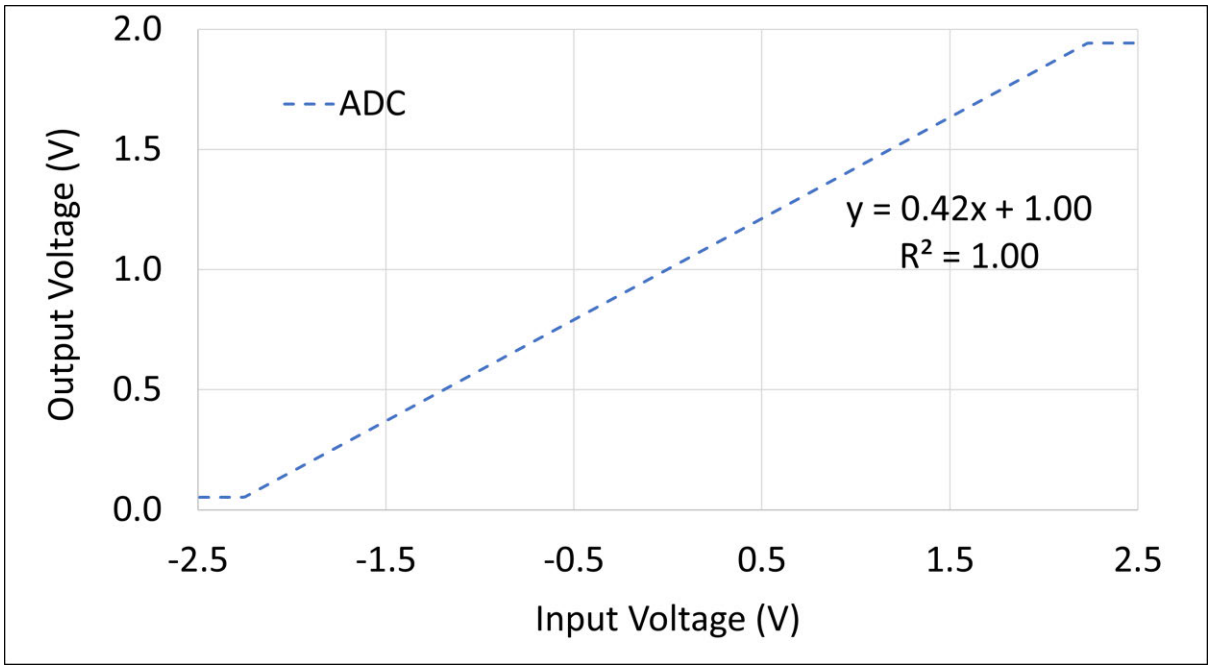

Figure A3. Modelled TIA circuit output voltage response to various CE input voltages. Equation to the line is between ±2.25 V.

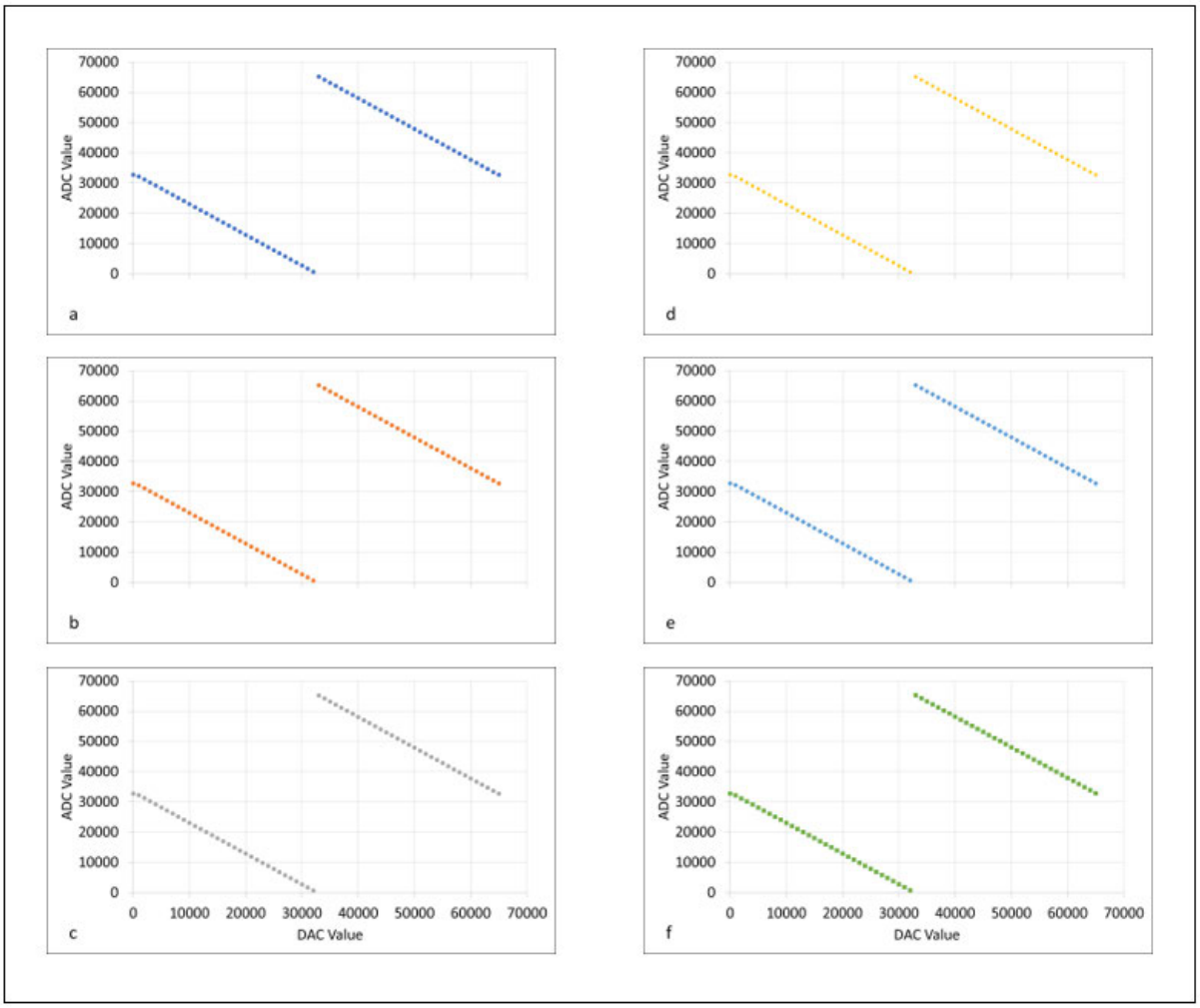

Figure A4 The raw ADC value response to the DAC value sweep for each potentiostat

APPENDIX B

Additional Component Information

Operational Amplifier

Many of the circuits in the potentiostat design employ an op-amp to convert the various voltages and current. It is important that the op-amps have significant noise immunity and especially important that no or very little current flows through the op-amp, which would distort the output.

Figure B1 represents a standard op-amp. Terminal 1 is the inverting input, terminal 2 is the non-inverting input and terminal 3 is the output. Here, terminals 4 and 5 are the power supply positive and negative respectively and are normally implied in circuit drawings (Sedra & Smith, 2011). The function of the op-amp is to output the differential voltage between terminals 1 and 2 (depending on external circuitry), multiplied by the gain (A), therefore, $v_3 = A(v_2 - v_1)$. The input resistance of an ideal op-amp is infinite and therefore signal current should be zero (Sedra & Smith, 2011).

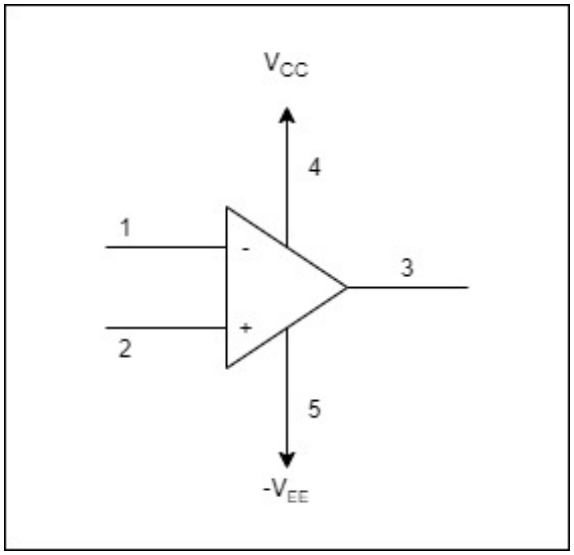

Figure B1 Operational amplifier

Reference electrode

The reference electrode (RE) is used to overcome cell effects, such as diffusion resistance, electrolyte conductivity, and allow the working electrode to be poised at the experimentally required potential. The RE is a half-cell reaction that allows the measurement to be referenced to standard potentials, such as the standard hydrogen electrode (SHE). The RE is used to counteract cell resistance due to electrolyte properties.

The RE can only allow for spatial resistance between the counter electrode (CE) and RE, although, a small uncompensated resistance still exists between RE and the working electrode (WE). Within the cell, RE must be placed as close as possible to WE, but no closer than twice the diameter of the RE capillary tip to avoid shielding errors (Bard & Faulkner, 2001).

Theory of operation; the Voltage applied to the non-inverting input V_a is reflected on the output V_o, this configuration is known as a voltage follower or buffer. The op-amp circuit shown (Figure B1) connects V_o to the inverting pin of the op-amp via a feedback loop, this produces unity gain ($V_a = V_o$). The input impedance of the op-amp is essentially infinite, this is essential so that no current flows through the op-amp from RE, which could affect cell measurement. Without the contribution from the RE the potential of the WE cannot be accurately controlled or easily compared with other microbial electrochemical cells.

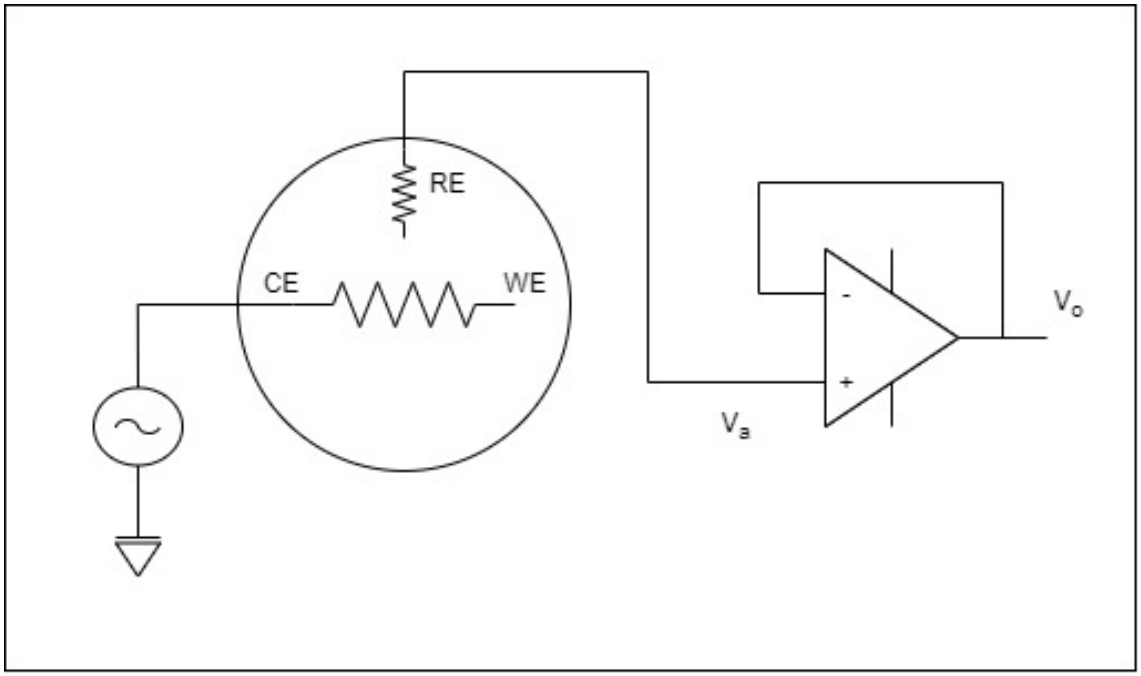

Figure B2 Reference electrode feedback circuit

Figure B2, the circuit shows how the RE is connected to the electrochemical cell and the potentiostat. The current that flows through the RE half-cell is ideally zero, although, practically some electrons move through the circuit. The current through the RE is minimised by placing an operational amplifier in series reducing the impact from electron flow through RE.

Transimpedance Amplifier (TIA)

The design of the potentiostat will vary depending on the current measurement method. This design incorporates a transimpedance amplifier (TIA) as the method for current measurement, this topography is designed to reduce circuit resistance (Figure B3). Unlike other methods for measuring current, the TIA takes advantage of a virtual ground (V_g) created by the feedback loop of the TIA op-amp.

The TIA theory of operation, V_a is connected to the WE of the cell, V_b is either connected to power ground or variable supply (this case power ground). The op-amp with output a voltage directly proportional to the difference between inputs V_a and V_b, with V_b = 0V, the output will be determined by the current flow from V_a for example; V_o will be, $V_o = -V_a/R$ resulting in equal but opposite current flow through R (V_a is negative as current direction is into the inverting pin of the op-amp). For the circuit to obey Kirchhoff's current law, the two currents of equal but opposite current will cancel, thus producing a virtual ground at V_g, V_g = 0V. Therefore, the voltage at V_o will be directly proportional to the current flowing through the cell.

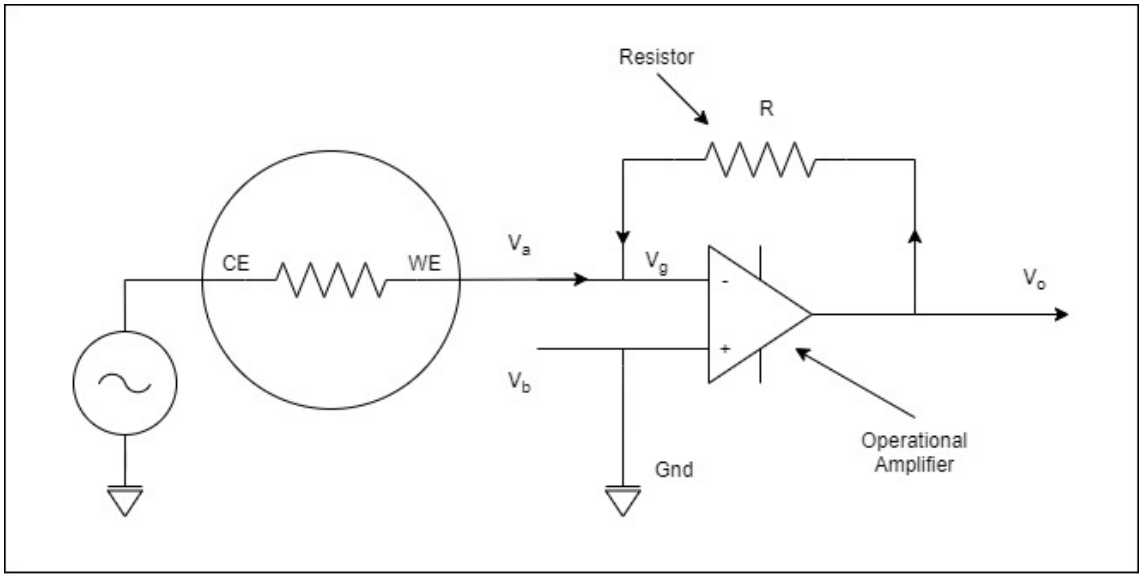

Figure B3 Transimpedance circuit

APPENDIX C

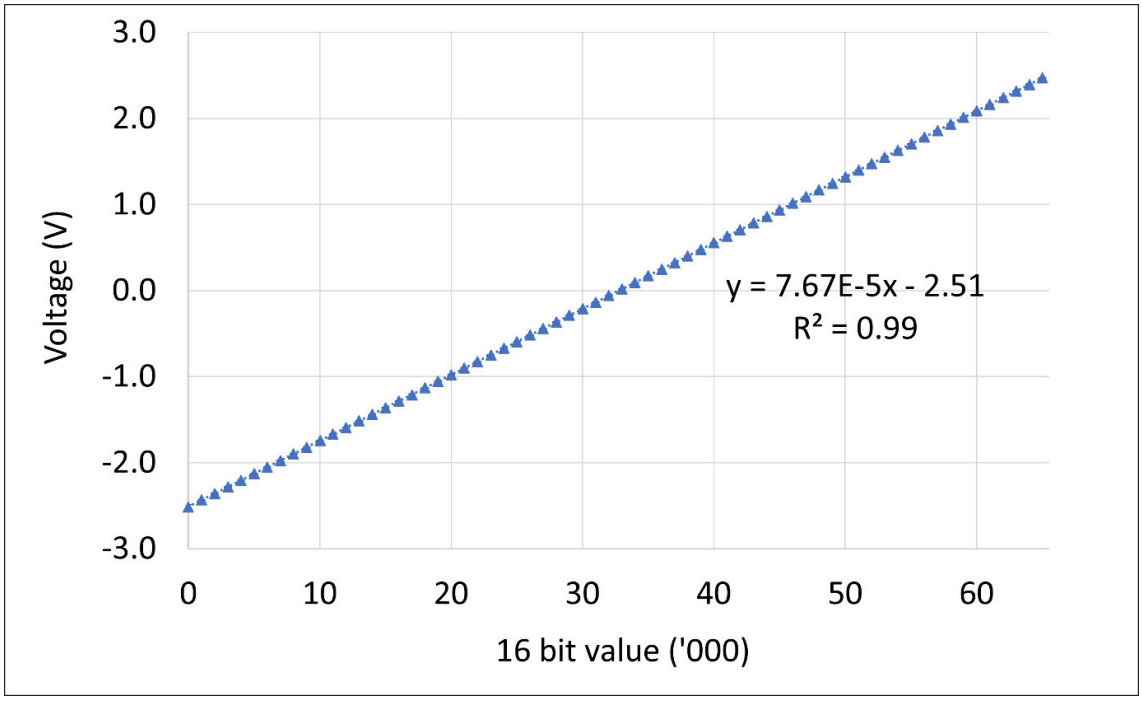

Figure C1 Mean voltage drop across 100 ohm resistor of all six potentiostats. Voltage sweep performed using digital to analog converter 16 bit value (x-axis), standard deviation was applied but is too small to visually identify.